UNITED STATES
NUCLEAR REGULATORY COMMISSION
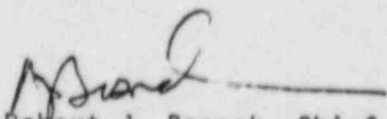WASHINGTON, D. C. 20555

MAR 2 8 1984

MEMORANDUM FOR: George Knighton, Chief
Licensing Branch #3
Division of Licensing

FROM: Robert J. Bosnak, Chief
Mechanical Engineering Branch
Division of Engineering

SUBJECT: PALO VERDE VIBRATION PROBLEMS - REQUEST FOR
ADDITIONAL INFORMATION

As a result of the March 20, 1984 meeting with the applicant, the
following additional information is needed to complete our review:

1. We were notified in the meeting that the thermal liners of the surge
lines will also be removed in addition to the liners in the safety
injection system as originally indicated in the licensee's
submittal. Information regarding the nature and number of occur-
rences of pressure and thermal transients induced by various flow
modes during the expected life span of the surge line should be
provided and reviewed by the Reactor System Branch in order that
MEB's evaluation of fatigue effects can be completed. This is
necessary to ensure the nozzle structural integrity without the
thermal liner.

2. We also were advised during the course of the meeting that the four
"snubbers" (nominally keyways) at the top of the CEA shroud are the
first-of-a-kind design being used initially in the CE system 80
reactor internals. Due to the lack of service experience, additional
information is needed to demonstrate that, with the reduced clearances
present in these "snubbers" over other designs now in service, these
devices can operate reliably for the service life of the internals.
Further, to eliminate confusion, we recommend the use of the term
"Keyways" in lieu of "snubbers".

Robert J. Bosnak, Chief
Mechanical Engineering Branch
Division of Engineering

cc: See Page 2.

8404110148

cc: R. Vollmer
    D. Eisenhut
    J. Knight
    T. Novak
    M. Licitra
    H. Brammer
    F. Cherny
    S. Hou
    B. Liaw

Document No. CEN-264(V)-NP

REPORT ON

PALO VERDE UNIT 1

SAFETY INJECTION NOZZLE

THERMAL LINER

Prepared by: COMBUSTION ENGINEERING, INC.

WINDSOR, CONNECTICUT

LEGAL NOTICE

PALO VERDE UNIT 1
SAFETY INJECTION NOZZLE THERMAL LINER

1.0 Introduction

Palo Verde Unit 1 system is a 3800 Mwt class, pressurized water System 80 nuclear power plant. Figure 1 is a layout arrangement of the primary components. The hot-leg piping is a 42 inches in diameter and the cold-leg piping is 30 inches in diameter. The pumps in the coldleg piping are designated 1A, 1B, 2A and 2B and, hereinafter, the cold-leg pipe attached to a particular pump will carry the same designation.

There is one safety injection nozzle in each of the four cold-leg pipes. The nozzle is a 14 inch, schedule 160, full penetration weided nozzle mounted on an angle 30° from perpendicular to the axis of the pipe as shown in Figure 2. The nozzles are located near the discharge of the main coolant pumps (Figure 1) and serve as a conduit for the injection of water into the system for plant cooldown, loss of secondary pressure and loss of coolant accident conditions.

The pumps were operated for cold hydrostatic testing during July - September, 1982 (Figure 3), and for pre-core hot functional testing during May - July, 1983 (Figure 4).

During the post core HFT inspection on July 19, 1983, the reactor coolant pipe (RCP) 1A and 1B discharge piping was entered to look at the thermowells which failed during the HFT. It was noticed that the thermal liner in the safety injection nozzle for the 1B pipe was protruding into the pipe about one-half inch. Also, it was observed that the thermal liner was missing from the safety injection nozzle in the 1A pipe. Also, there were gouges in the clad on safety injection nozzle 1A near the nozzle-to-pipe juncture where the positioning pads were located. The missing liner was found in the reactor vessel below the inlet nozzle through which it had passed and wedged between the reactor vessel and the outside of the flow skirt. All other nozzles with thermal liners in the RCS piping were examined and the liners were found to be in place. As a result of the findings an intensive effort was initiated to understand the failure mechanism and develop a course of action to prevent any further occurrence. The intent of this report is to discuss efforts in both of these areas pertaining to the safety injection nozzle liner problem.

The safety implications of the failure have been evaluated. The transients and the number of cycles originally specified and analyzed were reviewed and were found to be applicable for this plant. An examination of the usage factors for the area of the safety injection nozzle under the liner was performed and the results are listed below:

a. With the liner in place the limiting usage factor is 9.4% of the allowable.

b. With the liner missing and the support groove in the "as is condition" the limiting usage factor is 60% of the allowable in the raised portion of the explansion groove (see Figure 7 thermal sleeve explansion groove and Figure 5).

c. With the explansion groove blended, the limiting usage factor is 34% of the allowable.

Therefore, with the explansion lands blended, the limiting usage factor under the liner has increased to 34% of the allowable without the liner as compared to 9.4% with the liner.

If the liner had become dislodged in service, the usage factor would have increased to 60% of the allowable, however, even at this value the nozzle is acceptable for use for its full 40 year design life.

The safety injection nozzle is located down stream of the pump (see Figure 1) and upstream of the reactor vessel. The potential for core flow blockage has been examined and it has been concluded that the dislodged liner would not lead to flow blockage. The liner would be prevented from entering the core region by the reactor flow skirt and would remain trapped between the flow baffle and the reactor vessel shell as found in Palo Verde I.

It has been a Combustion Engineering design practice to install a thermal liner in nozzles which could experience rapid temperature changes (thermal shock) during the life of the plant. In some instances, this was

done without regard to the necessity for a liner, but as an additional assurance of adequate "protection" for the nozzle. Therefore, the original calculations which justified the fatigue life of the safety injection nozzles included the nozzle liner. No calculations were made at that time to determine if the liner was actually required for the fatigue evaluation of the nozzles to be satisfactory.

As will be discussed in more detail in this report, subsequent fatigue evaluation of the safety injection nozzle without the liner indicates the fatigue life is well in excess of the specified requirements.

Other nuclear steam supply systems designed by Combustion Engineering have a safety injection nozzle and liner design similar to that described above. There are significant differences in primary coolant pump design and in fluid flow rates. Generally, the pump impeller blade passing frequencies and fluid flow rates for the other plants are less than for the System 80 plants. The significance of this will be discussed in another section of this report.

2.0 Summary

When the safety injection nozzle liner at the 1A coolant pipe was discovered missing, an intensive effort was begun (1) to determine why this occurred, (2) to determine the effect on the safety injection nozzle, and (3) to determine if a similar condition existed in other safety injection nozzles. Initial inspection of the explansion groove in the nozzle clad

suggested either improper groove design or improper fabrication. Later, the liner was found in the reactor vessel against the flow skirt below the 1A inlet nozzle. The recovered thermal liner 1A was sent to C-E Chattanooga Metallurgy Laboratory for further examination which revealed an inside explansion groove area corresponding to what would be expected from a properly made joint. However, the outside explanded and centering pad areas (see Figure 11) showed very definite signs of wear corresponding to the plaster molds made of the nozzle inside surface (Figure 7). From this evidence it was concluded that the nozzle groove had been correctly machined, the liner had been explanded properly into place, and that the liner had vibrated and worn the nozzle clad so as to become loose and eventually exit the nozzle.

To prevent loosening of the safety injection nozzle liners at other locations, the liners were removed. Any damage done to the nozzle cladding was repaired and operational suitability verified by non-destructive examination. The explansion ridge in the clad was also removed and the surface examined. No base metal was exposed.

The above solution to the problem has been verified by analysis. The maximum cumulative usage factor in the part of the nozzle that is protected by the liner when it is in place is calculated to be .094. The usage factor at this location without the liner is .34. The .34 usage factor would allow three times the number of transients that are listed in the RC piping specification. The specific nozzle transients are listed in Figure 17. Another location, namely the explansion groove,

is calculated to have a cumulative usage factor of .60 in its "as is" configuration in which a stress concentration factor is used. If this surface is machined smooth so that a stress concentration factor would not be present, the usage factor at this location would be .16. Thus, the largest usage factor in the area that was behind the liner will be .34 when the liner is not present.

The usage factor in the safe end portion of the nozzle, which is not protected by the thermal liner, is 0.6[1]. Therefore, the absence of the liner will not change the operating capability of the nozzle.

3.0 Inspection and Examinations

The initial examination of the clad surface in nozzle IA revealed that the explansion groove was non-existent for about 1/3 of the circumference and greatly reduced for the remaining portion. Diameters on appropriate surfaces were measured at several circumferential locations and compared to drawing requirements as shown on Figure 5. This indicated that either the groove had been machined incorrectly or that it had been worn significantly. Pad height measurements taken at the same time (dimension "D" on Figure 5) did not completely agree with the diameter measurements even though some reduction of groove length was again indicated.

_____

(1) This was previously reported to the staff incorrectly as .32.

To further verify the explansior groove dimensions in safety injection nozzle 1A, a set of molds were made in areas where a groove could be seen. Examination of these molds showed a severe reduction in groove depth more in agreement with the diameter measurements taken previously.

Molds were taken of impressions in the nozzle clad that were caused by one of the centering pads on the liner. It appeared from the indentations that the liner had vibrated at its original location while turning slowly. At some time, the liner slipped out of the nozzle about 1" and lodged there while vibrating and rotating slowly again (Figure 6). Finally, the liner slipped out of the nozzle completely and was eventually found in the reactor vessel under the 1A pipe inlet location.

An inspection of the three (3) remaining safety injection nozzles at the site showed that the liners were still in place, but the 2A liner was protruding about 1/2" into the primary pipe (Figure 8). Eventually, this liner as well as the others were removed exposing indentations in the nozzle clad very similar to those found under liner 1A with definite, but reduced, evidence of rotation (Figures 9 and 10). All indentations were acid-etched to check for exoosed base metal, but none was found. Repairs were made by blending the worn areas and machining out the explansion groove area flush with surrounding surfaces. A liquid penetrant inspection was done on finished surfaces to identify any indications that might have been uncovered during the rework. No weld repair was required.
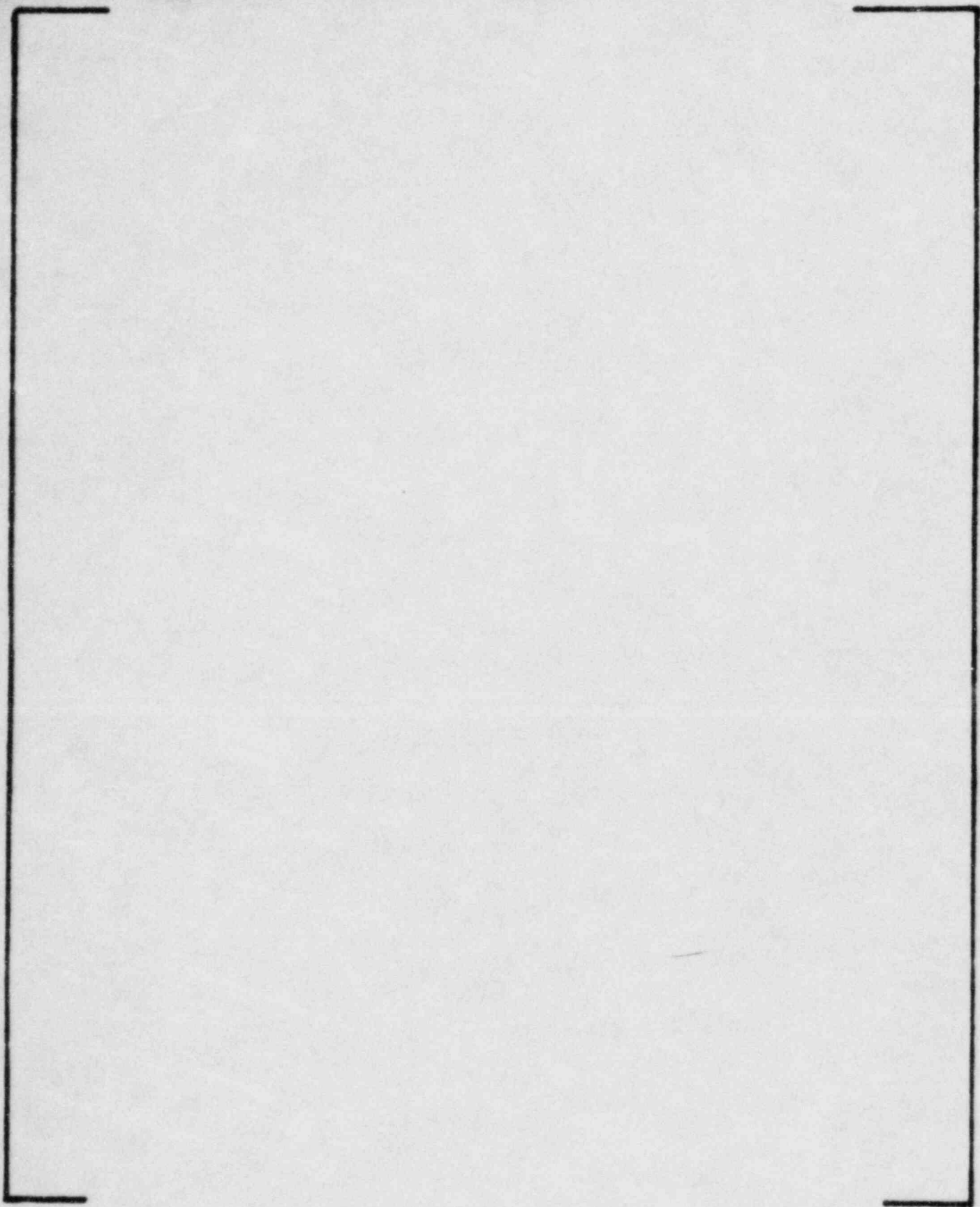
4.0 Problem Definition

One end of the cylinder is cut on a 30 degree angle to conform to the nozzle-to-pipe juncture. The liner is held in place in the nozzle by explansion into a specially prepared groove in the clad on the nozzle inside diameter. The groove is approximately 0.1 inch deep. Also, three equally spaced tabs on the liner near the nozzle-to-pipe juncture tend to limit lateral movement of the liner. Figures 11 and 12 show the liner details and the liner installed in the nozzle.

The cantilever length significantly influences the natural frequency and the "leverage" that forces can exert upon the liner.

By reviewing the operating history and the design of the liner, a failure mechanism can be developed to explain the post Core Hot Functional Testing findings. The following conditions were found:

1. The liner in the safety injection nozzle in the 1A pipe was missing.

2. The liner in the safety injection nozzle in the 2A pipe protruded into the main pipe between 1/2 inch and 1 inch. (This was found to result from rotation of the liner.)

3. The liners in the safety injection nozzles in the 1B and 2B pipes were apparently in the proper position.

By observing the operating history provided on Figure 4, a pattern is evident which suggests a reason for the liner problem. The following table contains data from Figure 4.

Liner	Total RC Pump Run Time, Hrs	Time @ Maximum Flow Rate*	Liner Condition
1A	1136	528	Missing
2A	1041	137	Rotated
2B	986	81	Acceptable
1B	686	77	Acceptable

The data suggests some correlation between liner condition and total run time and a fairly strong correlation between liner condition and the time at a high flow rate.

*   The maximum flow rate in a cold leg (>137%) occurs when only one of two pumps in a steam generator loop is operating. See Figure 1 for RCS loop configuration.

The failure mechanism is further substantiated by the indentations observed in the nozzle clad at the liner tab locations. Figure 6 shows photographs of the clad surface in nozzle 1A. Apparently, the liner vibrated against the nozzle wall and then dropped a short distance where both vibration and rotation within the explansion groove occurred. As the liner rotated, more of the liner end protruded into the fluid flowing in the main pipe. Ever increasing flow induced forces impacted the liner and was magnified by the cantilevered design. Eventually, the combination of vibration and flow load caused the liner to "lose its grip" at the explansion groove and fall into the main pipe.

Figure 8 shows photographs of the liner in nozzle 2A which has experienced some rotation. This is evidenced by the fact that the liner does not conform to the pipe surface, but protrudes into the pipe.

There were other factors which may contribute significantly to the mode of failure. The fundamental pump rotational frequency is about 20 cycles per second. Since the pumps have six blades, the blade passing frequency would be about 120 cps. If the natural frequency of the nozzle liner is sufficiently close to either of these frequencies or other harmonics, a resonant or near resonant condition could result which could cause liner failure. A finite element analysis was made to determine the natural frequency of the liner.
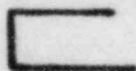
5.0 Design Verification

Two analyses were performed to demonstrate the acceptability of operating the primary piping and safety injection systems without a thermal liner and expansion groove in the safety injection nozzle. Since the purpose of the liner is to protect the nozzle from large thermal gradients (stresses), the analyses performed are (1) a thermal analysis to evaluate the new thermal gradient conditions in the nozzle and (2) a structural stress analysis to incorporate the results of the thermal analysis into the primary plus secondary stress and fatigue stress evaluations. These two analyses are "Thermal Analysis of Safety Injection Nozzle Without Thermal Liner" and "Fatigue Analysis of the Safety Injection Nozzle Without a Thermal Liner". It was not necessary to include a re-evaluation of the nozzle safe end in these analyses because the thermal liner did not offer protection in that area of the nozzle.

Using analytical criteria of the ASME Boiler & Pressure Vessel Code Section III Article NB3000 and the assumed transients in Figure 17, the results are summarized below.

Figure 13 shows the different places in the nozzle where stresses were calculated. Figure 14 shows the resulting range of stress and Figure 15 shows the corresponding fatigue usage factor[1] at each location. Note that the highest fatigue usage factor is at location D in the clad and is 0.34. This is only about one-third of the ASME Code, Section III allowable fatigue usage factor of 1.0 and is less than the 0.6 usage factor in the safe end. Therefore, removing the thermal liners will not adversely affect the operating capability of the safety injection nozzles or the primary coolant system.

---

(1) The usage factor is a cumulative measurement of fatigue damage to the nozzle resulting from specified transients (ratio of anticipated number of cycles ÷ allowable number of cycles, with a limit of one).

FIGURE 1
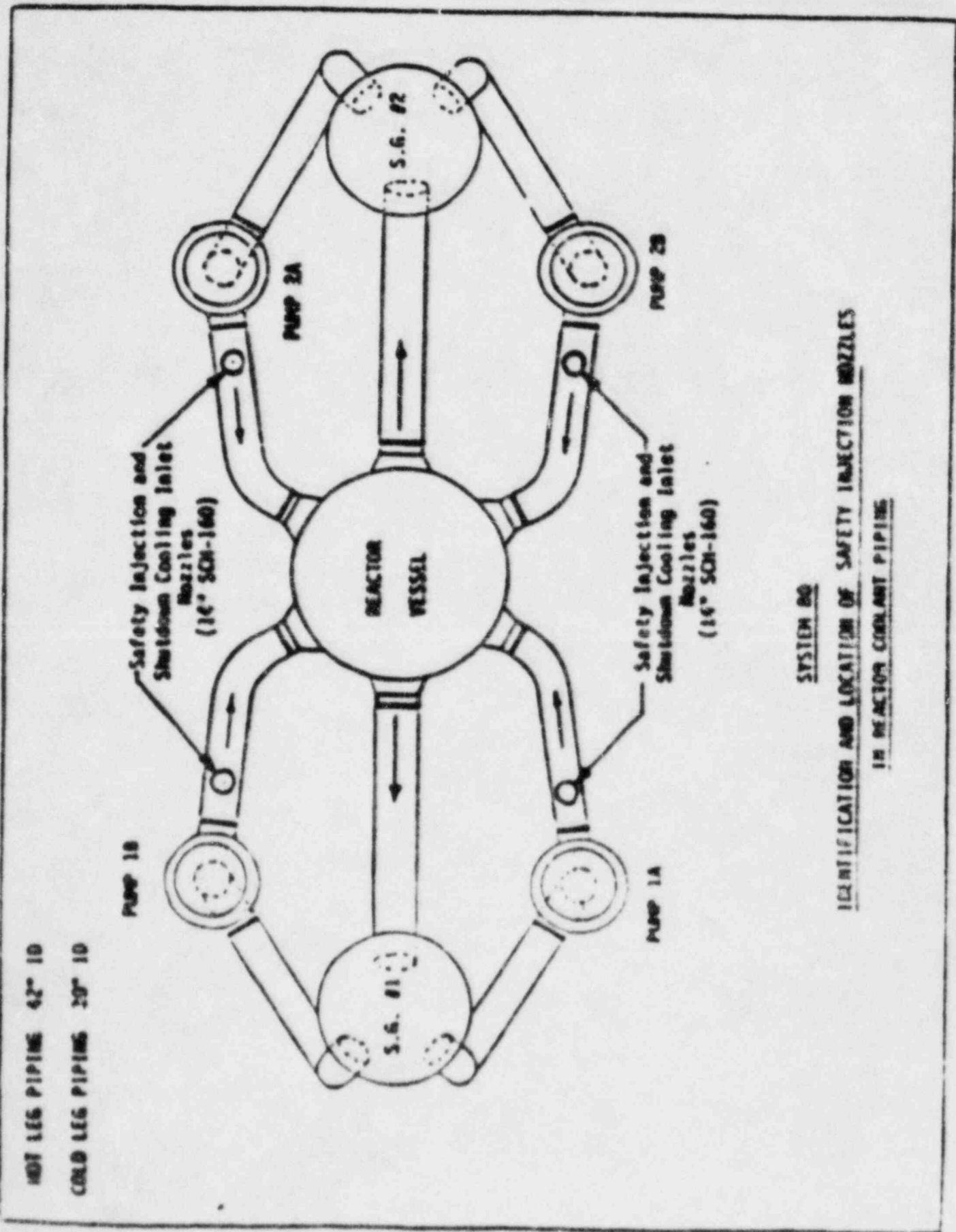
HOT LEG PIPING 42" ID

COLD LEG PIPING 30" ID

PUMP 1B

PUMP 2A

S.G. #2

PUMP 2B

Safety Injection and
Shutdown Cooling Inlet
Nozzles
(16" SCH-160)

Safety Injection and
Shutdown Cooling Inlet
Nozzles
(16" SCH-160)

REACTOR
VESSEL

PUMP 1A

S.G. #1

SYSTEM 80

IDENTIFICATION AND LOCATION OF SAFETY INJECTION NOZZLES

IN REACTOR COOLANT PIPING

FIGURE 2

SYSTEM 80
LOCATION OF S.I.S. NOZZLES

FIGURE 3
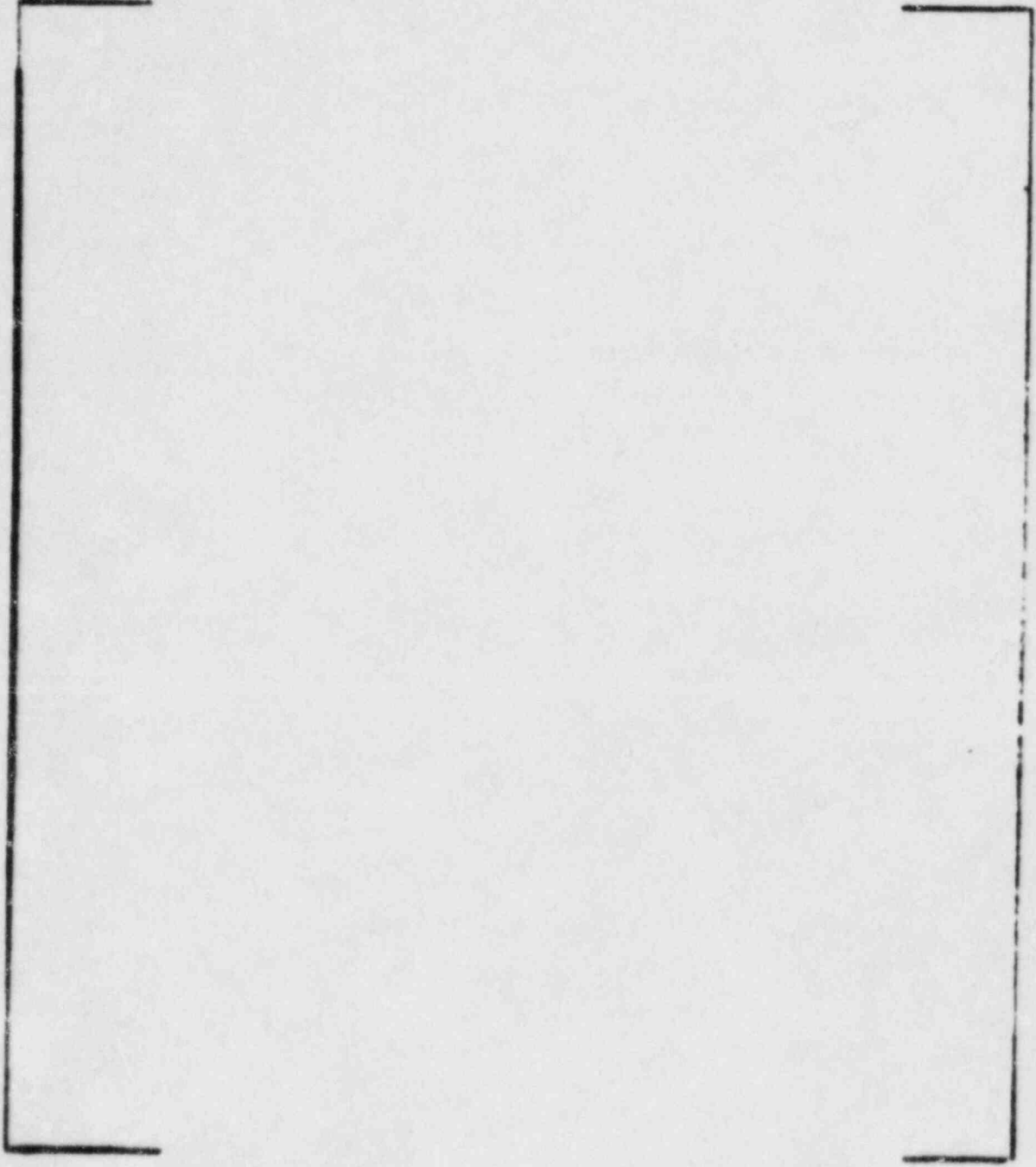
HISTORY OF PUMP OPERATION DURING COLD HYDRO TESTING
AT
ARIZONA PUBLIC SERVICE COMPANY PVNGS UNIT #1
JULY - SEPTEMBER, 1982

DESCRIPTION	RCP 1A	RCP 1B	RCP 2A	RCP 2B
Total Starts	10	36	31	12
Cold Starts	10	36	31	12
Starts with three other pumps running	0	0	0	0
Starts with two other pumps running	0	0	0	0
Starts with one other pump running	1	3/12*	15/24*	7
Starts with no other pumps running	9	33/24*	16/7*	5
Run Time - Hours (Total)	11	18	11	13
Two Pumps, One steam generator (Two pumps other steam generator)	0	0	0	0
One Pump, One steam generator (Two pumps other steam generator)	0	0	0	0
One Pump, One steam generator (One pump other steam generator).	5	10	4	10
One Pump, One steam generator (No pumps other steam generator)	6	8	7	3

*9 Starts were not sequence identified.

Information obtained from Control Room Operators Log supplement by CE-KSB Log.

Cold is defined as less than 300 F.

FIGURE 4

HISTORY OF PUMP OPERATION DURING HOT FUNCTIONAL TESTING
AT
ARIZONA PUBLIC SERVICE COMPANY PVNGS UNIT #1
MAY - JULY, 1983

DESCRIPTION	RCP 1A	RCP 1B	RCP 2A	RCP 2B
STARTS				
TOTAL	16	18	15	18
COLD	11	9	10	10
WITH THREE OTHER PUMPS RUNNING	0	8	1	0
WITH TWO OTHER PUMPS RUNNING	2	4	1	10
WITH ONE OTHER PUMP RUNNING	1	0	8	5
WITH NO OTHER PUMPS RUNNING	13	6	5	3
RUN TIME - HOURS				
TOTAL	1136	686	1041	986
TOTAL COLD	332	132	234	181
COLD TO FIRST HEAT UP	178	132	81	51
ONE PUMP COLD	58	26	0.1	0
ONE PUMP, ONE STEAM GENERATOR (NO PUMPS OTHER STEAM GENERATOR)*	69	27	2	1
ONE PUMP, ONE STEAM GENERATOR (ONE PUMP, OTHER STEAM GENERATOR)*	55	50	55	50
ONE PUMP, ONE STEAM GENERATOR (TWO PUMPS, OTHER STEAM GENERATOR)*	404	0	80	30
TWO PUMPS, ONE STEAM GENERATOR (NO PUMPS, OTHER STEAM GENERATOR)	0	0	2	2
TWO PUMPS, ONE STEAM GENERATOR (ONE PUMP, OTHER STEAM GENERATOR)	111	111	404	404
TWO PUMPS, ONE STEAM GENERATOR (TWO PUMPS, OTHER STEAM GENERATOR)	498	498	498	498
*FLOW GREATER THAN 137%	520	77	137	31

INFORMATION OBTAINED FROM CONTROL ROOM OPERATORS LOG
SUPPLEMENTED BY HOT FUNCTIONAL TEST LOG.
COLD IS DEFINED AS LESS THAN 300 F AND 400 PSIA.
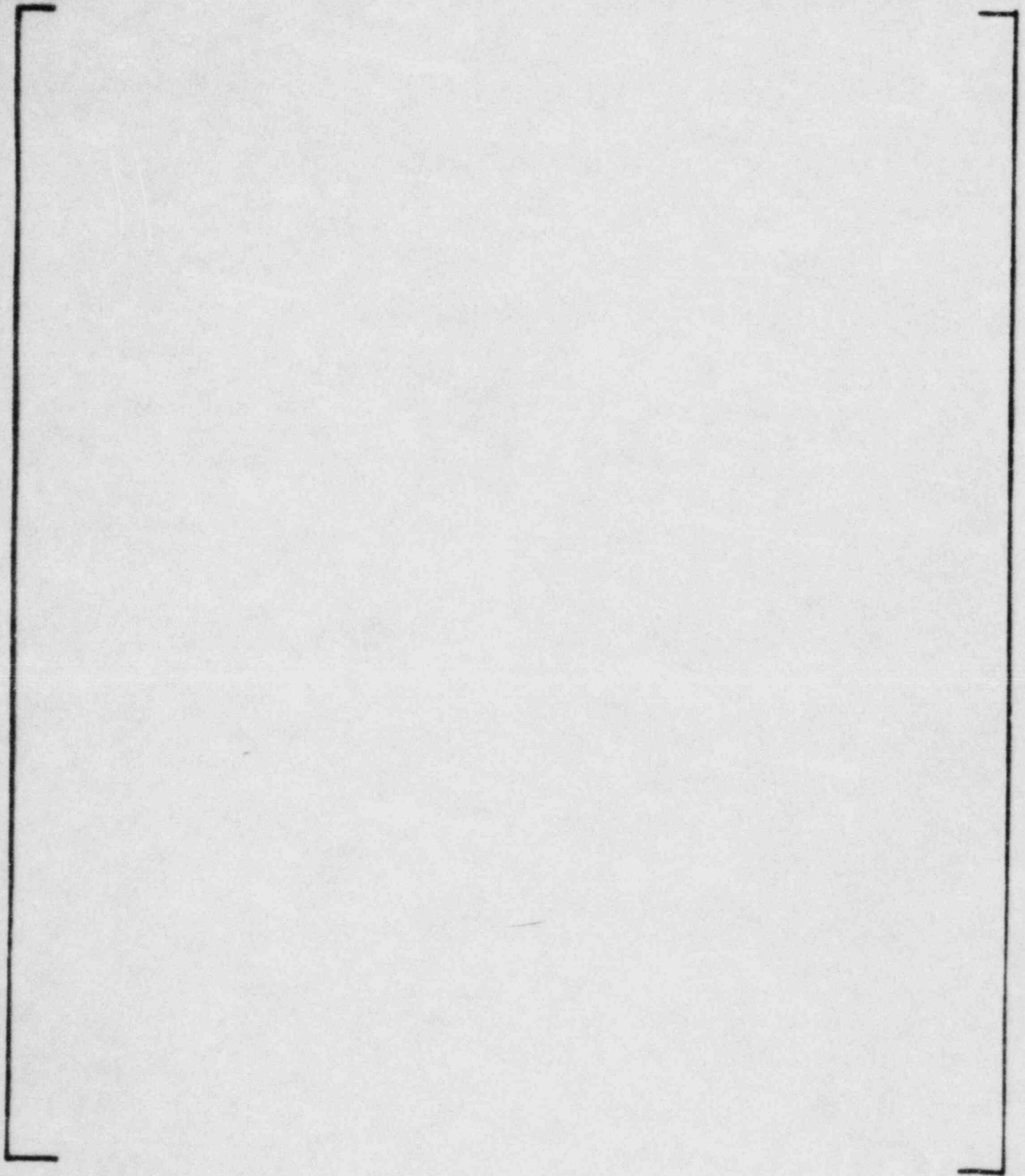
FIGURE 5

FIGURE 5

FIGURE 6

CLAD DAMAGE ON S.I. NOZZLE 1A
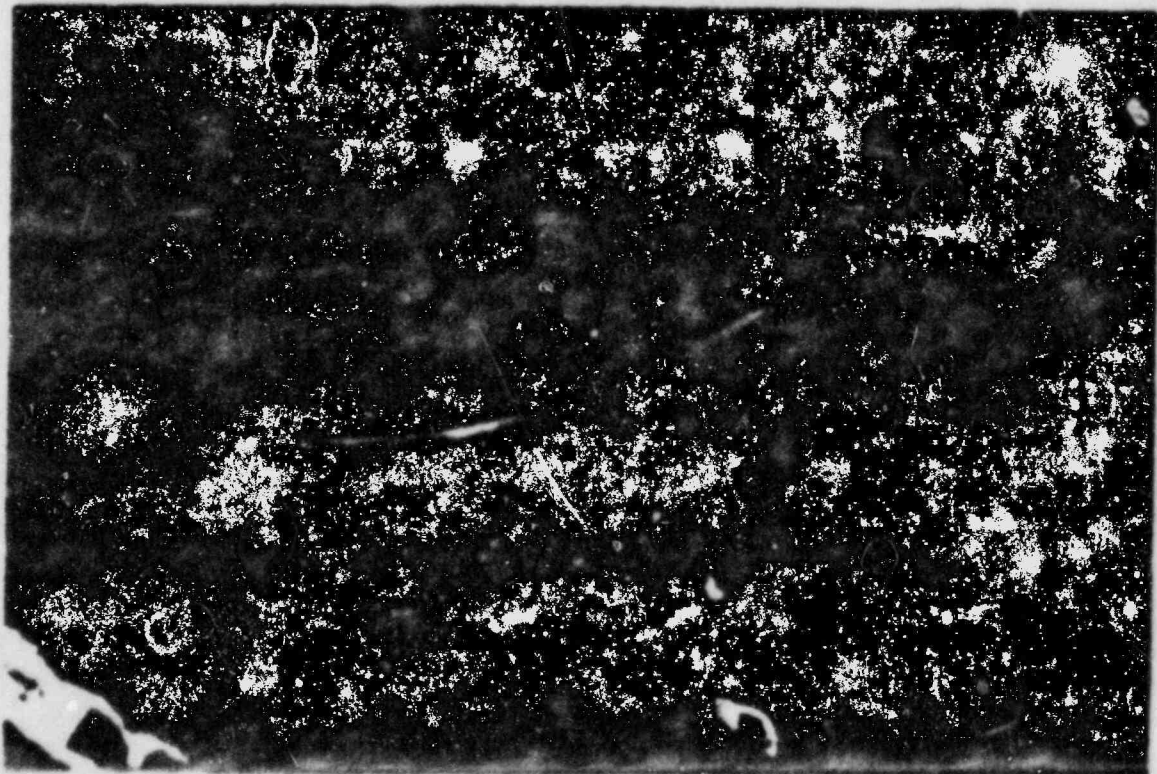
FIGURE 7

THERMAL LINER
EXPLANSION GROOVE
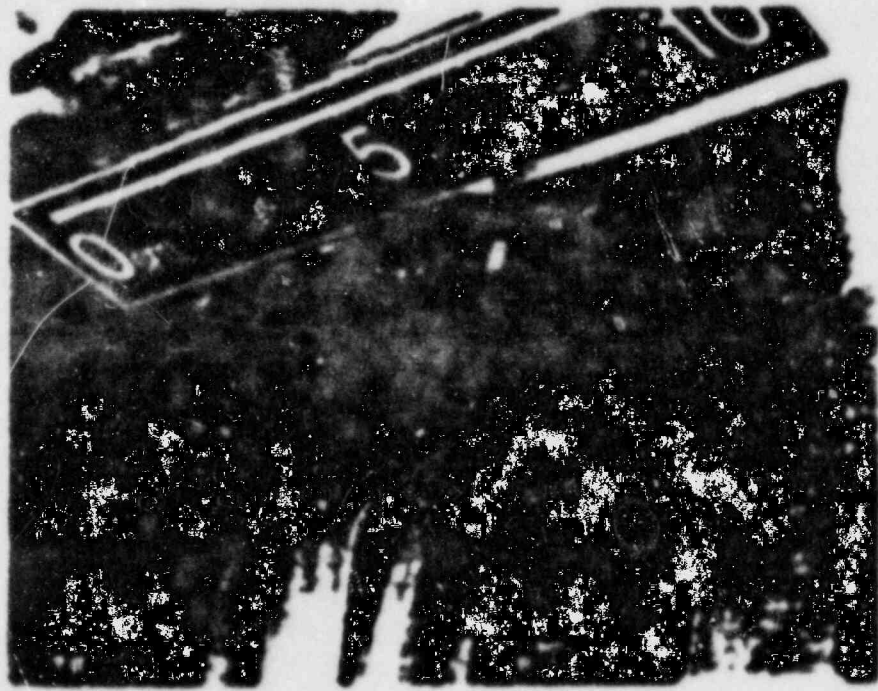
THERMAL LINER
EXPLANSION RIDGE

FIGURE 8

2A THERMAL LINER

PARTIAL ROTATION OF LINER IN THE NOZZLE
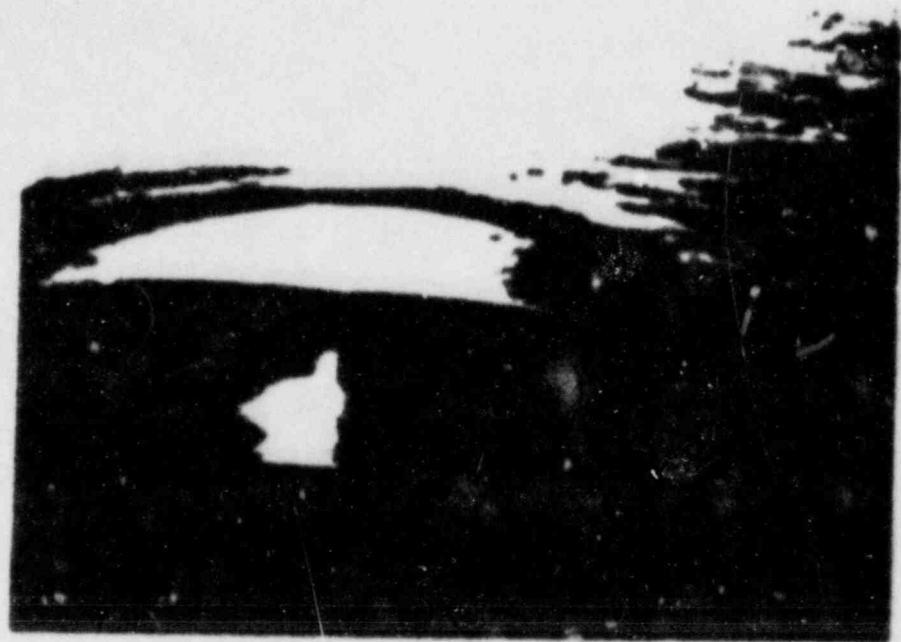
FIGURE 9

Pump Loop 1-B

This sketch is The Actual Size of The indentation Located at the 0°Axis And The 240° Axis of The Safety Injection Nozzle. Viewed from open End of The Nozzle Looking in.
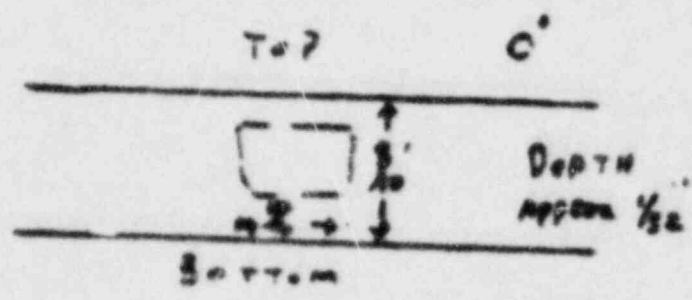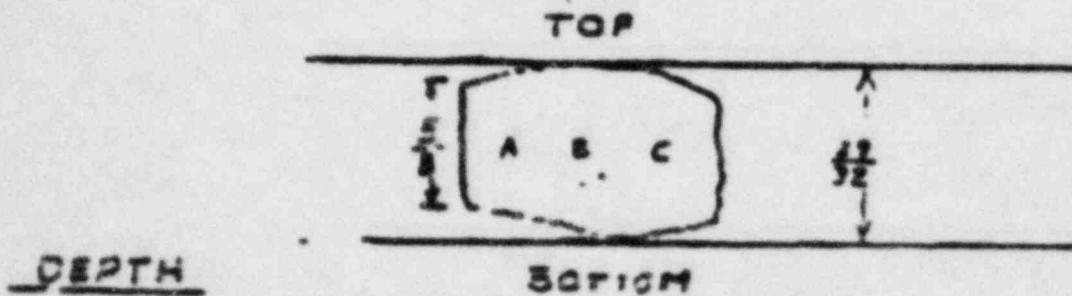

Top   0°

Depth
Appr. 3/32

Bottom

Top   240°

Depth
Appr. 1/16

Bottom

FIGURE 10

23
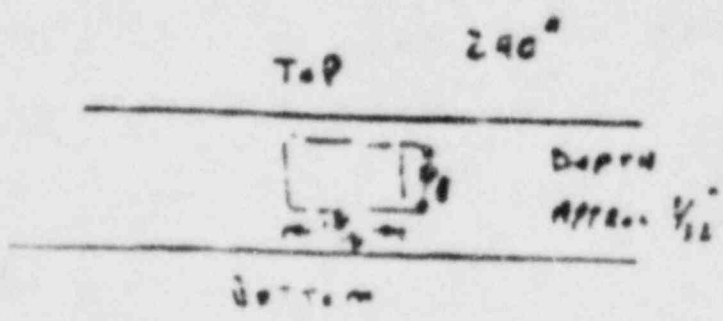
PUMP LOOP 2-B

THIS SKETCH IS THE ACTUAL SIZE AND SHAPE OF THE INDENTATION LOCATED AT THE 0° AXIS OF THE SAFETY INJECTION NOZZLE. VIEWED FROM OPEN END OF THE NOZZLE LOOKING IN.

DEPTH

A = .090

B = .094

C = .095

THIS SKETCH MADE FROM A RUBBING OF THE INDENTATION.

FIGURE 11

SAFETY INJECTION NOZZLE
THERMAL LINER

FIGURE 12

SAFETY INJECTION
NOZZLE

LINER INSTALLED FLUSH
WITH I.D. OF PIPE
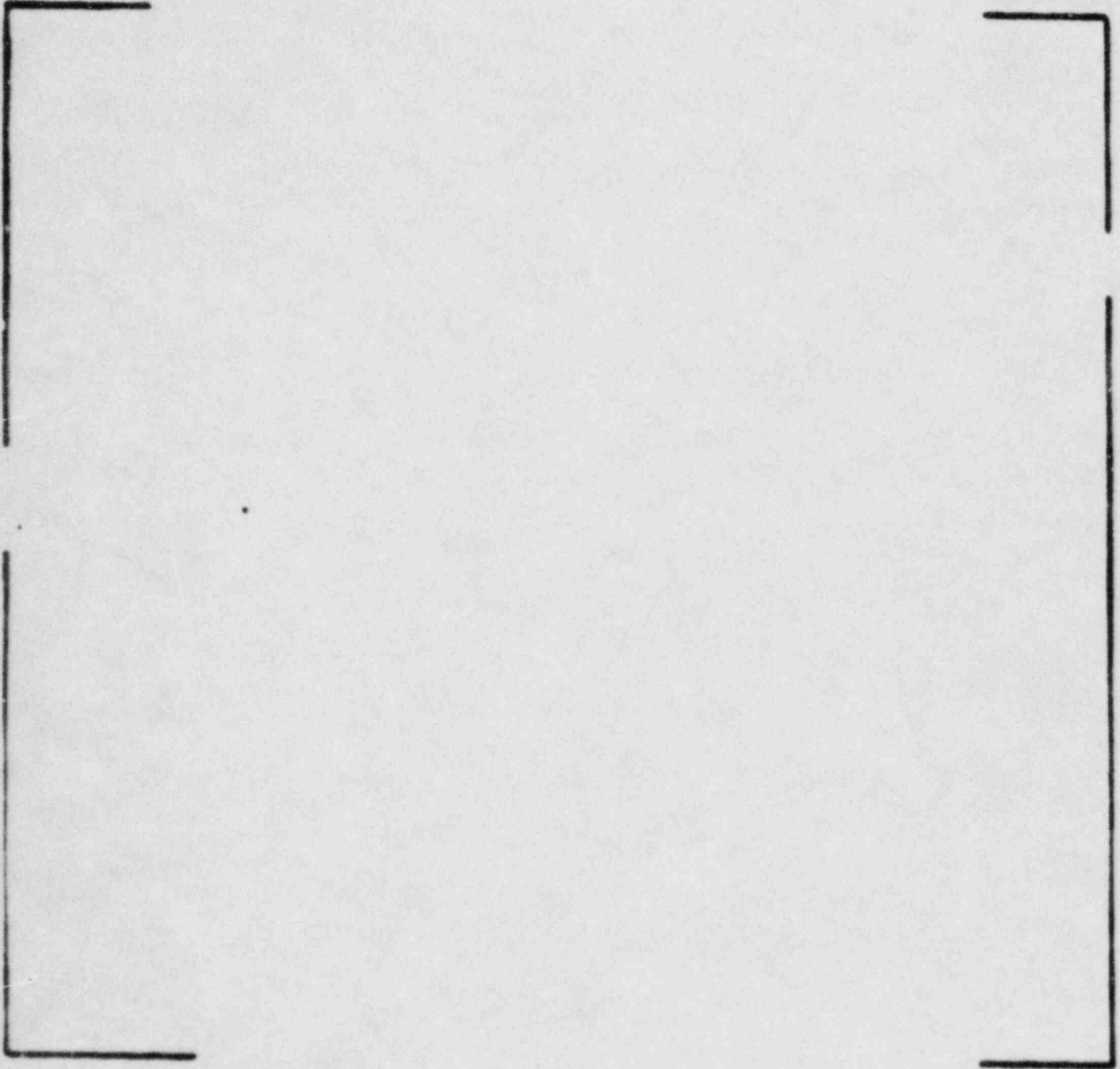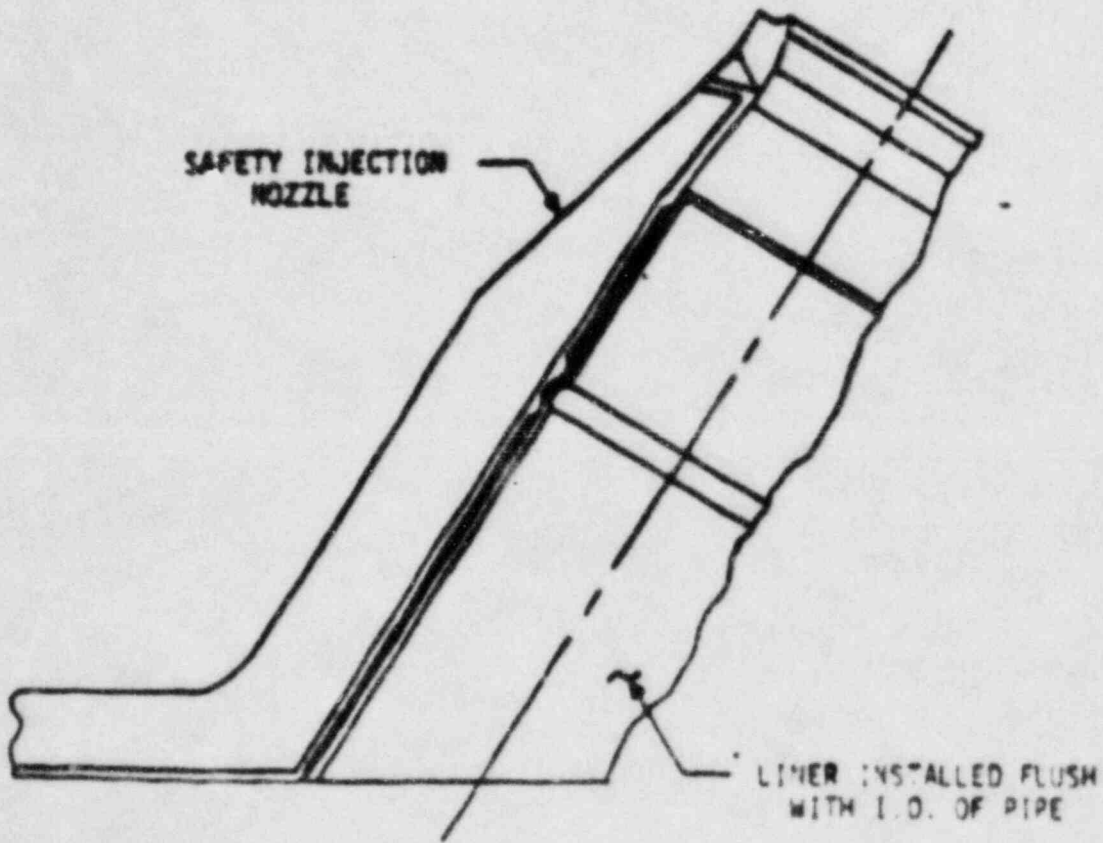
FIGURE 13

SAFETY INJECTION NOZZLE

SIGNIFICANT RESULTS

Critical Locations

Results are presented at the locations shown below:
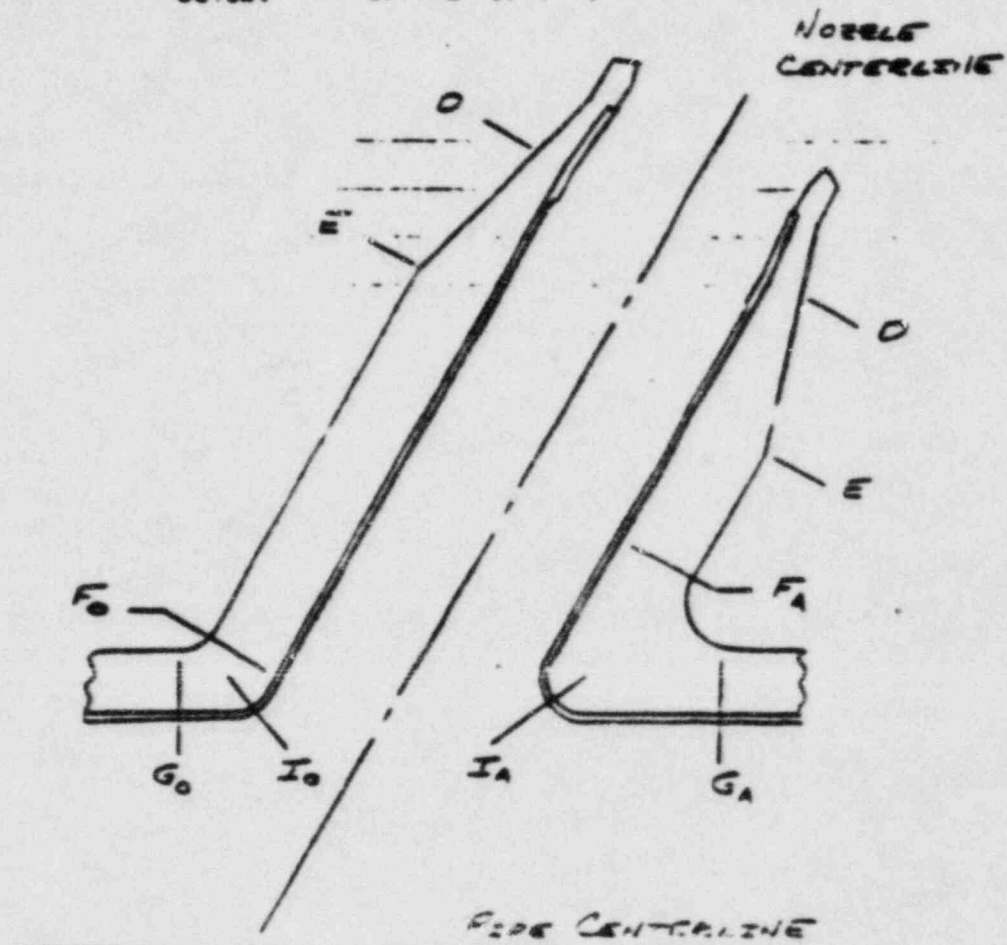
In the following tables, "INSIDE" and "OUTSIDE" refer to the inside and outside surfaces of the base metal and "CLAD" refers to the inside or wetted surface of the clad.

FIGURE 14

SAFETY INJECTION NOZZLES
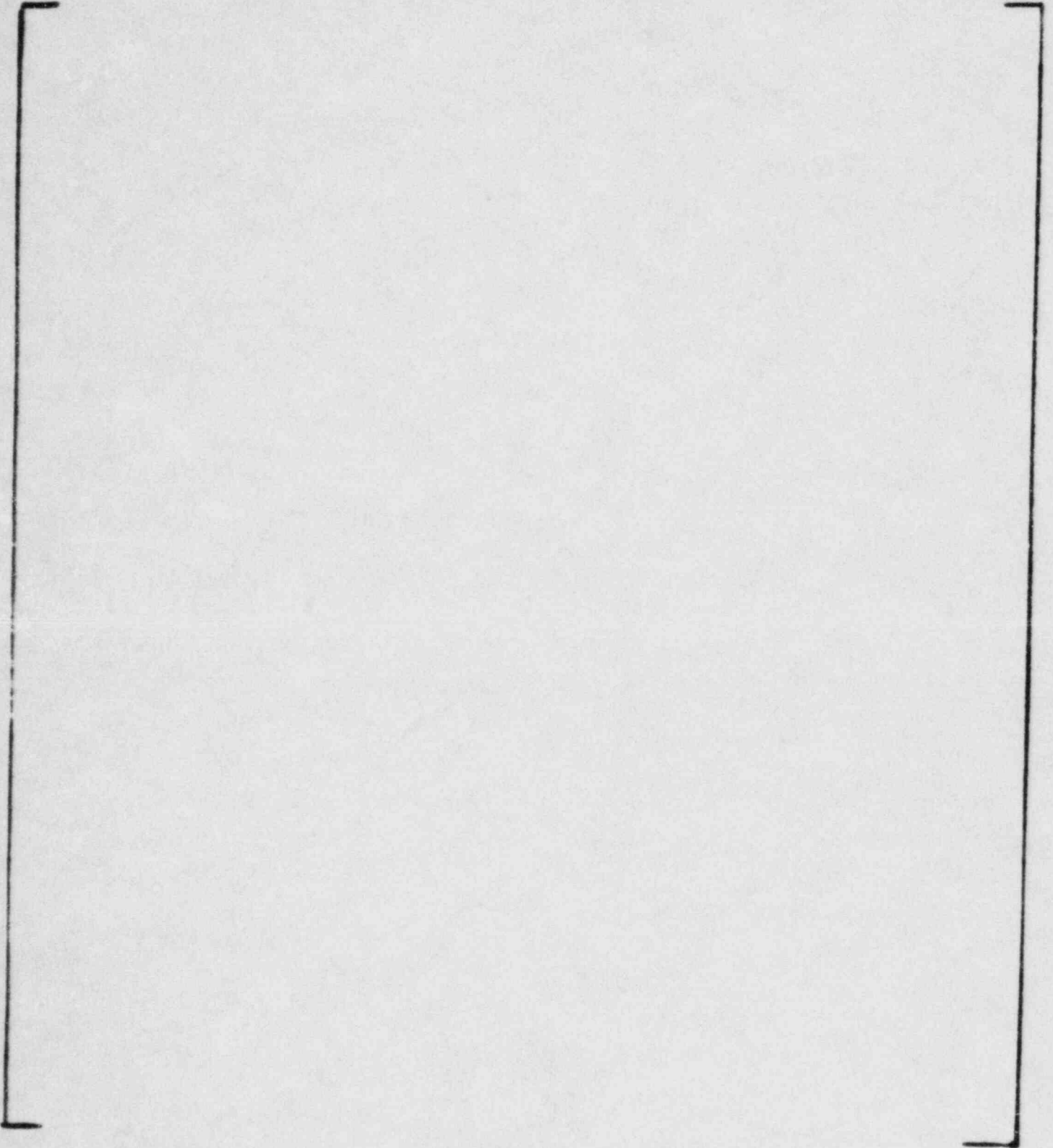
FIGURE 15

SAFETY INJECTION NOZZLE
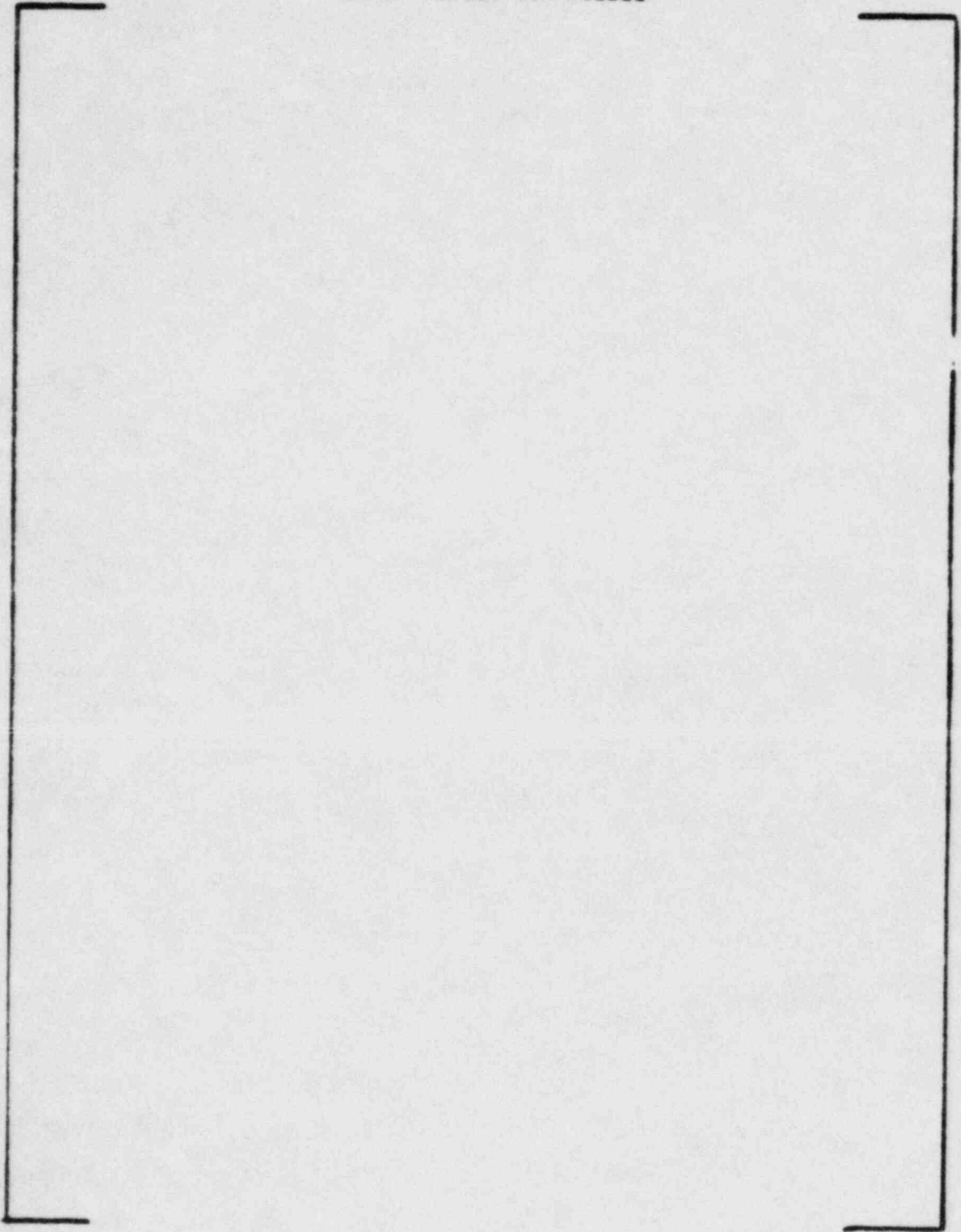
FIGURE 16
1A THERMAL LINER

CENTERING PAD CRACKS
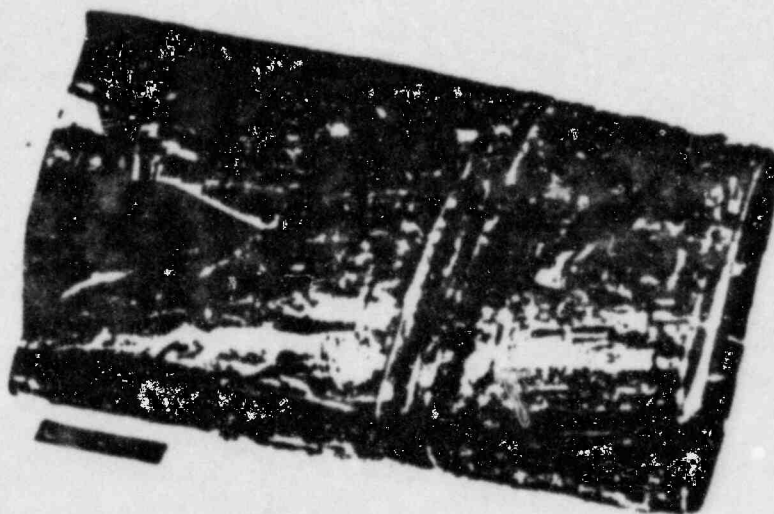
LARGE TEAR

FIGURE 17

SAFETY INJECTION NOZZLE
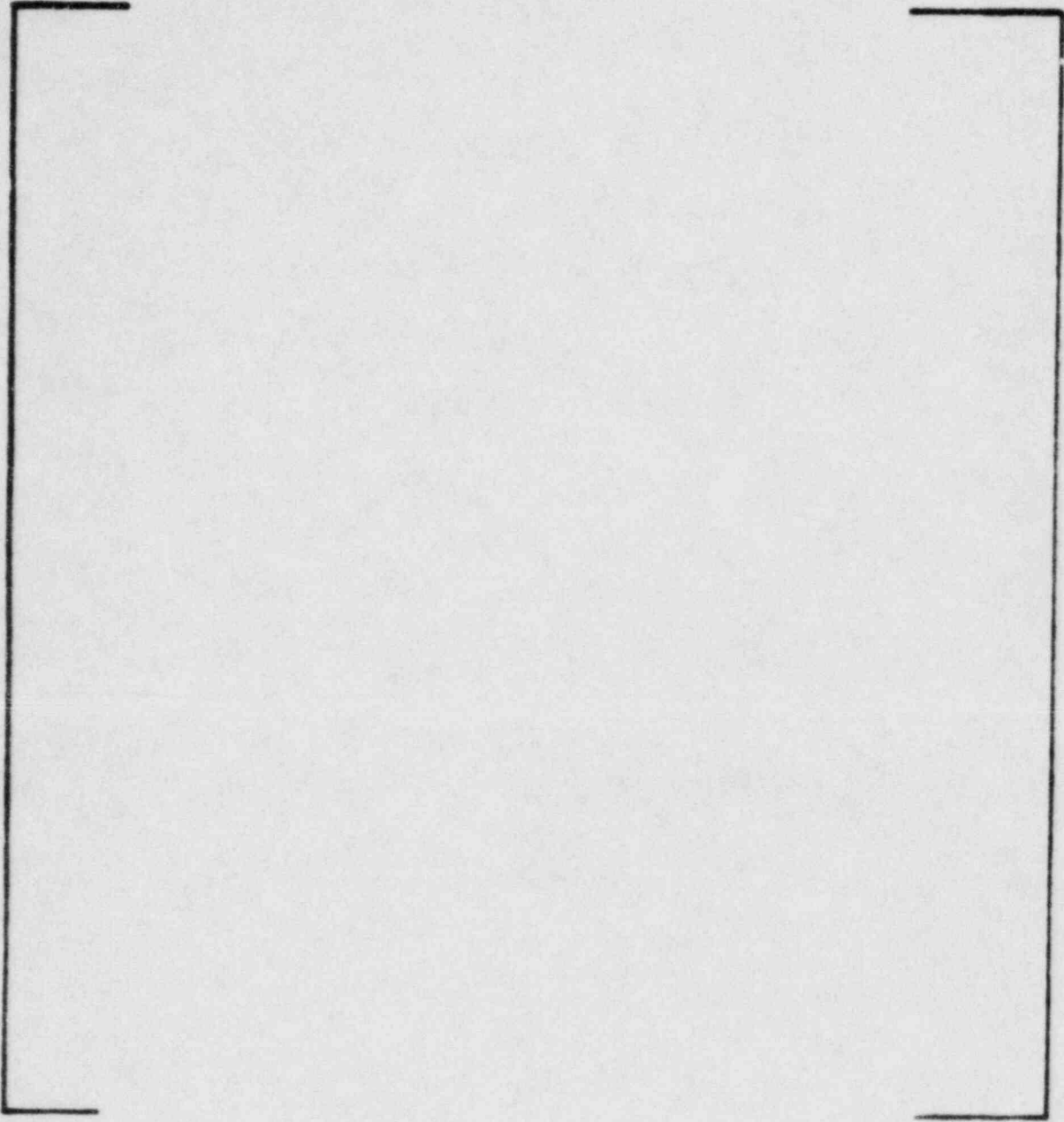
REPORT ON
PALO VERDE UNIT 1
RESISTANCE TEMPERATURE DETECTOR
THERMOWELL

Prepared by: COMBUSTION ENGINEERING, INC.
WINDSOR, CONNECTICUT

LEGAL NOTICE

TABLE OF CONTENTS

Section	Title	Page No.

TABLE OF CONTENTS (Cont'd)

LIST OF TABLES

LIST OF FIGURES

LIST OF FIGURES (Cont'd)

LIST OF FIGURES (Cont'd)

1.0   INTRODUCTION

1.1   DESCRIPTION OF THERMOWELL DAMAGE AND DISCOVERY AT SITE

Pre-Core Hot Functional Testing (PCHFT) of C-E's first System 80 Nuclear Steam Supply System (Arizona Nuclear Power Project (ANPP) Palo Verde Nuclear Generating Station (PVNGS), Unit 1) was initiated in early May 1983. The first indication of Resistance Temperature Detector (RTD) and related equipment problems developed at the site when the first of five RTD's failed in the electrically open position on May 31, 1983. The RTD/thermowell installation of the original design is shown on Figure 1.1-1. Hot functional testing (HFT) was about three quarters complete on June 17 when a leak was detected in the thermowell corresponding to the first RTD that failed electrically. Several days later, June 21, a leak developed in the thermowell associated with the second RTD that failed. Arizona Public Service Company and Combustion Engineering site personnel analyzed the pattern that had been established with the failure of the RTD's and thermowells and proceeded to plug the associated thermowell for each of the failed RTD's.

When the loop 2A reactor coolant (RC) pump was disassembled for its planned inspection following hot functional testing (HFT) an attempt was made to visually inspect the cold leg thermowells in loop 2A through the reactor coolant pump casing with the pump diffuser in place. No thermowell failure was detected. Further testing of ANPP Unit-1 (PVNGS) was performed. Structural vibration data for the thermowells was obtained during this time by placing an accelerometer in one of the thermowells. Inspection of the thermowells from the inside of the RC piping during the week of July 18, 1983 showed damage to several cold leg thermowells. Some cold leg thermowells were broken flush with the inside of the RC pipe; one was bent but intact; and one was broken both at the intersection between the large section at the top of the thermowell and at the lower end adjacent to the inside wall of the pipe. Another thermowell was

broken at the top and had fallen into the flow stream of the RC pipe cold leg. Other thermowells showed no visible damage. A total of 5 of the cold leg thermowells were found to have failed. Initial inspection of the hot leg thermowells did not show any visible damage, except about half of them were slightly bent in the direction of the reactor vessel (against the flow).

RTD/TW INSTALLATION ORIGINAL DESIGN

FIGURE 1.1 - 1

RTD ENCLOSURE HEAD

RTD CABLE CONNECTION

NIPPLE

THERMOWELL

PIPE NOZZLE

RTD SENSING ELEMENT

HOT LEG PIPE WALL

COLD LEG PIPE WALL

LOCATION OF FAILURES

.001 - .006" DIAMETRAL CLEARANCE

2.13"

2½"

.375"

1-3

1.2   DISCUSSION OF SAFETY IMPLICATIONS
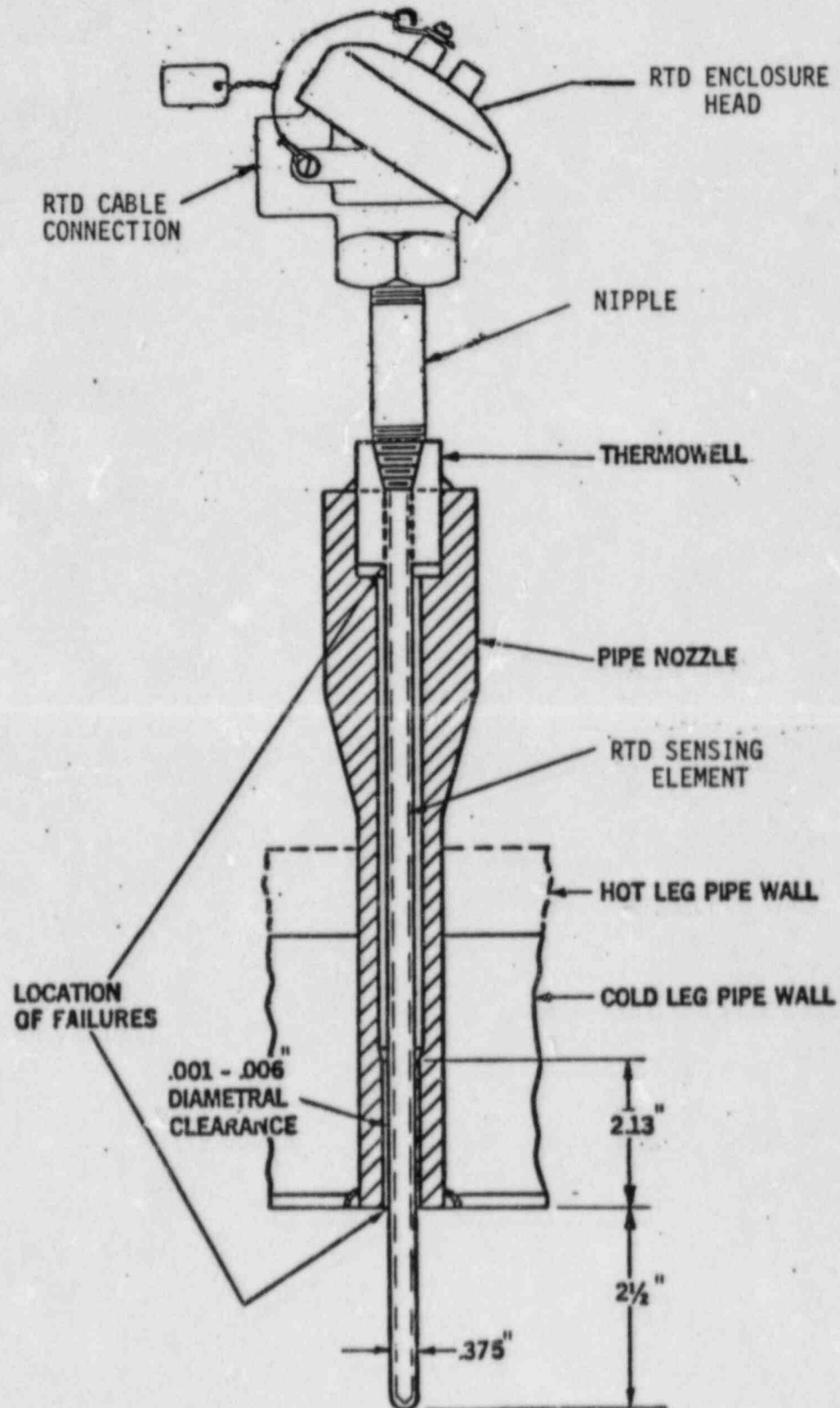
Failure of one or a few thermowells would not jeopardize the safe operation of the plant. Thermowell failure causes a leakage of primary coolant through the thermowell and around the RTD. RCS leakage can be controlled, via make-up from the charging pumps, even though several thermowells were to fail simultaneously.

The broken pieces of thermowell probably entered the cold leg flow stream and most likely settled at the reactor vessel flow skirt or in the bottom of the reactor vessel. Because of its small size and weight, flow velocities necessary to propel a broken piece of thermowell through flow holes at the ccre inlet are generally available. It is theoretically possible for the System 80 thermowell, which has a .375 outside diameter, to flow through the Lower End Fitting (LEF) of the fuel assembly.

If this were to happen, no measurable impact on heat transfer (fuel cooling) is expected due to blockage of one flow channel.

The broken tip of the thermowell most likely would be captured by the flow in an attitude where the longer dimensions of the fragments would be transverse to the flow direction. In this orientation it could become lodged against the LEF and cause partial flow blockage of up to five of the   diameter flow holes. Under this condition no impact on heat transfer of the fuel would occur.

2.0   SUMMARY

2.1   GENERAL DESCRIPTION AND RESULTS OF INSPECTION, TESTING, AND ANALYSIS OF THE ORIGINAL DESIGN

Both visual and metallurgical examinations were performed on the thermowells. The visual examination included wear measurements. Wear measurements show that the most significant wear was experienced in the cold legs, which can have higher than normal, four pump operation, flow. The high flow conditions were experienced in various cold legs during Hot Functional Testing; when only one of the two reactor coolant pumps inducing flow in a particular steam generator was operated, and the other pump was secured. The majority of the thermowells that failed (3 out of 5) were located in the particular cold leg that had the highest number of hours in this high flow mode of operation. The detailed results of wear and damage are presented in the tables of Section 4.1.

The wear measurement and damage correlation also showed that thermowells at a particular location in the reactor coolant pipe cold legs were the most susceptible to both wear and damage. On each cold leg, three thermowells are installed approximately 30 inches from the pump. They are oriented at 10, 12 and 2 O'clock when viewed from the pump in the direction of flow. The 10 O'clock position thermowells received the worst damage in 3 out of 4 loops. This position is the one almost in a direct line with the flow axis of the reactor coolant pump diffuser vanes. Flow measurements were taken during the CE-KSB pump performance testing to determine if there are significant flow variations at this particular thermowell radial location. This data is in the process of being evaluated.

A metallurgical examination was performed on the five failed RTD thermowells. The results indicated that the chemical and mechanical properties and the microstructure were within the normal limits. There were no indications of pre-existing flaws on the fracture surfaces. The fracture surfaces exhibited relatively large areas of

fatigue cracks. The cracks indicate high cycle (low stress) fatigue as the failure mechanism. Possible crack initiation points were identified on the outside of the thermowell tubular sections at approximately 90 degrees to the flow direction. Portions of the fracture surface were smeared due to relative motion of the two surfaces.

A visual examination of the wear surfaces on the downstream side of the thermowells classified the wear as adhesive wear. This wear is typical of that produced by oscillatory motion of loaded contact surfaces.

Based on the metallurgical results it is concluded that the most likely excitation mechanism to cause this type of failure would be vortex shedding. The higher than normal operating flow rates also appear to have aggravated the situation.

To determine if vortex shedding mechanism is responsible for thermowell damage, tests have been run at a flow loop test facility (TF-2) at CE-Windsor. The results of these test are being evaluated and other failure mechanisms are being considered. It does appear that vortex shedding is the most significant cause of thermowell excitation.

Calculations have shown, that for normal operating flow rates, the vortex shedding frequencies for the cold legs would be approximately   cps. When compared to a predicted natural frequency of   cps there appears to be adequate separation between the flow excitation frequency and the predicted natural frequency. For the higher flow conditions, that existed during some portion of the hot functional testing (HFT), the vortex shedding frequency can be analytically shown to be as high as   cps and thus could have stimulated the thermowell at its natural frequency.

2.2   GENERAL DESCRIPTION OF THERMOWELL AND NOZZLE REDESIGN

As a result of the damage and the postulated failure mechanism, C-E undertook a program to redesign the thermowell in order to increase its strength and stiffness and raise the natural frequency.

The redesigned thermowell is shown on Figure 2.2-1. The assembly of the thermowell into the nozzle is shown on Figure 2.2-2. The outside surface of the thermowell has two tapered transition sections and a conical tip. The first tapered section forms a transition between the tip diameter (.375 inch - the original system 80 thermowell O.D.) and a increased cross section (.5 inch OD) which resists the maximum bending moment from flow induced loads. This tapered section also serves to break down the formation of vortices. The second tapered section serves as a support to wedge the thermowell into the mating tapered section of the nozzle ID. Above this tapered section the thermowell has a 0.7 inch diameter. The increased thermowell shank diameter from .375 inch to .7 inch in addition to the .125 inch fillet at the top increases the stiffness of the thermowell and reduces the local stresses. The 1 1/2 inch male thread on the thermowell and mating female thread on the nozzle provide a means of pre-loading the thermowell into the nozzle. The pre-load force ensures the thermowell is permanently supported by the nozzle via the support taper on the thermowell and nozzle. A fillet weld shown on the assembly sketch, Figure 2.2-2, between the thermowell and the top of the nozzle provides the pressure boundary. Pressure loads on the thermowell are taken up in the 1 1/2 inch threads and are not transmitted to the seal weld.

The redesigned thermowell also reduces the inserted length in the flow stream. The original thermowell had an inserted length of 2 1/2 inches, which was reduced to 2 1/8 inches for the revised design.

ANPP-1 THERMOWELL

FIGURE 2.2 - 1

MODIFIED THERMOWELL & PIPE NOZZLE

FIGURE 2.2 - 2

RTD LOCATION

FILLET WELD

THREADED
TO FACILITATE
PRELOAD
ON TAPER

0.700"

CHROME PLATED
OVER THIS LENGTH

PIPE WALL

2.0"

.500" DIA.

2.125"

0.375"
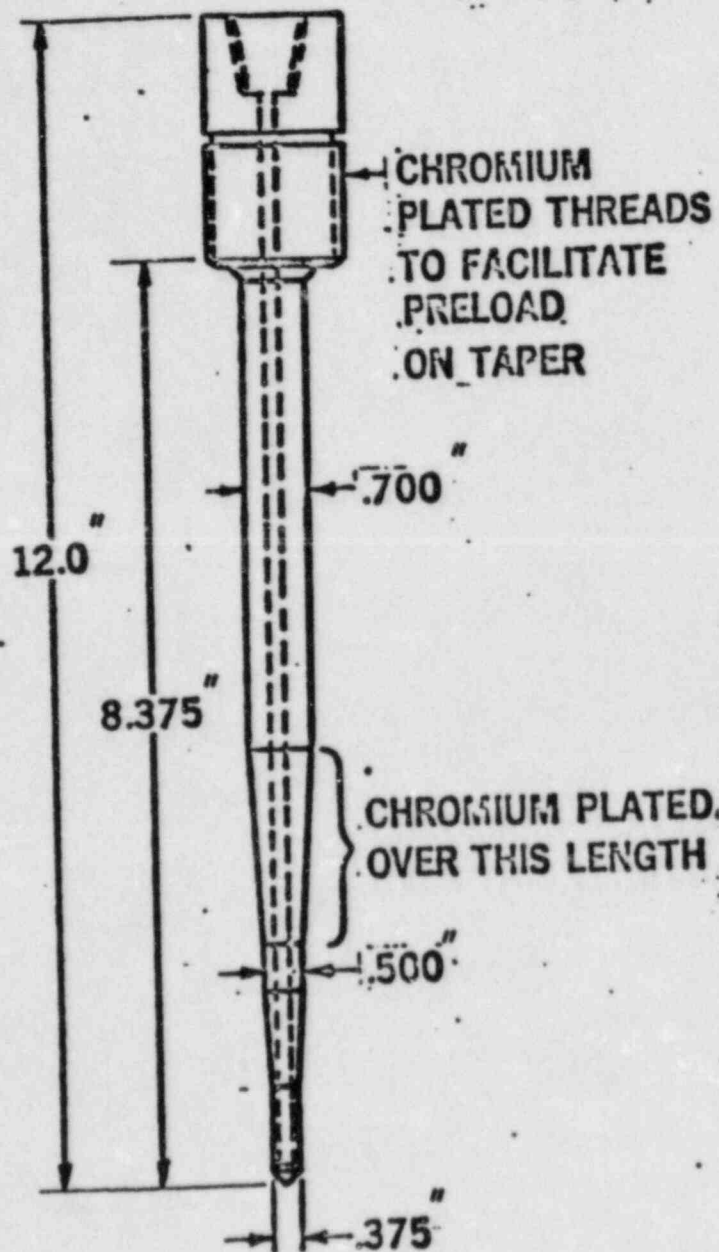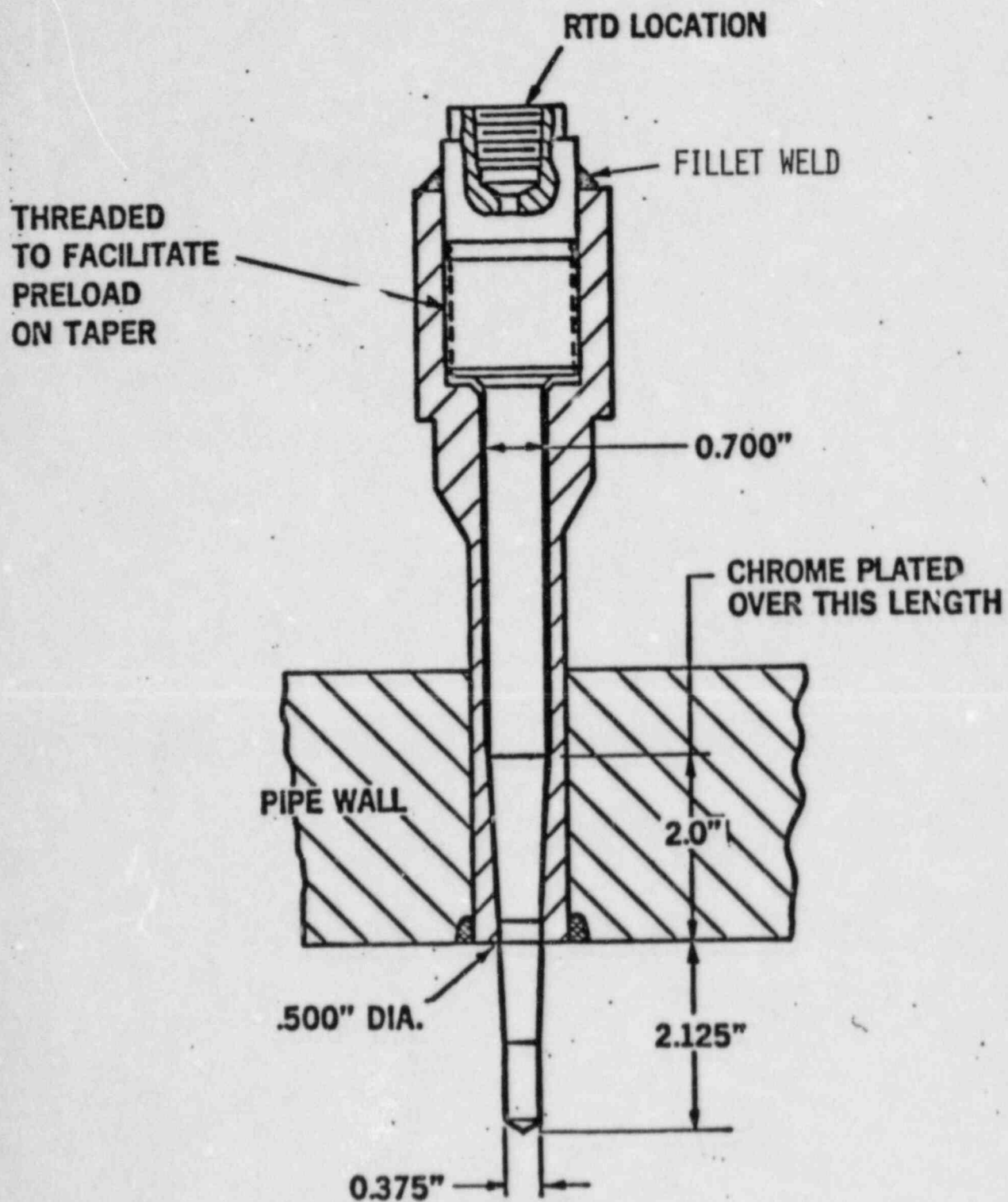
2.3 GENERAL DESCRIPTION OF ANALYTICAL AND TEST RESULTS WHICH JUSTIFY THE DESIGN MODIFICATIONS

The redesign of the thermowell, as described in the previous section, is based on maintaining the original interfaces, design parameters and thermal response times for the RTD instrument. In addition to this, it was desired to provide as much margin as possible to flow induced excitation. Four major design objectives were established:

1) Increase the natural frequency of the thermowell to keep it from being close to potential vortex shedding frequencies.

2) Eliminate the clearance at the support area between thermowell and the nozzle and thus eliminate any relative motion that could cause wear.

3) Because the failure mode was high cycle fatigue, a significant reduction in possible stress level was desired to eliminate the possibility of high cycle fatigue.

4) Provide a flow profile that would minimize the capability of large vortex induced loading.

A structural analysis was performed for pressure, thermal, seismic and mechanical loadings for both the original and the redesigned thermowell. Both were found to be acceptable to the requirements of ASME Boiler and Pressure Vessel Code Section III for Class 1 components. Flow tests were conducted in C-E's hot flow test facility (TF-2) and in the reactor coolant pump test loop in Newington to verify mechanical load input assumptions to the structural analysis. All of this test data has not yet been analyzed. However, preliminary results show that the redesigned thermowell is not responding to vortex shedding frequencies well above those experienced during the Palo Verde start-up test.

Therefore the thermowell natural frequency is well above the maximum potential vortex shedding frequency. Due to the slight taper on the thermowell tip, vortices will be shed in a range of frequencies. This is due to the fact that the vortex frequency is directly related to the local diameter of the flow path obstruction. If the vortex shedding takes place at a range of frequencies, it will reduce the total energy at each discreet frequency and thus reduce the load that can be imposed along the thermowell span.

Because the original design was damaged by a high cycle fatigue mechanism, a stress reduction as significant as this would eliminate any concern of high cycle fatigue that could be caused by vortex shedding or any other high cycle phenomenon.

The redesigned thermowell was installed in the CE-KSB reactor coolant pump test loop at C-E Facility at Newington, New Hampshire. It was installed near the reactor coolant pump outlet, similar to its arrangement in the reactor coolant system at Palo Verde. The thermowell was tested at various pump flow rates while the reactor coolant pump modifications were being qualification tested. This amounted to 180 hours of operation. Acceleration data was recorded during this testing. This data will be used to demonstrate that the design calculation assumptions were adequately conservative.

Upon completion of the extensive testing program at both TF-2 and
Newington, the redesigned thermowells used in both tests were given
a complete visual inspection. No signs of wear or damage were
observed.

3.0 INSPECTIONS AND EXAMINATIONS (Original Design)

3.1 DESCRIPTION AND RESULTS OF SITE INSPECTIONS

Figure 3.1-1 is a schematic showing the location of the thermowells in the Reactor Coolant System (RCS). Table 3.1-1 summarizes the results of the site inspection of the cold leg thermowells. Note that a total of 5 thermowells were broken, all in the cold legs. Also, one thermowell was bent approximately 45° with the flow in Cold Leg No. 2A and 8 thermowells were slightly bent. The thermowell that was not initially removed, 122CB, did not appear to have been damaged from observation inside the RCS piping. Two broken pieces of thermowells were subsequently retrieved from the reactor vessel and returned to C-E for examination.

Figure 3.1-2 shows the removed thermowells arranged to illustrate their respective locations within the RCS. As can be seen, all three thermowells (112CC, 111Y and 112CA) in Cold Leg 1A fractured at the lower end, at the reactor coolant piping surface. One thermowell (112CD) in Cold Leg 1B was fractured at the upper end near the head. One thermowell (122CA) in Cold Leg 2A was fractured at both ends. A second thermowell (125CC) in Cold Leg 2A was bent approximately 45° with the flow and had "chatter marks" on the upstream side of the bent section. This indicates that impact by a large piece of debris, most likely a piece of reactor coolant pump impeller, had bent the thermowell. All remaining thermowells were intact.

Liquid penetrant examination of Thermowells No. 112CC, 111Y and 112CA, performed at the site, showed no indications of cracks at the upper end at the junction with the head.

All the hot leg thermowells were inspected at the site. Examination results are also given in Table 3.1-1. All hot leg thermowells were intact. Some were slightly bent (1/16" - 9/32") against the flow (towards the reactor vessel).

Table 3.1-2 lists measured diameters adjacent to and at three axial locations in the wear area of examined thermowells. The amount of wall thinning was determined from the difference in diameter between a given location and an unaffected adjacent area.

As can be seen, severe wall thinning occurred on thermowells located at the 10 o'clock position in the RC pipe as viewed from the reactor coolant pump (i.e., in excess of 80% wall reduction). Moderate amounts (20%) occurred on thermowells located at the 12 o'clock position. Only slight wear occurred at the 2 o'clock position. It is important to note that the 10 o'clock position experiences the most severe flow conditions because it is approximately on a tangent line to the reactor coolant pump diffuser vanes which deflect the pump discharge directly at this thermowell. The geometry and pump cross section is provided in Figure 3.1-3. It should also be noted that the two thermowells with failures at the upper head junction were the two 10 o'clock thermowells and had the greatest amount of wear.

Examination of the wear surface indicates that the amount of wear damage is greatest on the thermowell circumference on the downstream and tapers off to no damage at 90° to the direction of flow. Also, the wear pattern indicates relative motion between the thermowell and the RTD nozzle in a direction transverse to the flow direction. There is no indication of impact damage on the downstream side indicating this damage was not caused by motion of the thermowell in the direction of the flow stream (as opposed to wear resulting from motion in the transverse flow direction).

Table 3.1-3 gives the results of wear measurements on the hot leg thermowells. The worst case thermowell, No. 121HD, experienced a wall reduction of .002" or 3.2% using an .0625" nominal wall thickness.

Site inspection showed that corresponding wear also occurred on the RTD nozzle. Some RTD nozzle inside diameters (ID)s were found to appear to be elongated in the flow direction. This could be wall thinning due to wear. Also, some of the nozzle edges were rounded and some were square (could be manufacturing or installation related).

At location 122CA (10 o'clock in 2A), a depression or gouge was found in the nozzle end on the piping both upstream and downstream of the thermowell. The maximum dimensions of these gouges was 5/32" long x .050" deep. Table 3.1-4 gives the results of wear measurements taken on the ANPP Unit-1 cold leg thermowell nozzles.
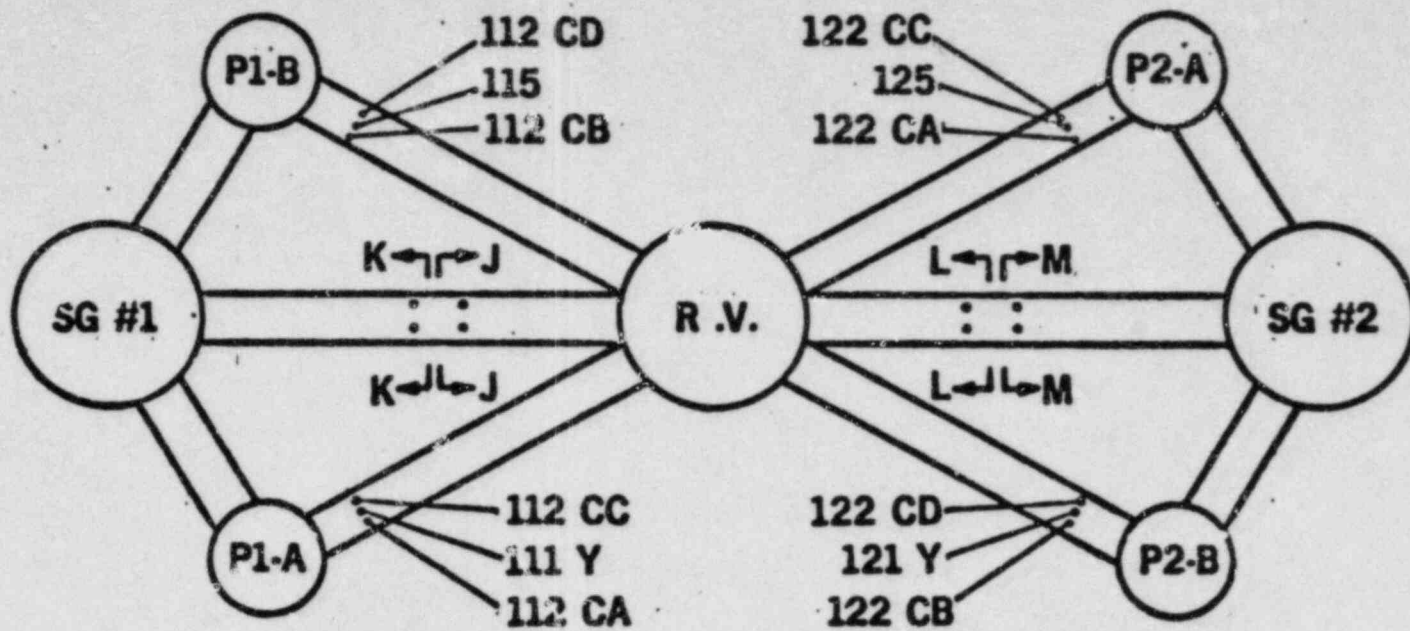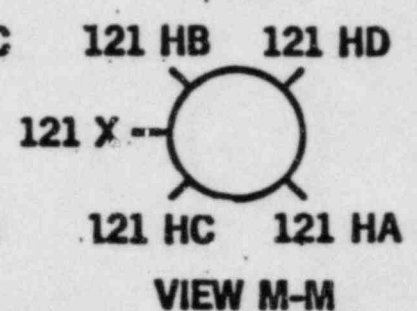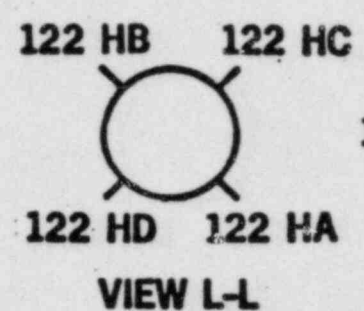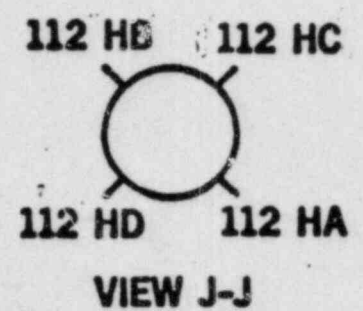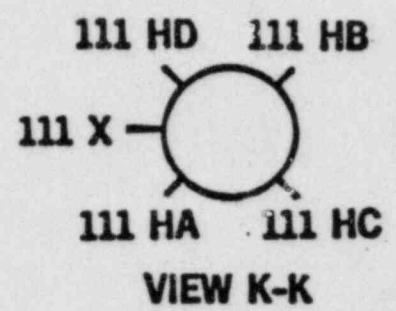
**LOCATION OF THERMOWELLS
REACTOR COOLANT SYSTEM
ANPP-1**

FIGURE 3.1-1
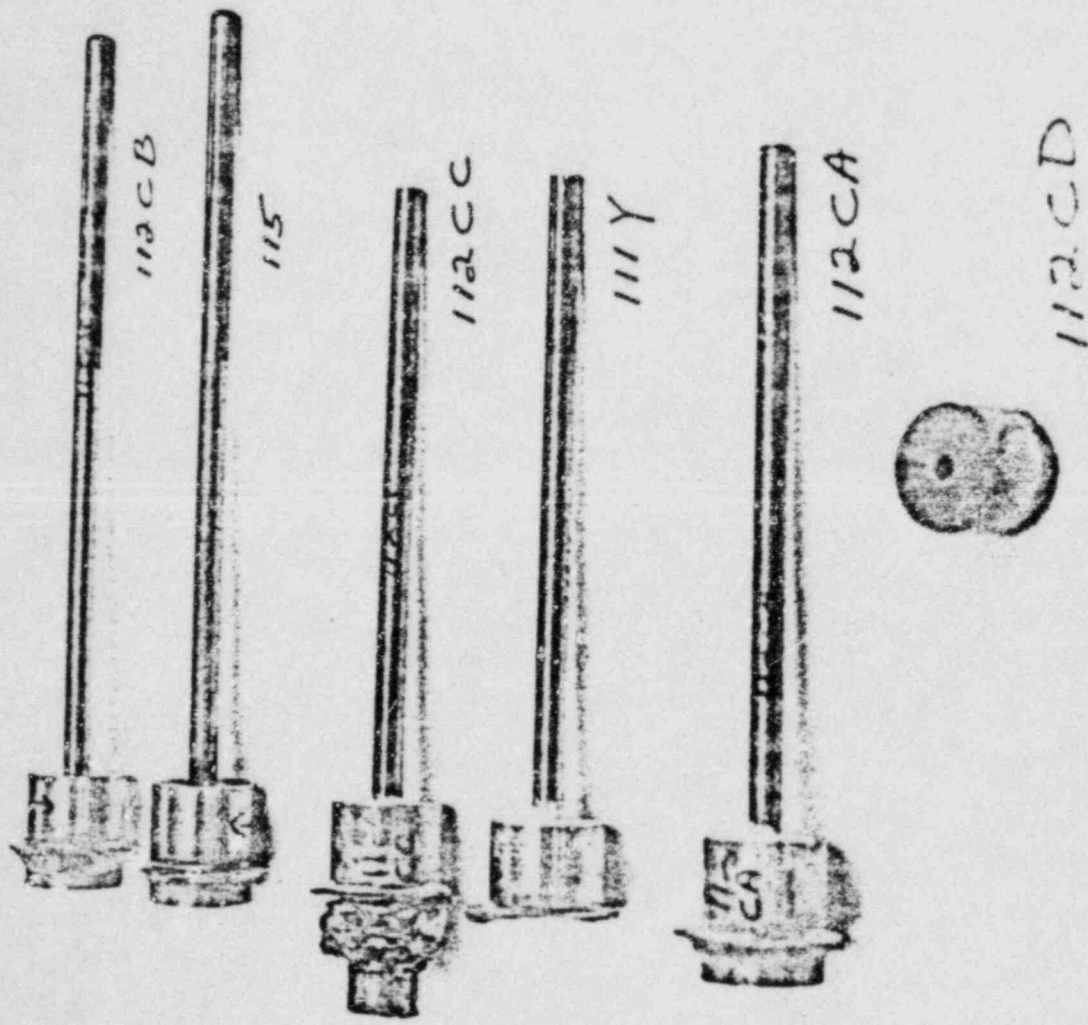
Figure 3.2-1
Overall View of Several of
the Removed Thermowells
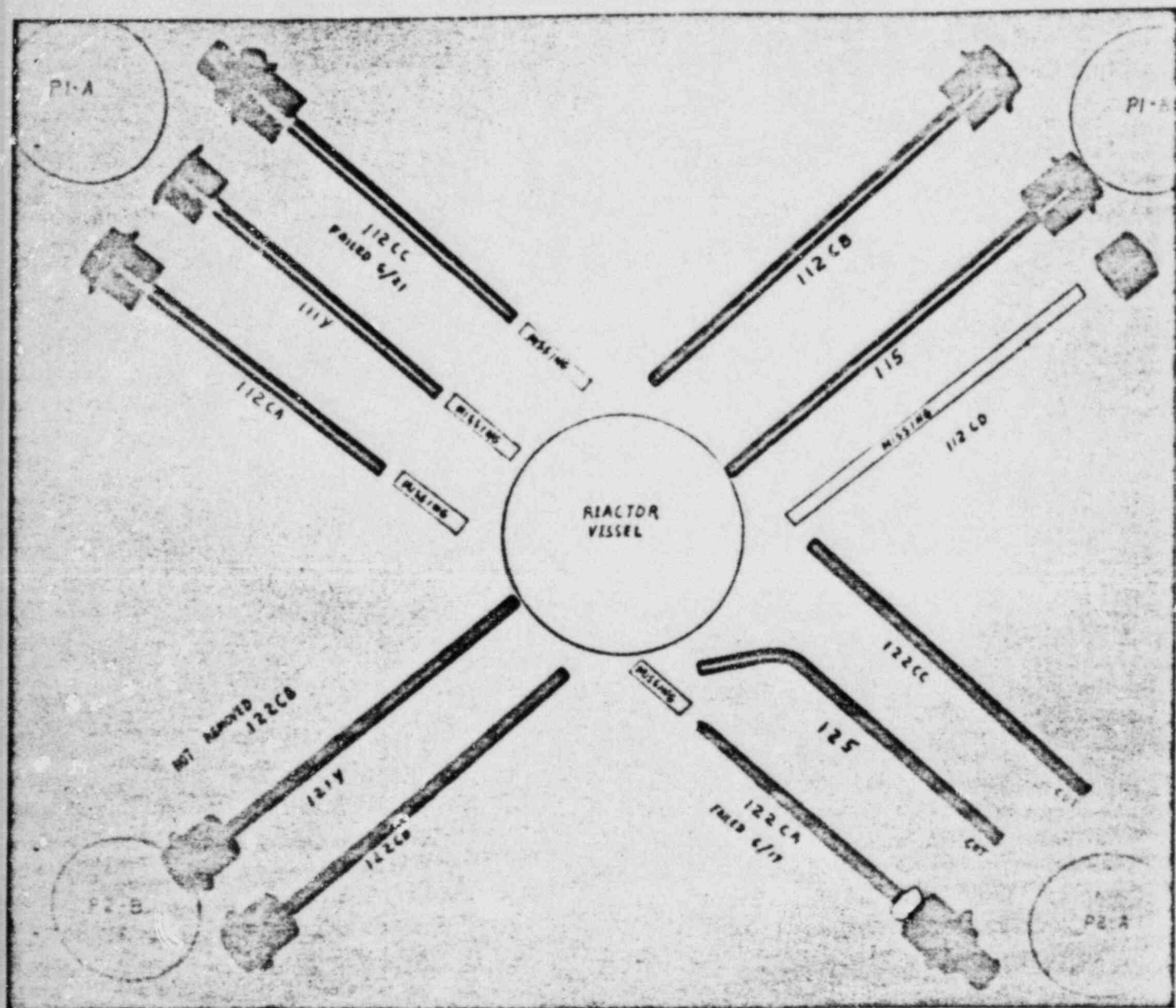
Figure 3.1-2

Arrangement of Removed
Thermowells Showing Location
Within Reactor Coolant System

10 O'CLOCK POSITION
THERMOWELL

VIEW A - A

THERMOWELL

IMPELLER
DIFFUSER
SUCTION PIPE
CASING
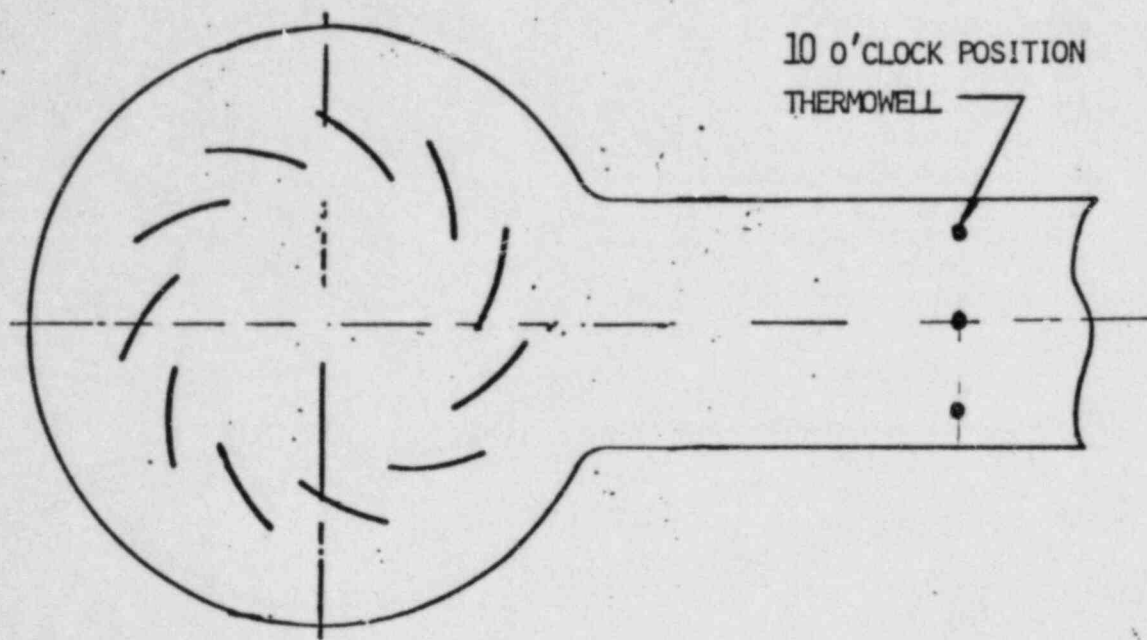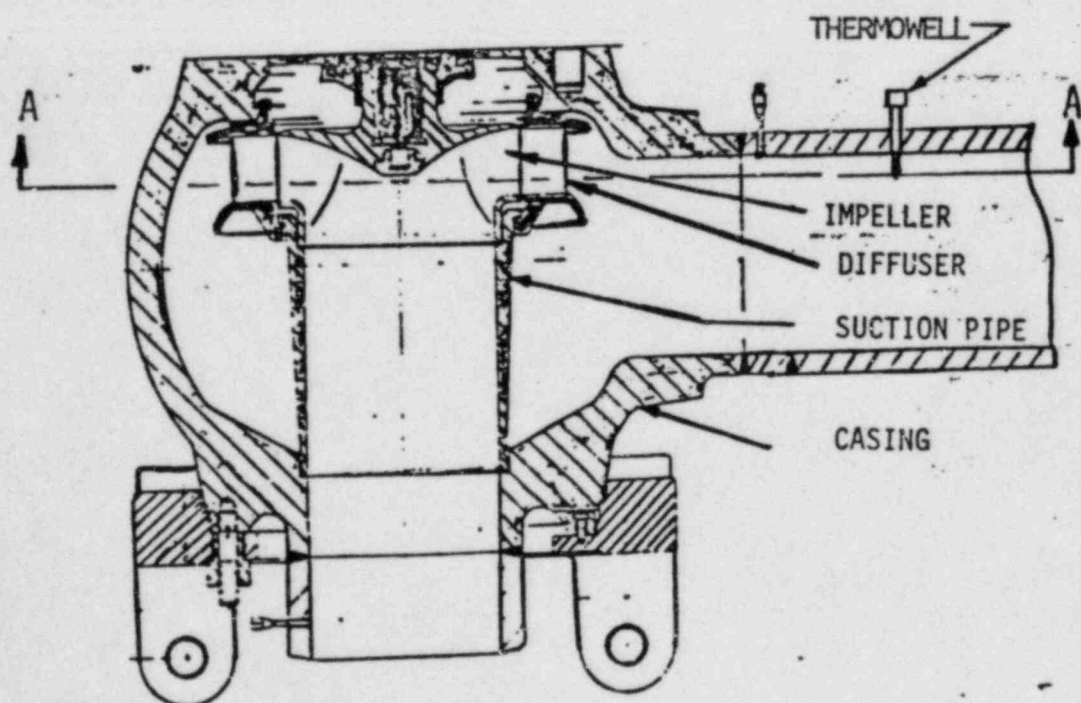
REACTOR COOLANT PUMP ASSEMBLY
(LOWER SECTION)

FIGURE 3.1 - 3

62403
Figure   3.2-3
Close-up View of
Wear Area on
Thermowell No.115

115

1 Brown & Sharpe 2   U.S.A   3   TEMPERED   4 No 899-323-605 5
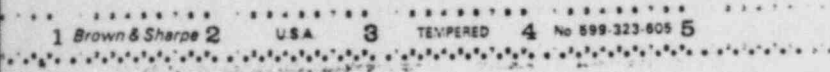
Figure   3.2-4   62415
Higher Magnification
of Wear Transition
Area of Figure   3.2-3
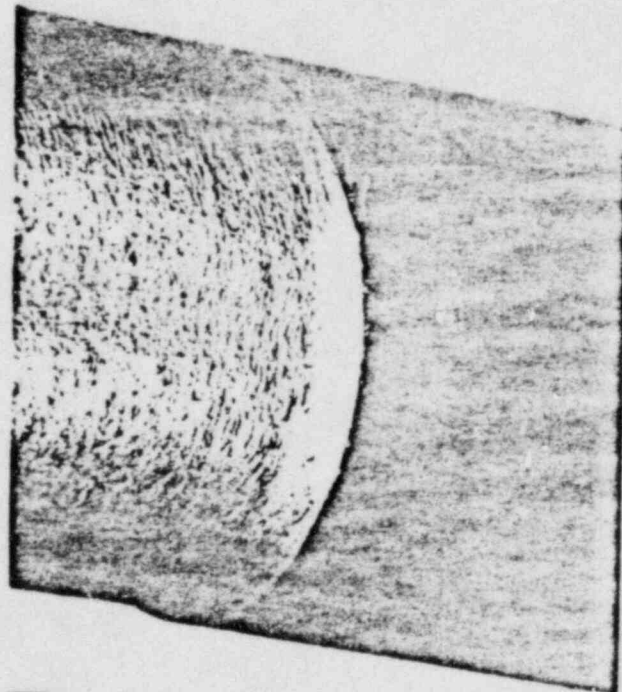
62705
Figure 3.2-5
Wear Area on
Thermowell No.112CD
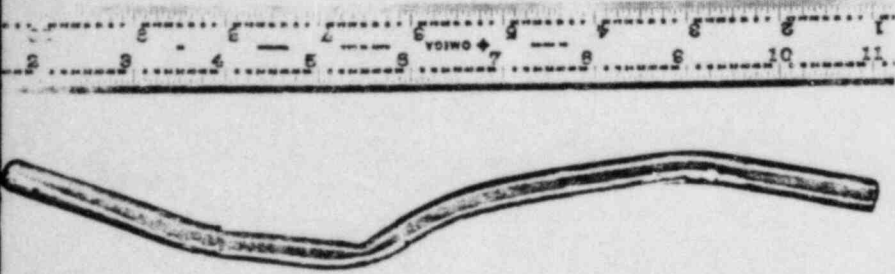
Figure 3.2-6   62706
Higher Magnification
of Wear Transition
Area of Figure 3.2-5
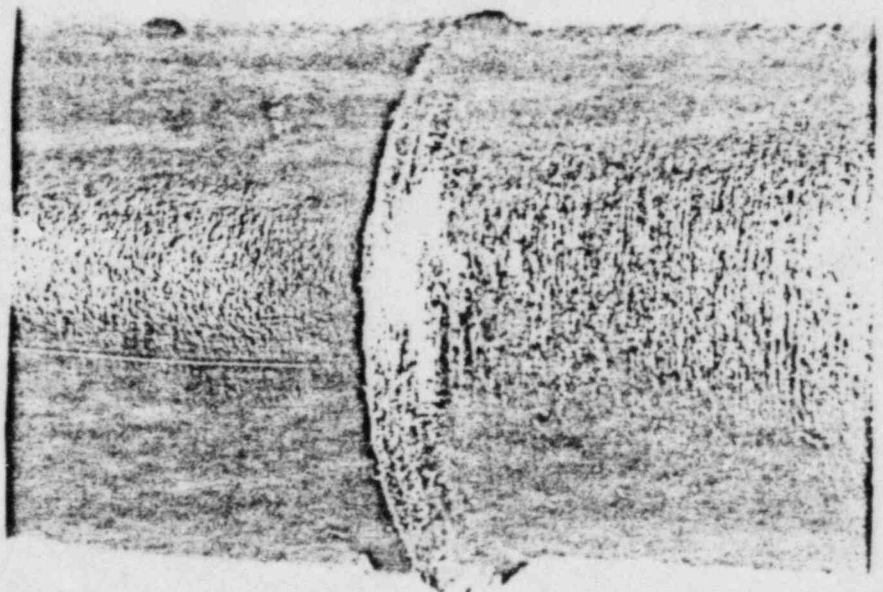
62404
Figure   3.2-7
Close-up View of
Wear Area on
Thermowell No.122CD

1 Brown & Sharpe 2   .84   3   TEMPERED   4   NO 899 923 603 5

Figure   3.2-8   62412
Higher Magnification
of Wear Transition
Area of Figure   3.2-7

42
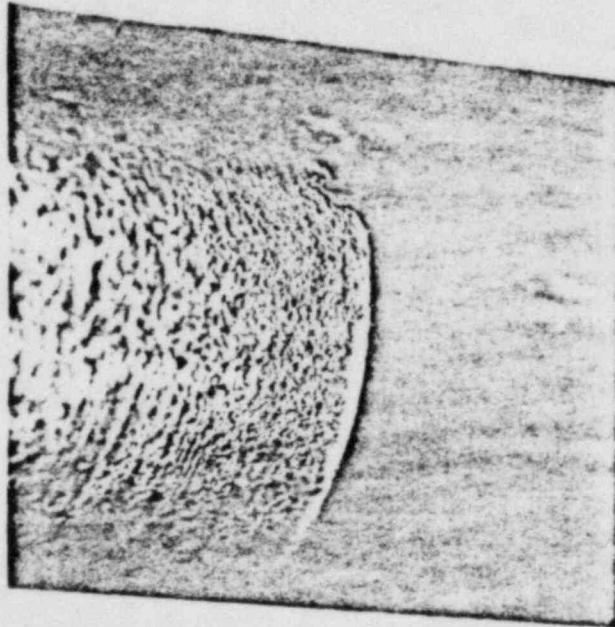
Figure 3.2-9 62406
Close-up of Wear and
Fractured Surfaces of
Thermowell No. 112CA.
The wear area is as
indicated; the fractured
end is on the right
hand side.
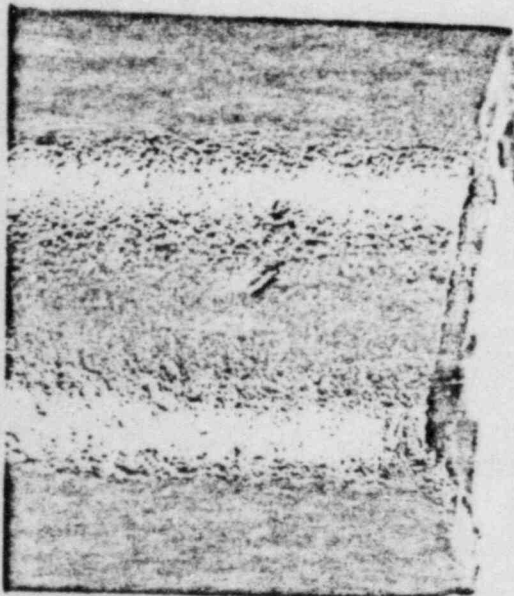
62413
Figure 3.2-10
Higher Magnification
of Fractured End in
Figure 3.2-9

Figure 3.2-11 62405
Close-up of Wear and
Fractured Surfaces of
Thermowell No. 111Y.
The wear area is as
indicated; the fractured
end is on the right
hand side.
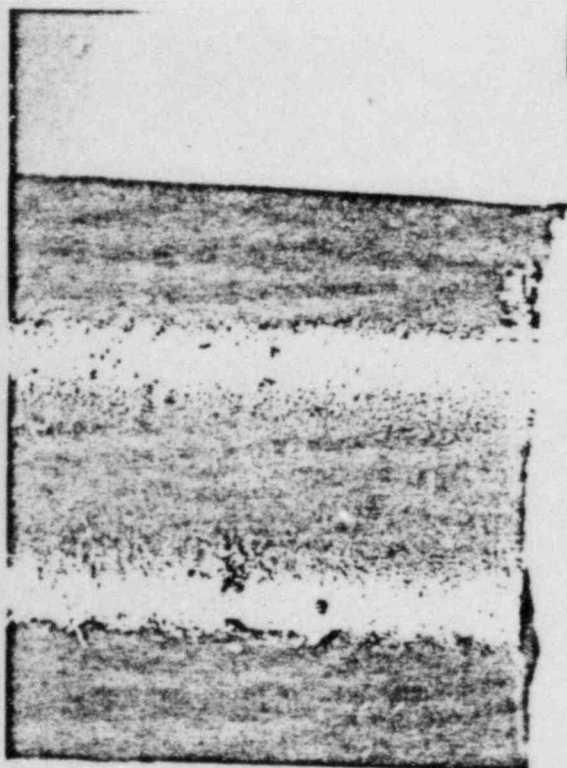
62414
Figure 3.2-12
Higher Magnification
of Fractured End in
Figure 3.2-11

_122CA_

62408
Figure   3.2-13
Close-up of
Failed End of
Thermowell No.122CA

Figure   3.2-14   62411
Higher Magnification
of Failed End Shown
in Figure   3.2-13
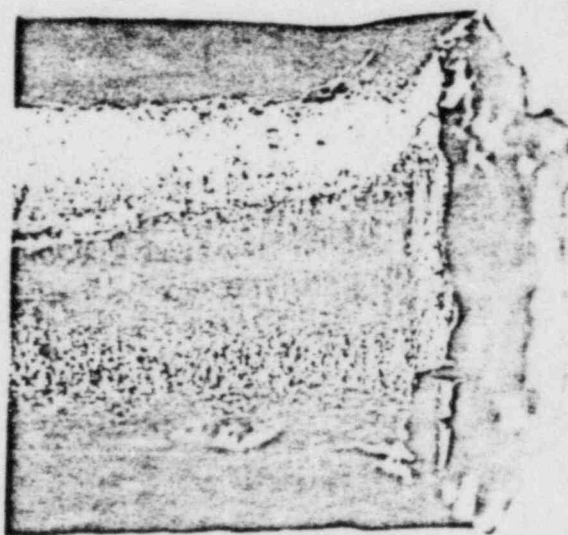
Figure   3.2-15   62407
Close-up of Failure
at Head Area of
Thermowell No. 122CA
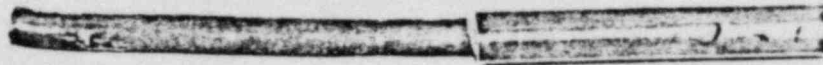
1 Brown&Sharpe 2   U.S.A   3   TEMPERED   4   No 889-223-605 5
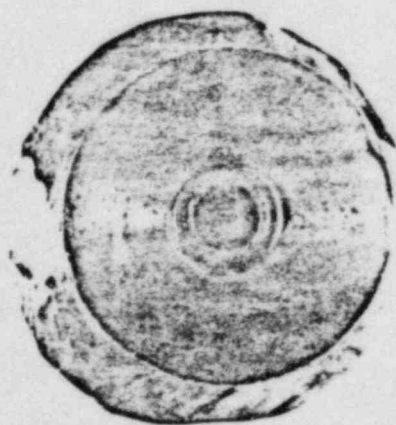
62410
Figure   3.2-16
Mating Part of the
Failure Shown in
Figure   3.2-15
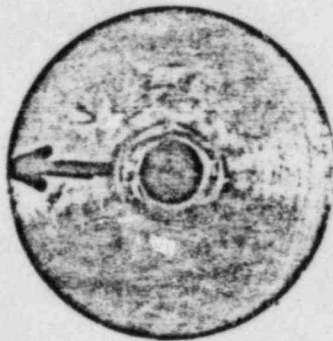
&Sharpe 2   U.S.A.   3   TEMPERED   4   No.

112CD

Figure   Fracture Surface of Head
3.2-17   of Thermowell No. 112CD

62814

Figure   EDS Spectrum of
3.2-18   Thermowell 111Y.
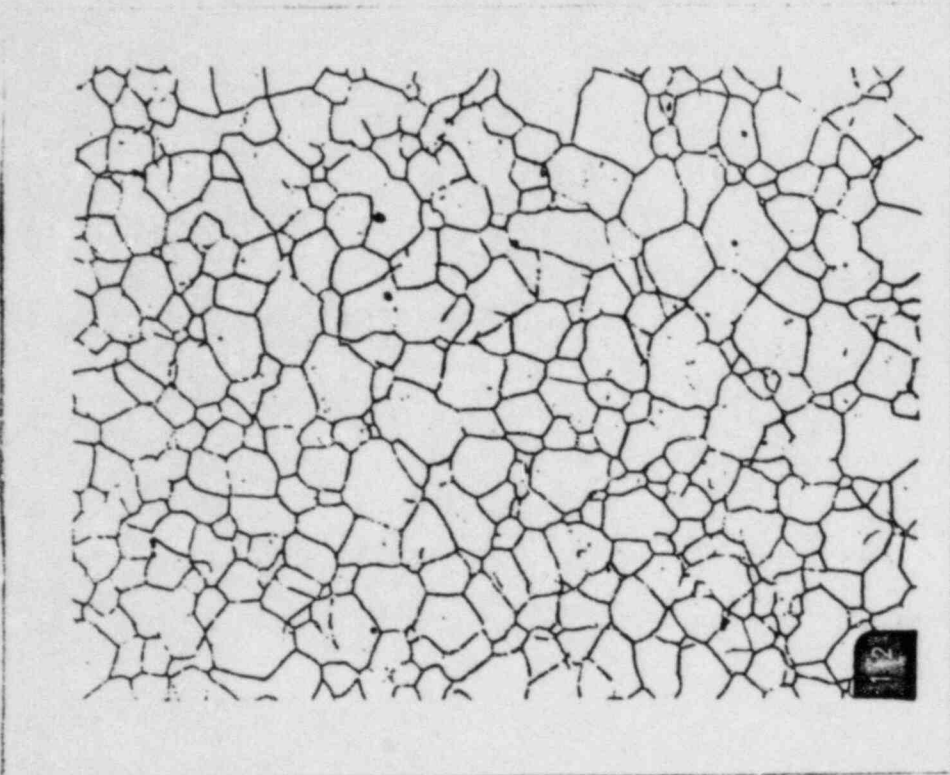
62938

200X

Etchant: Nital

Figure
3.2-19

Microstructure of Thermowell 111Y,
Transverse Cross Section
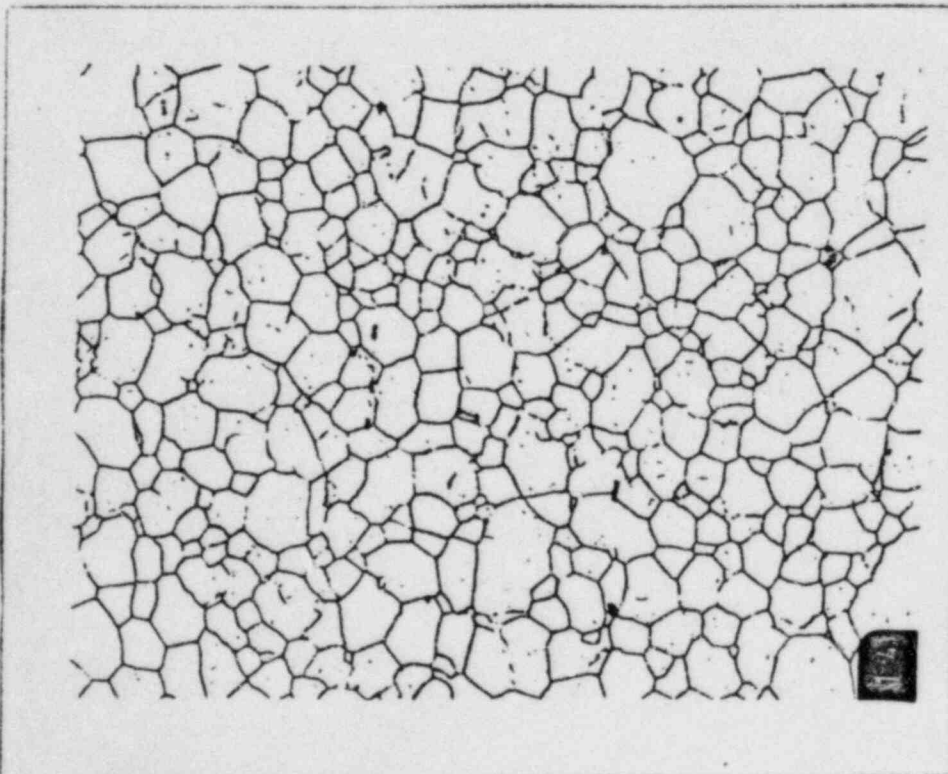
62939

200X

Etchant: Nital

Figure
3.2-20

Microstructure of Thermowell 111Y,
Longitudinal Cross Section

62569

8X

Figure
3.2-21   Optical Fractograph of Fracture
         Surface of Thermowell No. 112CD

10X

Figure
3.2-22   SEM Fractograph of Fracture
         Surface of Thermowell No. 112CD
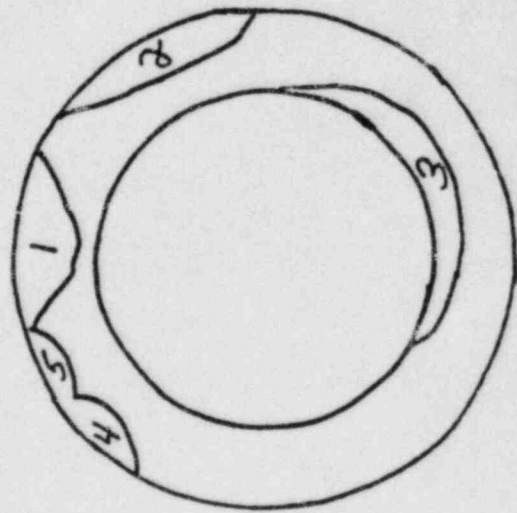
Figure
3.2-23   Sketch Identifying
         Areas in Figures 24 and 25.

61987
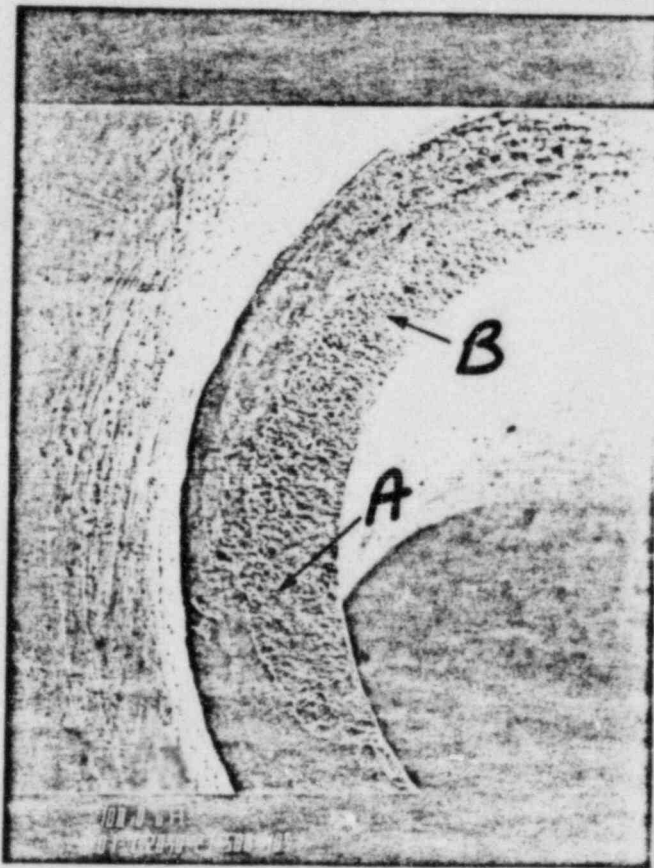
10X

Figure 3.2-24   Close-Up View of Area 3, Thermowell No. 112CD
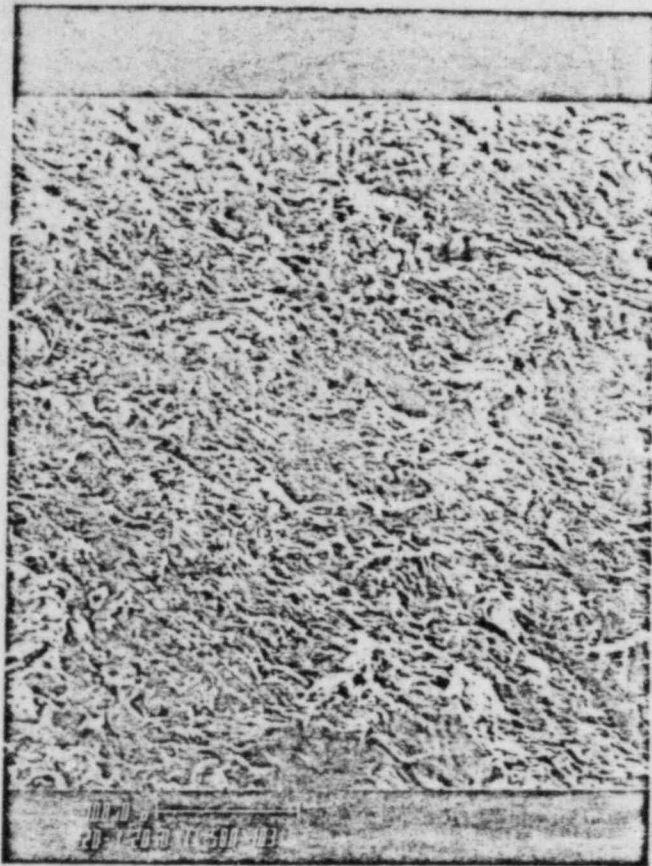
61985
Figure   3.2-25
Striations in
Location A, Area 3
of Thermowell No.112CD

20X

Figure   3.2-26   61986
Higher Magnification
of Figure   3.2-25
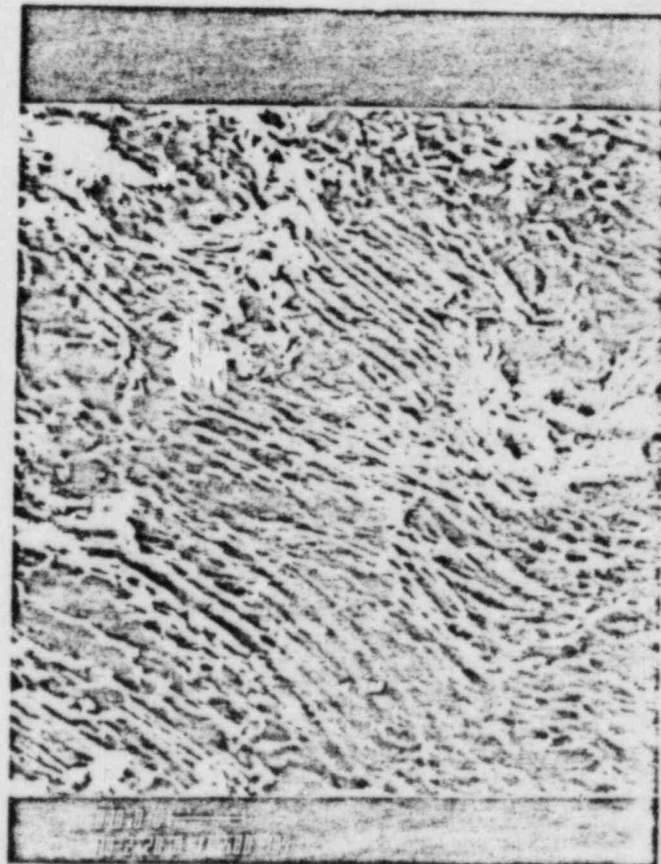
1000X
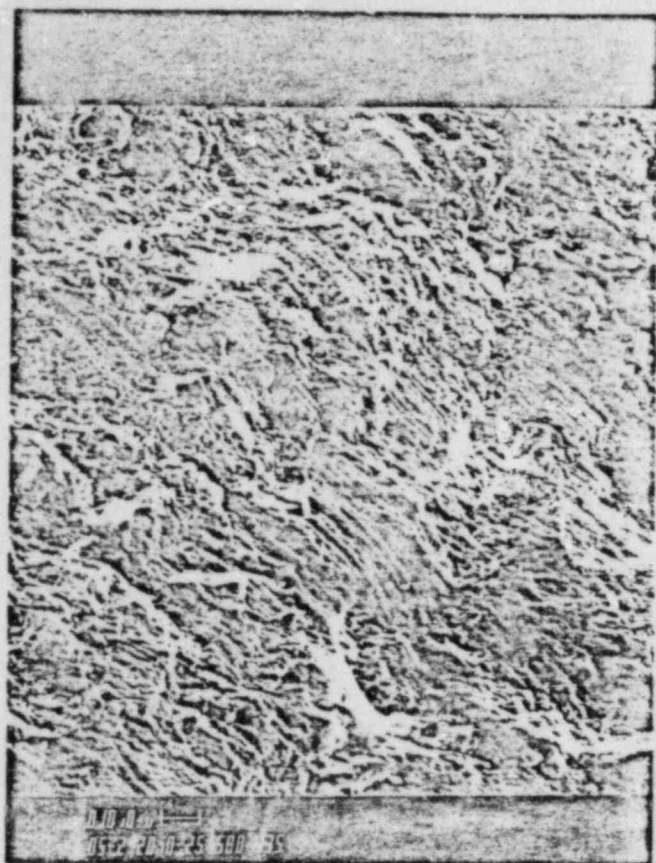
62565
Figure   3.2-27
Additional Striations in
Location A, Area 3
of Thermowell No.112CD

500X

Figure   3.2-28   62571
Higher Magnification
of Figure   3.2-27

1000X

Figure   3:2-30   62566
Areas 4 and 5 of
Thermowell No. 112CD

5

4
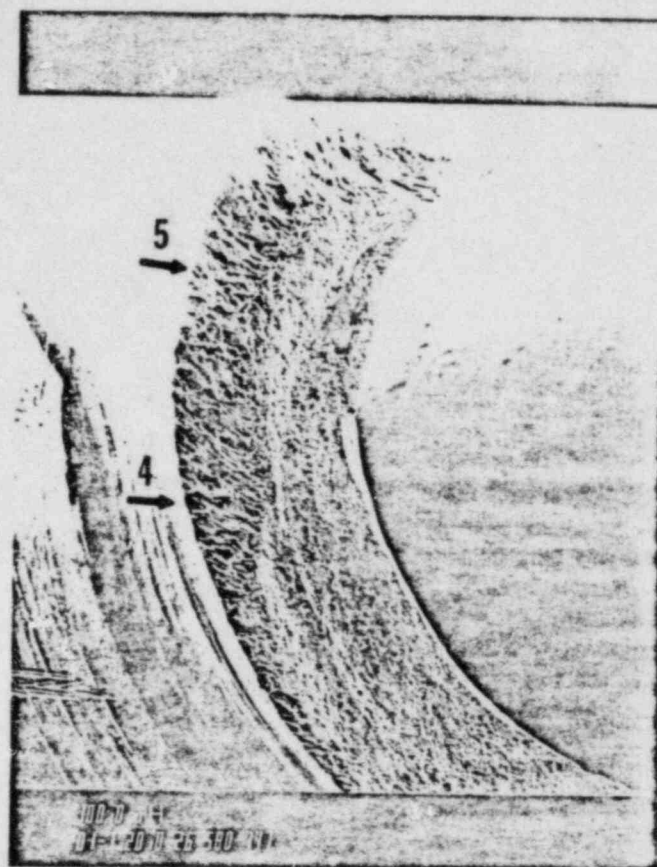
10X
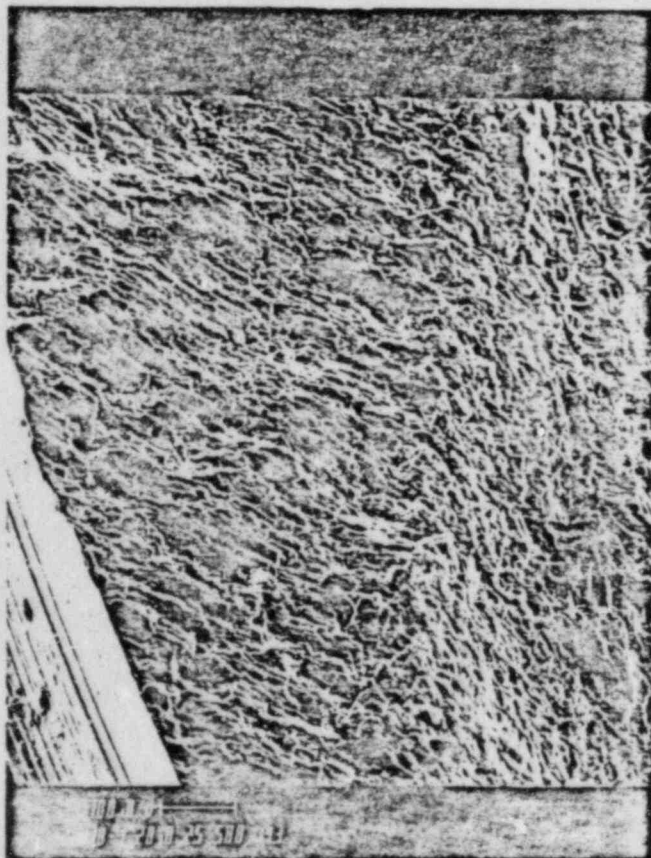
62568
Figure   3.2-31
Higher Magnification
of Area 4 of Thermowell
No. 112CD

100X

8X
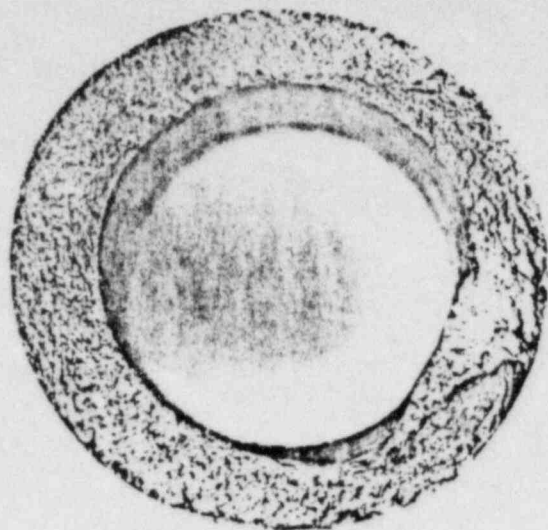
Figure
3.2-32   Optical Fractograph of Fracture
           Surface of Thermowell No. 111Y

62545

10X

Figure   SEM Fractograph of
3.2-33   Fracture Surface of Thermowell
           No. 111Y

Figure   Sketch Identifying
3.2-34   Areas in Figures 3.2-32 and 3.2-33

62546

30X

Figure   Area 1 of Thermowell
3.2-35   No. 111Y

Figure   3.2-36   62550
Higher Magnification
of Area 1 of Thermowell
No. 111Y, Showing
Ductile Tearing

100X

62548
Figure   3.2-37
Higher Magnification
of Figure   3.2-36

1100X

Figure 4 3.2-38   62551
Striations in Area 2
of Thermowell No. 111Y
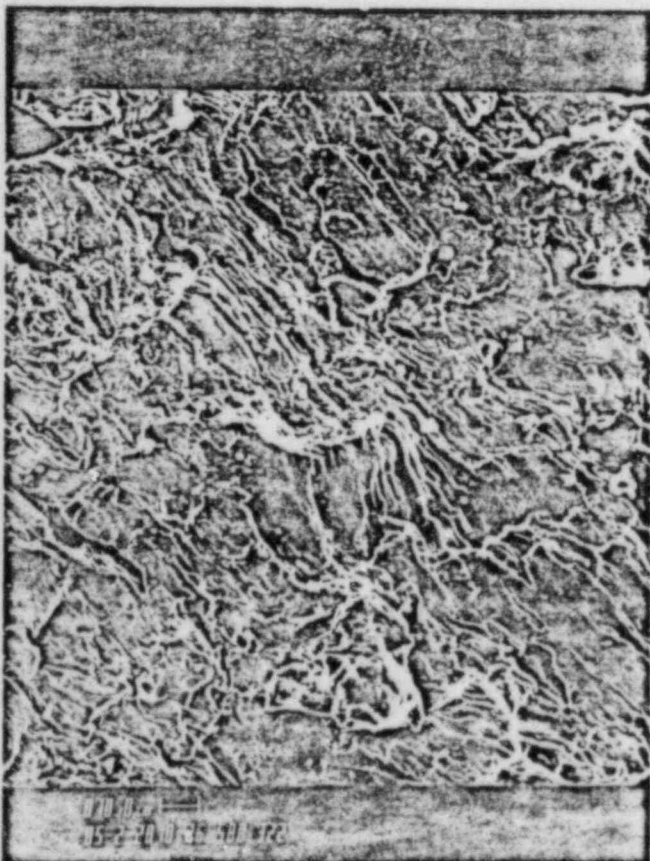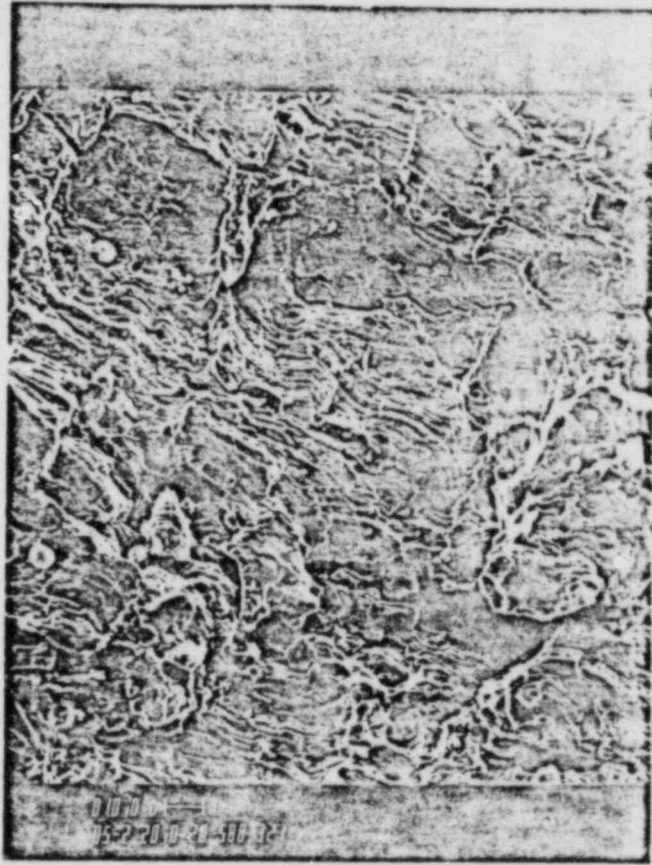
500X

62554
Figure   3.2-39
Additional Striations
in Area 2 of Thermowell
No. 111Y

500X
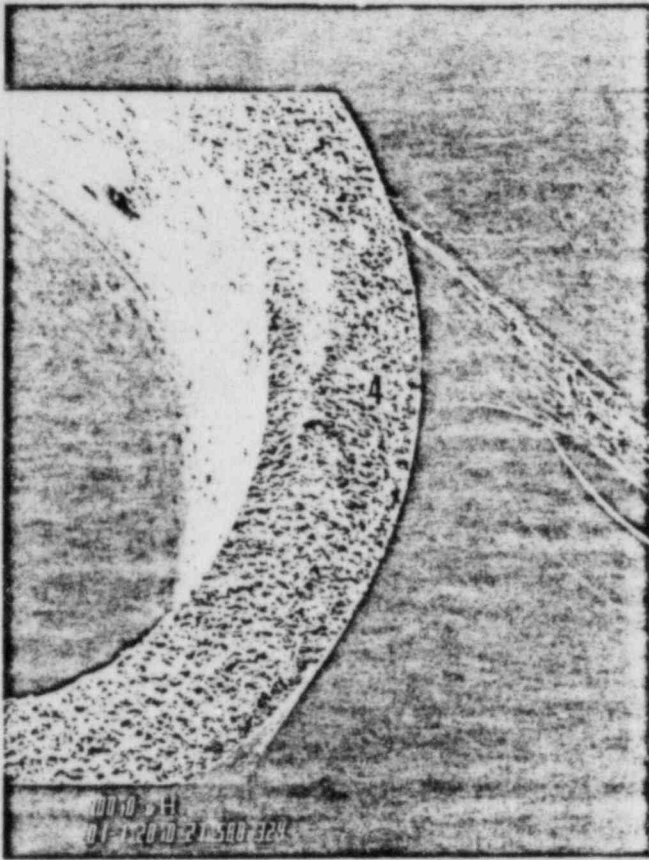
62556
Figure   3.2-40
Area 4 of Thermowell
No.111Y

10X

Figure   3.2-41   62557
Close-up of Area 4
of Thermowell No. 111Y
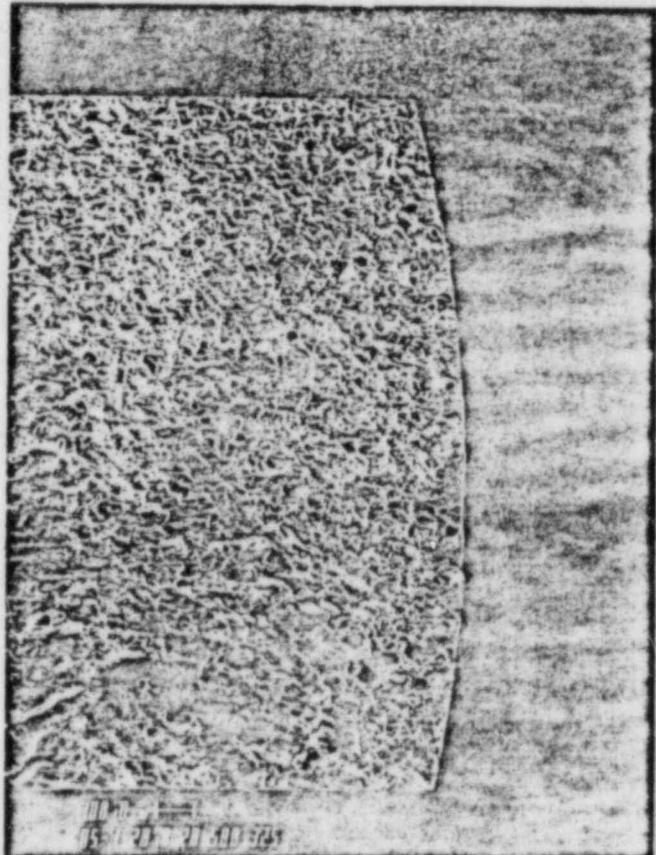
50X
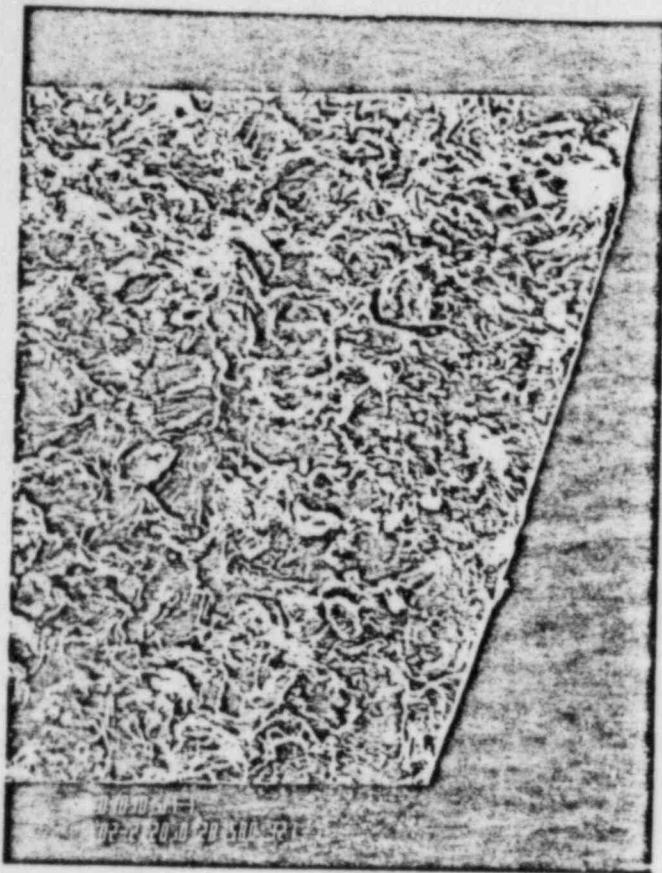
62559
Figure   3.2-42
Possible Crack Initiation
Point in Area 4 of
Thermowell No.111Y

200X

Figure   3.2-43   62560
Higher Magnification
of Figure   3.2-42

500X

8X
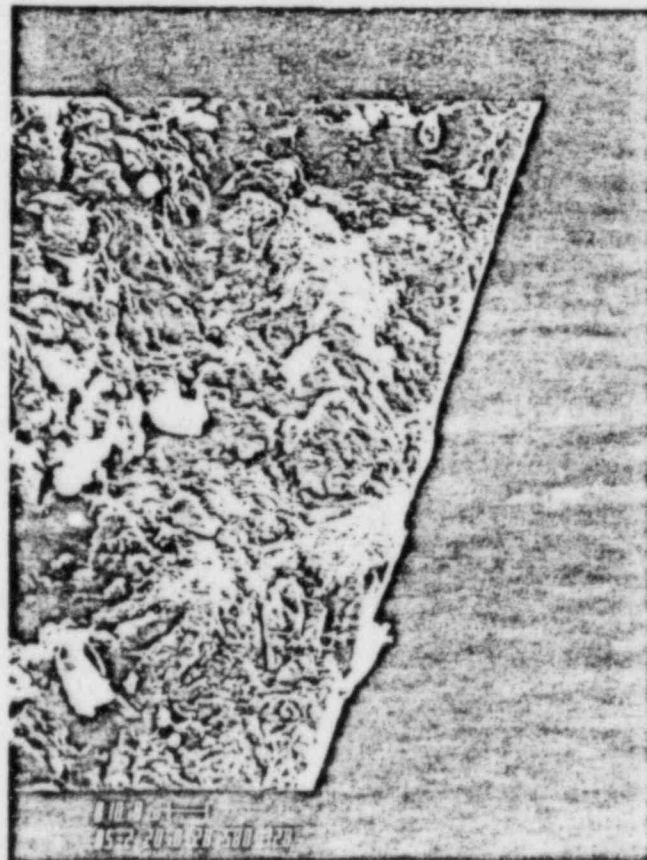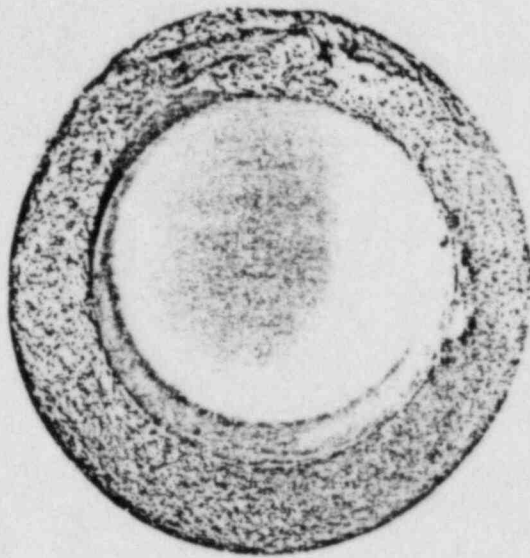
Figure   Optical Fractograph of
3.2-44   Fracture Surface of
              Thermowell 112CA

62419

8X
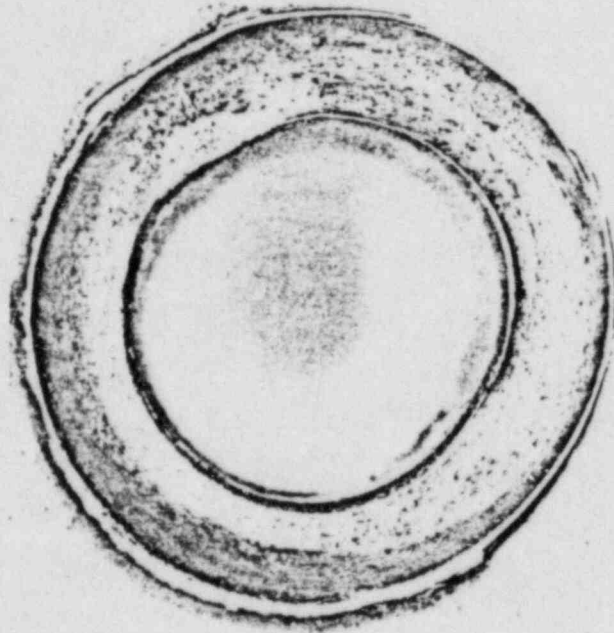
Figure   Optical Fractograph of
3.2-45   Fracture Surface of
             Thermowell 112CA

Table 3.1.1
Summary of Results of Site
Inspection of Thermowells

Location	ID	Position[8]	Condition	Location of Failure
1A-Cl[1]	112CA[5]	2 o'clock	Broken	Pipe
	111Y[5]	12 o'clock	Broken	Pipe
	112CCY(6)	10 o'clock	Broken	Pipe
1B-CL	112CB	2 o'clock	Intact	N/A[9]
	115[5]	12 o'clock	Intact	N/A
	112CD[5]	10 o'clock	Broken	Head
2A-CL	122CC	2 o'clock	Intact	N/A
	125CC	12 o'clock	Bent 45°[3]	N/A
	122CA[5][6]	10 o'clock	Broken	Head[4]
2B-CL	122CD[5]	2 o'clock	Intact	N/A
	121Y	12 o'clock	Intact	N/A
	122CB	10 o'clock	Intact	N/A
1-HL[2]	112HA	8 o'clock	Intact	N/A
	112HB	2 o'clock	Intact	N/A
	112HC	10 o'clock	Intact	N/A
	112HD	4 o'clock	Intact (1/16)[7]	N/A
	111HA	8 o'clock	Intact	N/A
	111HB	2 o'clock	Intact	N/A
	111HC	4 o'clock	Intact (1/16)	N/A
	111HD	10 o'clock	Intact (1/16)	N/A
	111X	9 o'clock	Intact (1/8)	N/A

Table 3.1.1
Summary of Results of Site
Inspection of Thermowells
(Cont'd.)

Location	ID	Position(8)	Condition	Location of Failure
2-HL	122HA	4 o'clock	Intact (9/32)	N/A
	122HB	10 o'clock	Intact	N/A
	122HC	2 o'clock	Intact	N/A
	122HD	8 o'clock	Intact (3/16)	N/A
	121HA	8 o'clock	Intact	N/A
	121HB	2 o'clock	Intact	N/A
	121HC	4 o'clock	Intact (1/16)	N/A
	121HD	10 o'clock	Intact	N/A
	121X	3 o'clock	Intact (1/16)	N/A

NOTES:

(1) CL = Cold Leg

(2) HL = Hot Leg

(3) Appears to have been bent by piece of RC Pump Impeller Vane.

(4) Original failure at head; subsequently broken off at pipe by Impeller Vane Piece and Thermowell dropped down ~2".

(5) Returned to Windsor for examination.

(6) Originally reported leaking.

(7) Value in parenthesis indicate amount thermowell was bent towards the RV.

(8) Location of thermowells are shown on Figure 3.1-1.

(9) Not applicable (Thermowell not broken)

Table 3.1-2

Cold Leg Thermowell Wear Measurements

Thermowell No.	Position	Status[1]	Location[2]	OD, in.	Wall Reduction[3] Inches	Percent[4]
122CD	2 o'clock	I	1	.375	.000	0
			2	.375	.000	0
			3	.375	.000	0
			4	.373	.002	3
112CA	2 o'clock	B/P	1	.375	.000	0
			2	.372	.003	5
			3	.371	.004	6
			4	.366	.009	14
115	12 o'clock	I	1	.377	.000	0
			2	.370	.007	11
			3	.369	.008	13
			4	.365	.012	19
111Y	12 o'clock	B/P	1	.375	.000	0
			2	.366	.009	14
			3	.366	.009	14
			4	.362	.013	21
122CA	10 o'clock	B/H	1	.375	.000	0
			2	.325	.050	80
			3	N/A[5]	N/A	N/A
			4	N/A	N/A	N/A
112CD	10 o'clock	B/H	1	.376[6]	.000	0
			2	.340	.035	56
			3	.344	.031	50
			4	.321	.054	86

Notes: (1) I = Intact; B = Broken; H = at head; P = at Pipe
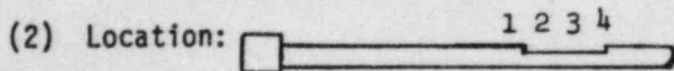
(2) Location:

(3) Wall Reduction = OD_1 - OD

(4) Based on nominal .0625" wall

(5) Not obtainable, tip is damaged.

(6) In this case, location 1 (unworn reference diameter) is to the right side of location 4 due to damage in the original location 1 area.
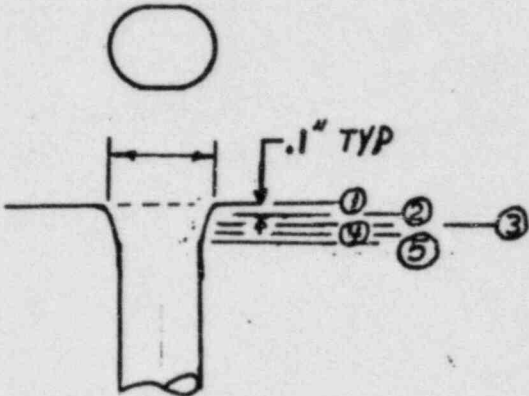
Table 3.1-3

Hot Leg Thermowell Wear Measurements

Thermowell No.	OD,$^{(1)(2)}$in	Inches	Wall Reduction[3] Percent[4]
112 HB	.374 - .375	.000 - .001	0 - 1.6
121 HB	.374 - .375	.000 - .001	0 - 1.6
121 HD	.373	.002	3.2

(1) Measured at worst wear location, i.e., at "Step" produced at junction with reactor coolant piping.

(2) Reference diameter = .375" for all three thermowells, measured outside of the wear area.

(3) Wall Reduction = Reference diameter - OD measured.

(4) Based on nominal .0625" wall.

TABLE 3.1-4
Cold Leg Thermowell
Nozzle Wear Measurements

Thermowell No.	Location[1]	ID (in.)	Notes
112CC	1	.500	1. Location
	2	.410	
	3	.405	
	4	.403	
	5	.400	
111Y	1	.400	
	2	.393	
	3	.390	
	4	.390	
	5	.378	
112CA	1	.387[2]	2. Hole edge appeared sharp all around.
	2	.386	
	3	.386	
	4	.383	
	5	.383	3. Downstream edge has 1/32 radius. Remainder of hole is round for entire length of support.
115	1	.420	
	2	.387	
	3	.387	4. Depression in end of nozzle (wear or erosion)
	4	.384	
	5	.377	
112CB		.377[3]	
122CA		(4)	
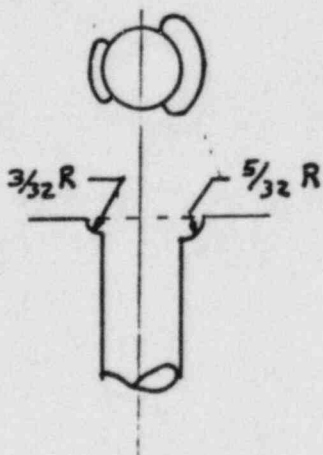
3.2 DESCRIPTION AND RESULTS OF EXAMINATION FOR THE ORIGINAL DESIGN

3.2.1 Metallurgical Evaluation

Laboratory examination consisted of visual examination, wear measurements, material evaluation, stereomicroscopy, and optical and scanning electron fractography. The visual examination and wear measurements were performed initially at site inspection of the thermowells. A more detailed visual examination of the thermowells was performed on thermowells returned to the laboratory. The thermowells examined are shown on Figure 3.2-1.

3.2.2 Visual Examination

Of the six cold leg thermowells returned to the laboratory, 2 were intact (115, 122CD), two were fractured at the RCS pipe surface (111Y, 112CA), one was fractured at the upper end at the junction with the head (112CD) and one was fractured both at the RCS pipe surface and at the junction with the head (122CA). Subsequently, a missing fractured piece from 112CD was retrieved by site personnel and returned to C-E Windsor.

All of the examined thermowells exhibited a pattern of wear on the downstream side in a 2" long section that corresponds to the reduced diameter section of the RTD Nozzle (.377" nominal, Figure 3.2-2). In this section, clearance between the thermowell and nozzle is .001" to .006" on the diameter.

Figures 3.2-3 to 3.2-8 illustrate this wear pattern. Figures 3.2-3 and 3.2-4 show a moderate amount of wear on Thermowell No. 115. Figures 3.2-5 and 3.2-6 show an extensive amount of wear on No. 112CD. Figures 3.2-7 and 3.2-8 show a slight amount of wear on No. 122CD. Section 3.1 of this report has additional details on wear measurements and damage.

The thermowells which fractured at the RCS pipe surface failed at the wear transition area seen in Figure 3.2-9 thru 3.2-12. The wear and fracture surfaces can be seen on Figures 3.2-9 and 3.2-10 for thermowell 112CA and on Figures 3.2-11 and 3.2-12 for thermowell 111G. In addition to the location of failure, these figures show that the fractured end is relatively flat, with little or no plastic deformation.

Figure 3.2-13 and 3.2-14 show the failed portion of Thermowell No. 122CA at the RCS pipe surface. Figure 3.2-13 shows two areas of wear, the second (left side in the Figure) occurring after the separation at the head, which allowed the thermowell tube to drop down, approximately 2 inches, further into the RCS flow. The broken end (Figure 3.2-13 and Figure 3.2-14) shows a ductile type break which probably occurred as a result of impact by reactor coolant pump parts.

Figures 3.2-15 and 3.2-16 show the failure of the Thermowell No. 122CA at the other end, i.e., at the junction with the thermowell head. Figure 3.2-15 shows the tube and Figure 3.2-16 shows the head portions, respectively. As previously seen, the fracture surfaces are flat and have little or no plastic deformation.

Figure 3.2-17 shows the fracture surface on the head of Thermowell No. 112CD.

3.2.3   Material Examination

The thermowell material was specified as Inconel 600 per ASME SB-166. Two heat lots of material were used to fabricate the thermowells for Palo Verde Unit 1. The material certifications for these heat lots were reviewed and found to meet the specification requirements for chemical and mechanical properties. Ultrasonic Testing inspection reports for the raw materials were reviewed. No defects were found.

An Energy Dispersive Spectroscopy (EDS) spectrum taken on a piece from Thermowell No. 111Y confirmed that the material is Inconel 600. Figure 3.2-18 is the EDS spectrum.

Transverse and longitudinal cross sections were taken from 111Y for microstructural evaluation. Figures 3.2-19 and 3.2-20 present the transverse and longitudinal microstructures, respectively. The microstructure is normal for annealed Inconel 600 rod.

3.2.4 Optical and Scanning Electron Fractography

The fracture surfaces of the 4 broken thermowells (112CD, 111Y, 112CA and 122CA) were examined using a stereomicroscope and scanning electron microscope (SEM) and photographs we e taken with a macro-camera and the SEM.

Figure 3.2-21 is an optical fractograph and 3.2-22 is a SEM fractograph of the fracture surface of Thermowell No. 112CD. This thermowell broke at the upper head location. The fracture surface examined is on the head portion. Figure 3.2-23 identifies the areas seen in Figures 3.2-21 and 3.2-22.

The macroscopic appearance of Area 1 suggests this is the area of final fracture. The surface features are smeared, making further examination at higher magnification not meaningful.

The remainder of the fracture surface is also smeared, except for Area 3. Figure 3.2-24 is an SEM photograph of Area 3. This entire area represents a fatigue crack, as evidenced by striations throughout the area. Figures 3.2-25, 3.2-26, 3.2-27 and 3.2-28 show two areas of striations in location A shown in Figure 3.2-24. Figure 3.2-29 shows striations in location B. The average striation spacing measured in Area 3 is approximately 4.3×10^{-4} inches/cycle. This, together with the relatively large area of the fatigue crack, indicates low stress, high cycle fatigue as the failure mechanism. This type of loading is associated with vibration. Because the

remainder of the fracture surface was smeared, the fracture origin was not found and therefore, it cannot be determined whether Area 3 is near the origin or tip of the crack.

Areas 2, 4 and 5, as mentioned above, are also smeared. Figure 3.2-30 shows Areas 4 and 5. Figure 3.2-31 is a higher magnification view of Area 4. Area 6, the balance of the surface, is smooth and featureless.

Figure 3.2-32 is an optical fractograph and Figure 3.2-33 is a SEM fractograph of the fracture surface of Thermowell No. 111Y. This thermowell fractured at the RCS pipe surface. The fracture surface is on the remaining portion of the thermowell. Figure 3.2-34 is a sketch identifying the areas seen in Figures 3.2-32 and 3.2-33.

Area 1 is the area of final fracture. It is essentially on the downstream side and shows a ductile tearing fracture mechanism, see Figures 3.2-35, 3.2-36 and 3.2-37. This indicates final failure was due to separation caused by either flow pressure or by impact from reactor coolant pump debris.

Area 2 shows evidence of fatigue striations. Figures 3.2-38 and 3.2-39 show two different patches within this area. The surface, including striations, is slightly eroded, most likely due to the flow of water po t the fracture surface. Again, the close spacing of the striations and the relatively large size of the fatigue area indicates low stress, high cycle fatigue.

Areas 3, 5 and 6 are smeared and featureless. Area 4 could possibly be an origin point for the fatigue crack. See Figures 3.2-40 through 3.2-43. If so, the crack started on the outer surface, approximately 90° to the flow. This is consistent with one possible vibration source, i.e., vortex shedding. The quality of the surface in Area 4, however, makes a definitive interpretation difficult. This area has a substantial amount of oxide and deposits on it and also has undergone some erosion or smearing.

Figure 3.2-44 is an optical fractograph of the fracture surface of Thermowell No. 112CA. This resembles No. 111Y on a macroscopic scale. However, the fracture surface was smeared and oxide coated and yielded no information.

Figure 3.2-45 is an optical fractograph of the fracture surface of Thermowell No. 112CA. This was completely smooth, also yielding no information.

The metallurgical evaluation confirms that low stress, high cycle fatigue was the cause of thermowell failure.

3.2.5 Vibration Response Frequency Tests

Vibration response tests were performed on installed thermowells in Palo Verde Unit-1 to determine the response frequency of the thermowell tip on the original system 80 thermowell.

The tests were performed by use of an accelerometer mounted in the tip of a simulated RTD. Thermowell 122CB, a 10 o'clock position thermowell located in loop 2B, was used to perform the tests. The first test was performed without any reactor coolant pump operating. A plot of these results is shown on Figure 3.2-46. The peak at 480 HZ corresponds to a LPSI pump which was operating at the time.

The next test was performed with two pumps in opposite loops operating (pumps 1A and 1B). The results shown on Figure 3.2-47 identify the blade passing frequencies associated with the operating pumps.

RTD/TW INSTALLATION ORIGINAL DESIGN

FIGURE 3.2 - 2

RTD LOCATION

THERMOWELL

PIPE NOZZLE

.44"

HOT LEG PIPE WALL

COLD LEG PIPE WALL

LOCATION
OF FAILURES

.001 - .006"
DIAMETRAL
CLEARANCE

.377"

2.13 "

2½"

.375"

No Pumps Running

Accelerometer @ T10

1228

Loop 2B Looking Toward Core

ACCELERATION

4kg

Frequency HZ

0   500   1000   1500   2000   2500
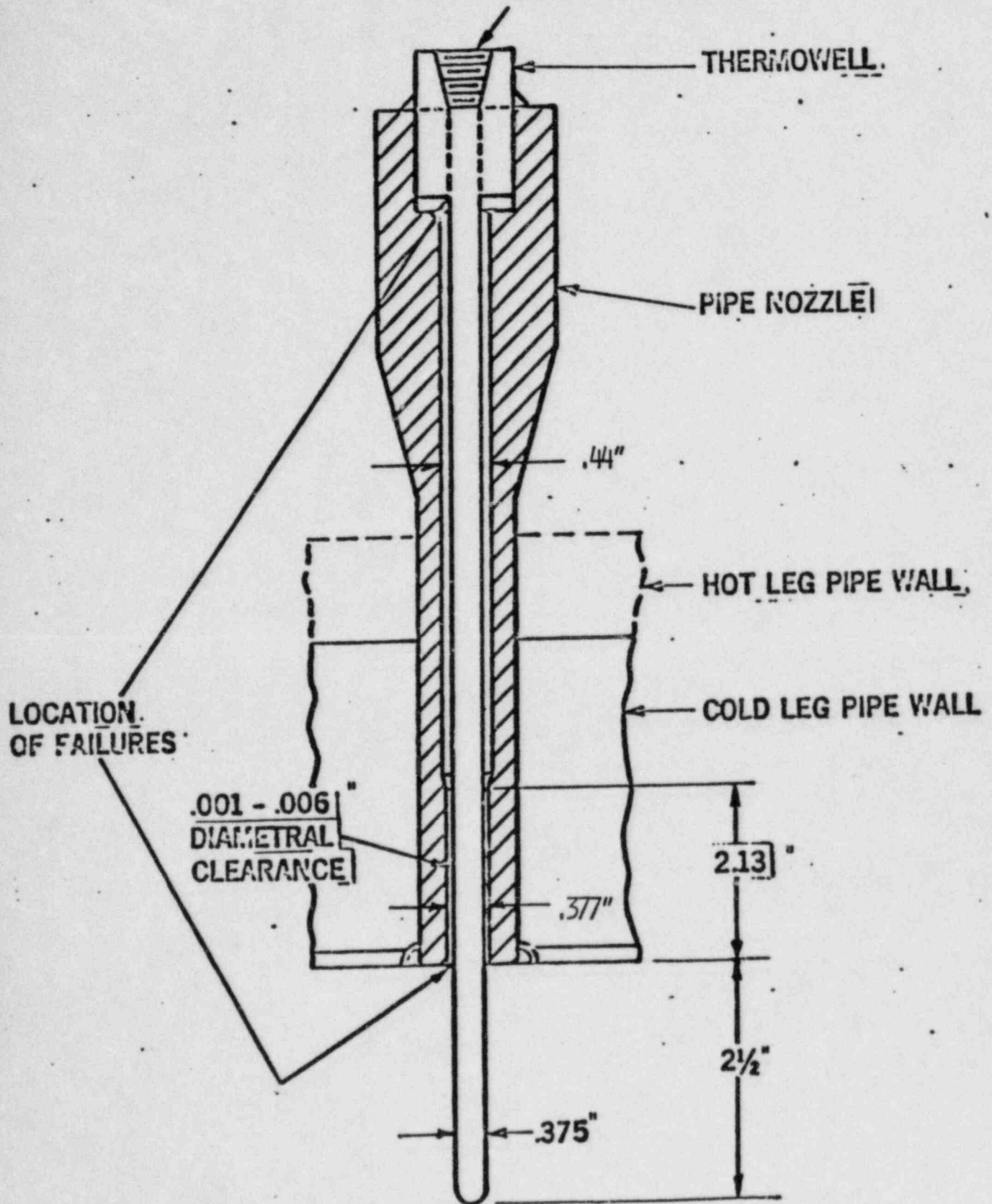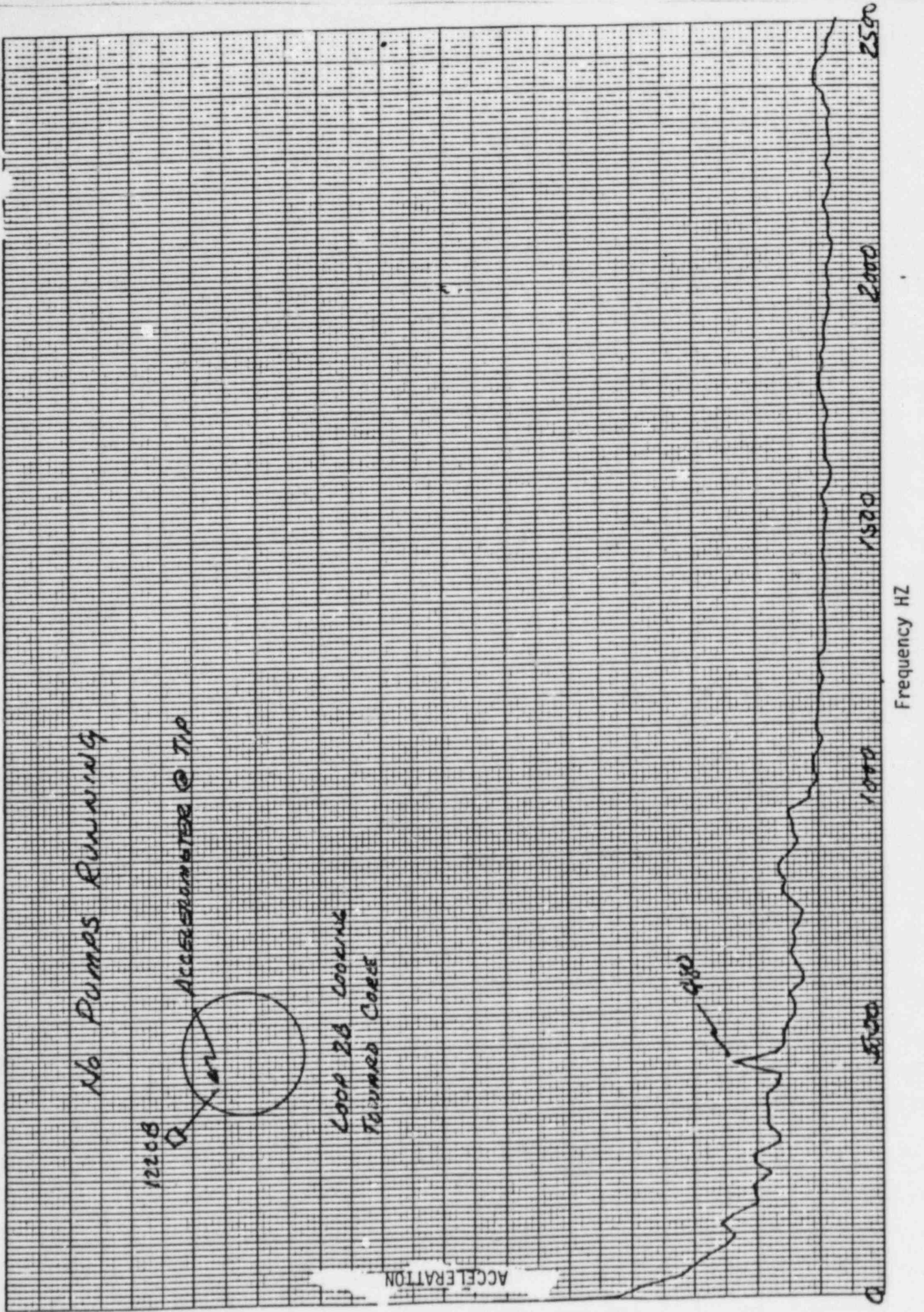
Figure 3.2-46
3-43

Two Pumps Running (10#18)

ACCELERATION

710

780

950

424

12" 1" 1"

Blade Passing

Frequency HZ
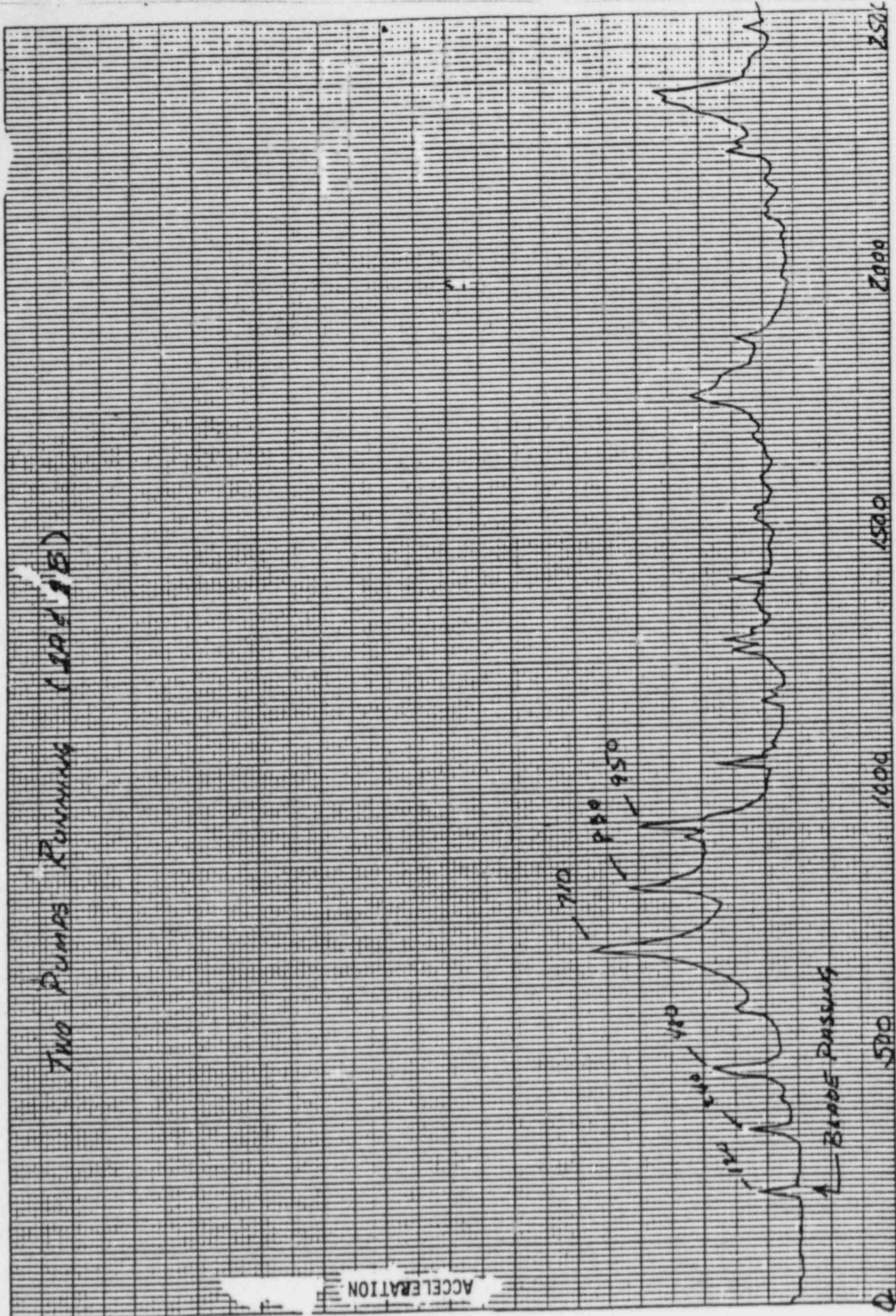
Figure 3.2-47
3-44

FIGURE 3.2-48

4.0 TEST AND ANALYSIS (Problem Definition)

4.1 DESCRIPTION AND RESULTS OF ANALYSIS TO DETERMINE CAUSE

Because vortex shedding was suspected as the failure mechanism, it's effects were evaluated. Vortex shedding can be described as follows: Flow across a tube produces a series of (Von Karmen) vortices in the downstream wake formed as the flow separates alternately from the opposite sides of the tube. This alternating shedding of vortices produces alternating forces which occur more frequently as the flow increases. For a single cylinder, the tube diameter, flow velocity and frequency of vortex shedding can be described by the dimensionless Strouhal number.

The original System 80 thermowell was analyzed to determine the effects of vortex shedding. First, this involved calculating the natural frequency of the original thermowell and investigating various conditions of support. As may be seen on Figure 4.1-1, the thermowell is supported from 2 1/2 inches to 4 5/8 inches from the tip by a clearance hole through the nozzle. Various assumptions can be made in evaluating this type of support. Three cases were considered, as shown in Table 4.1-1. The thermowell was first assumed to be unsupported by the nozzle and was fixed at the top of the thermowell. The second model considered the thermowell to be additionally supported at a point 2 1/2 inches from the tip of the thermowell (the edge of the nozzle at the inside of the pipe). The third model assumed additional support at a point 4 5/8 inches from the tip of the thermowell (the inner end of the nozzle support surface located 2 1/8 inches away from the inside of the pipe).

The natural frequency can be seen to vary significantly based on the type of support considered and may change with time as the nozzle support surface and adjacent surface on thermowell wear.

Flow velocities affecting the thermowells were evaluated. The highest flow velocity is associated with part-loop operation. The highest flows occur in a cold leg whose pump is operating, with a secured pump on the other side of the same steam generator (loop). This runout flow is about 43% higher than normal operating design.

It can be seen by comparing results shown in Tables 4.1-1 and 4.1-2 that the frequency ratio (vortex shedding frequency to natural frequency) can approach unity. A maximum frequency ratio value of .8 is recommended for design purposes. The evaluations conducted indicate that resonance could have developed in the original System 80 thermowells, based on the range of local flow velocities that may have existed during start-up testing. During full power operation, with all four pumps running, flow velocities would not have been high enough to resonate the thermowell.

The Palo Verde Unit-1 thermowells were analyzed for wear and the type damage incurred was characterized for comparison with pump operating time in associated loops for various high and low flow velocities. The pump operating time during cold plant hydro, which involves very few hours, was not included. The plant operating history was compared to thermowell wear and damage and is presented in Table 4.1-3 for the cold legs and 4.1-4 for the hot legs. Only those hot leg thermowells showing measurable wear were presented in Table 4.1-4.

An examination of the results listed in Table 4.1-3 shows cold leg thermowells in loop 1B and 2B saw the least number of hours (≈ 80 hrs.) of service at runout flow condition. Cold leg thermowells in loop 1A saw the most service time at runout flow (317.2-615.9 hrs.) while cold leg thermowells in loop 2A saw 110.5 to 119.1 hours of service at runout flow. The times listed represent hours of service up to the time of failure (no longer possible for thermowell to wear) or hours to completion of test. Normal flow service durations are also listed and varies from 358.8 to 594.8 hours for cold leg loop 1A thermowells to 1010.9 hours for loop 2B thermowells. A review of the hot leg thermowell flow data shown in Table 4.1-4 shows loop 1 thermowells to have 624.3 hours of service time at normal flow rates and 696.7 hours at lower flow rates associated with part loop operation. Loop 2 thermowells were exposed to 1010.9 and 200.3 hours of normal and lower flow service time, respectively.

4-3

It can also be observed, from the results in Table 4.1-3, that the 10 o'clock position thermowells, which broke at the top (Cold Legs 1B and 2A), have the most wear (35 to 54 mills) and saw the least (80.1 hrs.), to relatively low (110.5 hrs.) service time at runout flow conditions and relatively low service time at normal flow conditions (358.8-594.8 hrs.). A review of the pump damage which resulted during (PCHFT) of Palo Verde Unit-1 shows that the pump impeller vanes failed in loops 1B and 2A. An impeller vane was found to have a missing segment on pump 1B and two adjacent vanes were found with missing segments on pump 2A.

There is no physical evidence that a broken impeller part impacted any of the thermowells on loop 1B. On loop 2A, it appears thermowell No. 125 was struck very early in the testing period because little wear took place before it was bent at about 45° as a result of impact. Thermowell No. 122CA on the same loop (2A) was also struck but only after a considerable amount of wear occurred and the thermowell fractured at the top. All the thermowells on loop 1A fractured at the inside diameter of the pipe but do not appear to have been impacted. The failure of these thermowells is clearly from high cycle, low stress fatigue because little wear occurred while these thermowells were subjected to runout flow conditions for the longest duration. None of the thermowells in loop 2B failed, appeared to have been impacted, or incurred appreciable wear. Cross-sections of the System 80 RC pump (see Figure 4.1-3) and the layout of the associated RC piping show the 10 o'clock position thermowell to be directly in-line with flow coming off the impeller and through the diffuser vanes.

None of the hot leg thermowells failed and they exhibited relatively little wear.

RTD/TW INSTALLATION ORIGINAL DESIGN

FIGURE 4.1-1

RTD LOCATION

THERMOWELL

PIPE NOZZLE

HOT LEG PIPE WALL

COLD LEG PIPE WALL

LOCATION OF FAILURES

.001 - .006" DIAMETRAL CLEARANCE

2.13 "

2½"

.375"
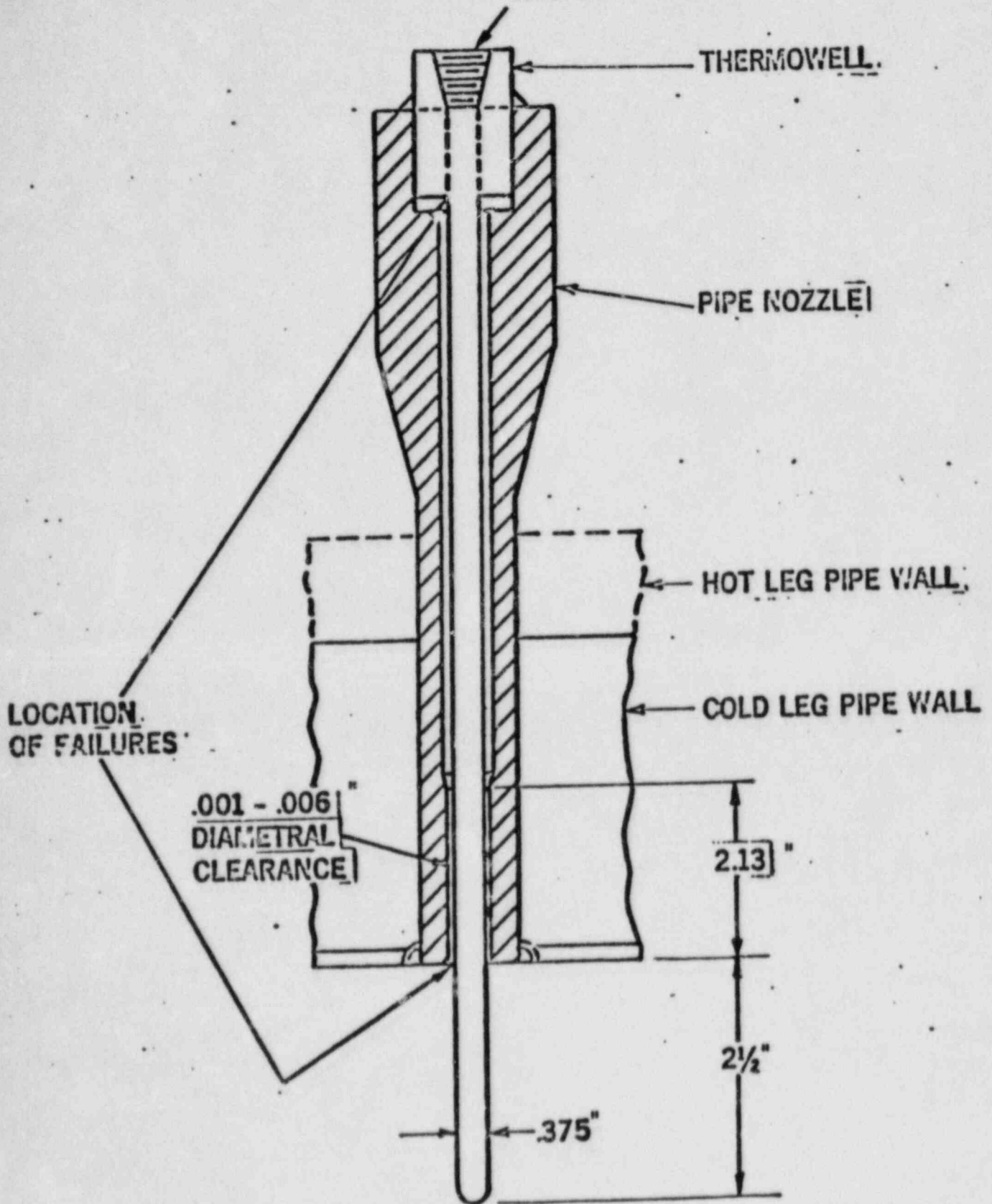
STROUHAL NUMBER
VS
REYNOLDS NUMBER
FIGURE 4.1 - 2

2 Experimentally determined Strouhal number S plotted against Reynolds number Re [4].
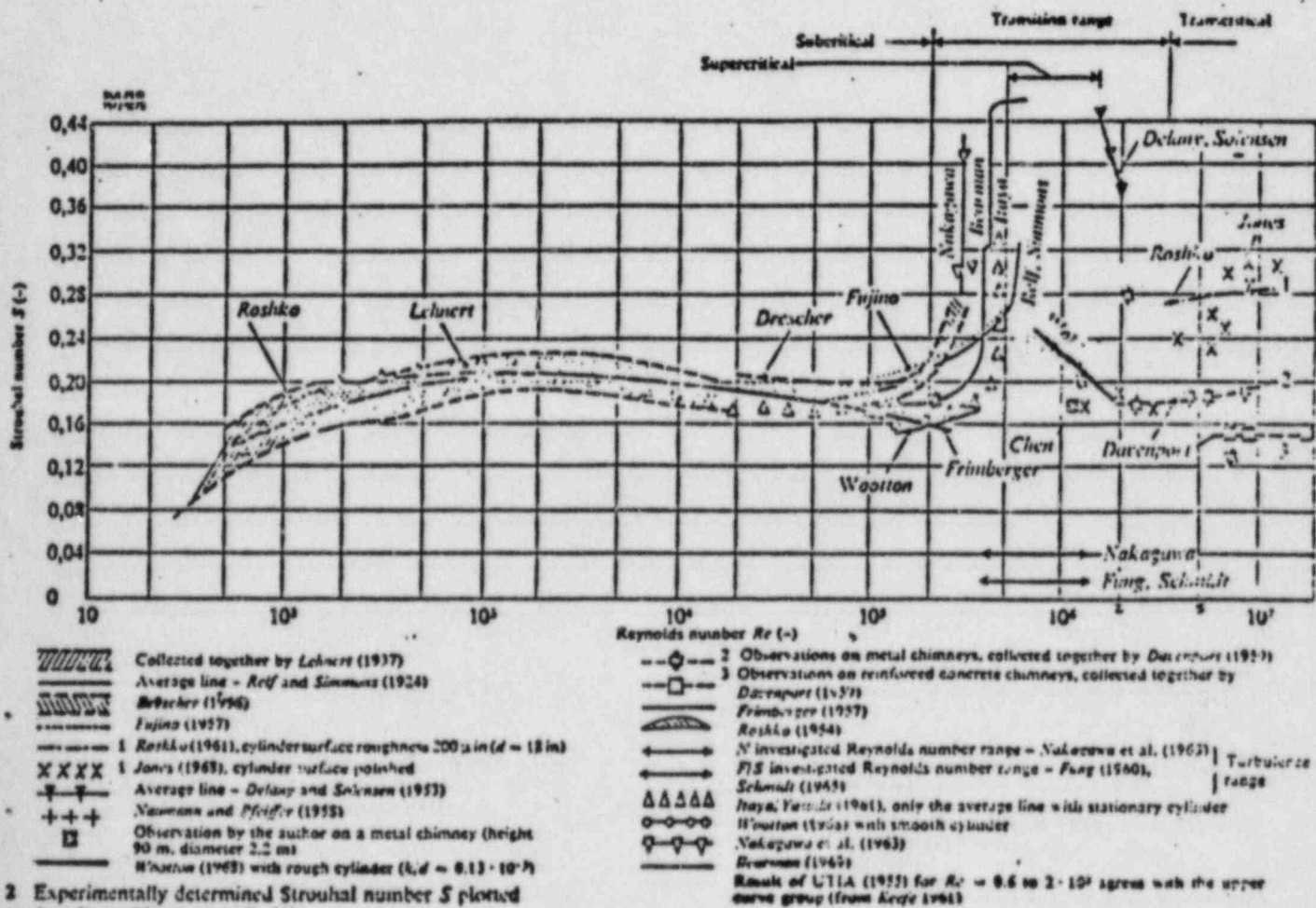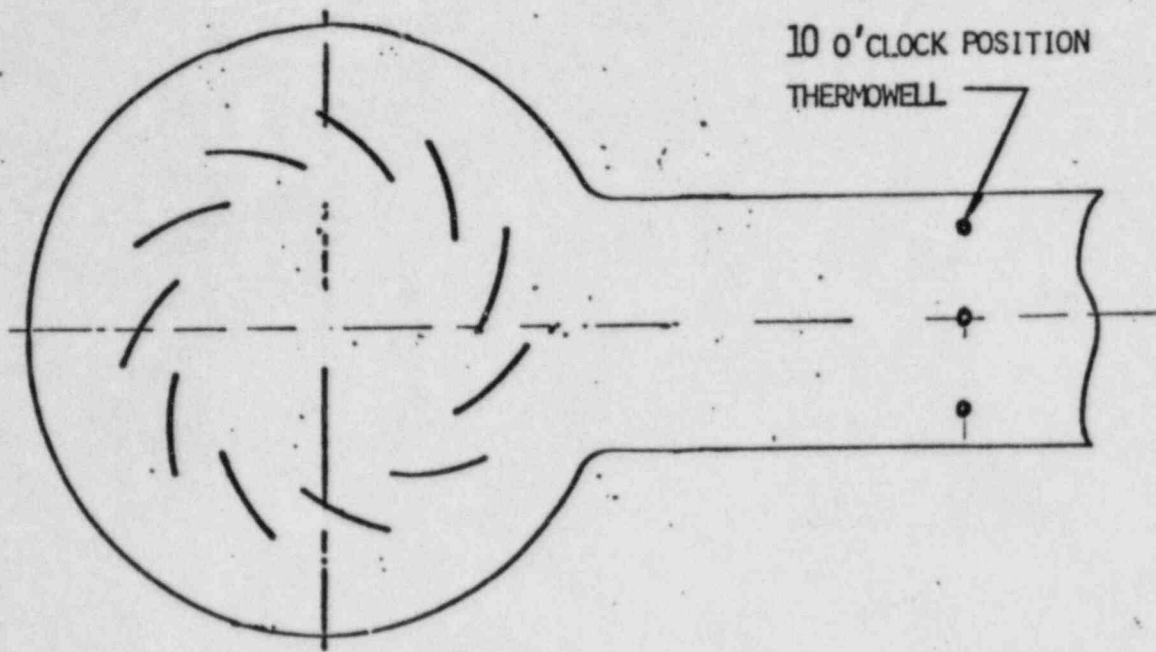
VIEW A - A
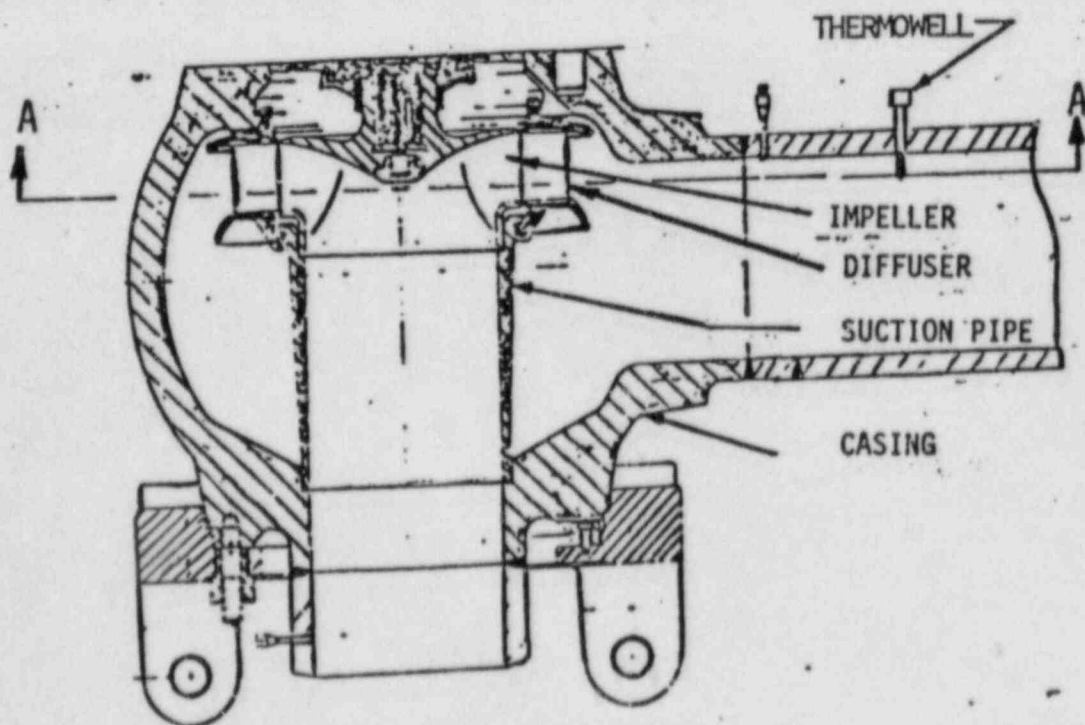
REACTOR COOLANT PUMP ASSEMBLY
(LOWER SECTION)

FIGURE 4.1 - 3

TABLE 4.1-3

THERMOWELL WEAR CHARACTERISTICS
(COLD LEG)
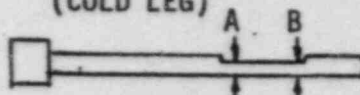
LOOP	LOCATION	TAG #	A-DIM INCH.	B-DIM INCH.	WEAR MILLS	FLOW DURATION (HRS) RUNOUT FLOW (4)	NORMAL FLOW (5)	REMARKS	THERMOWELL FAILURE
1A	10	112CC	(1)	(1)	(1)	317.2-615.9	358.8-594.8	2nd Thermowell to Leak	
								Not Known Exactly When Fractured	Yes
	12	111Y	.3660	.3620	9 -13	317.2-615.9	358.8-594.8	Not Known Exactly When Fractured	Yes
	2	112CA	.3720	.3660	3 - 9	317.2-615.9	358.8-594.8	Not Known Exactly When Fractured	Yes
1B	10	112CD	.3400	.3210	35 -54	80.1	358.8-594.8	Broken at Top	Yes
	12	115	.3700(2)	.3650(2)	7 -12	80.1	594.8		No
	2	112CB	.3750	.3752	.8- 1	80.1	594.8		No
2A	10	122CA	.3250	(3)	50	110.5	465.6	1st Thermowell to Fail, Broke at Top	
								Later Sheared by Pump Parts	Yes
	12	125	.3760	.3760	0	110.5	465.6	Bent by Pump Parts	No
	2	122CC	.3760	.3745	0 - 1.5	119.1	1010.9		
2B	10	122CB	.3748	.3748	0.2	81.2	1010.9		No
	12	121Y	.3745	.3738	1.5- 2.2	81.2	1010.9		No
	2	122CD	.3750	.3730	0 - 2.0	81.2	1010.9		No

(3) No obtainable tip damaged.
(2) Original thermowell dia. 1 mill O.H.L.
(1) No wear measurements taken.

4-8

TABLE 4.1-4

THERMOWELL WEAR CHARACTERISTICS
HOT LEG
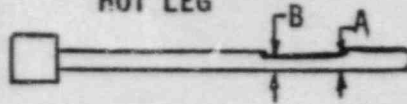
LOOP	LOCATION WRT CLOCK (1)	TAG #	A-DIM	B-DIM	WEAR MILLS	FLOW DURATION (HRS)	
						NORMAL FLOW (2)	LOW FLOW (3)
1	2	112HB	.374	.375	0-1	624.3	696.1
2	10	121HB	.374	.375	0-1	1010.9	200.3
2	2	121HD	.373	.373	2	1010.9	200.3
2	4	122HD	.373	.372	2-3	1010.9	200.3
2	4	121HA	.375	.374	0-1	1010.9	200.3
2	9	121X	.375	.374	0-1	1010.9	200.3
2	8	122HA	.373	.374	0-1	1010.9	200.3

(1) Looking toward generator.

4.2 SHAKER TABLE TESTS OF THE ORIGINAL DESIGN AND RESULTS OF THERMOWELL RESPONSE

A shaker table test of the original thermowell was performed. The tested assembly included the original System 80 thermowell, nozzle, RTD and associated RTD instrument head and hardware including actual cable. The objective of the test was to determine the natural frequency and damping properties of the thermowell assembly and to define the accelerations at various locations on the thermowell assembly; i.e., the RTD head , the upper part of the thermowell nozzle, the external tip of the thermowell and the internal tip of the thermowell via a modified RTD probe (accelerometer mounted in tip of RTD).

4.3 DESCRIPTION AND RESULTS OF FLOW LOOP TESTS AT C-E (NUCLEAR LABS) AND C-E KSB (PUMP LOOP TESTS)

The objectives of the C-E (Nuclear Labs) test and C-E KSB (Pump Test Loop) tests were to determine the cause of failure of the original thermowell design and to verify the thermowell redesign. This section of the report is devoted to the first part of the objective. Design verification of the redesigned thermowell by these tests is discussed in Section 6.1 of this report.

4.3.1 TF-2 Tests

The C-E (Nuclear Labs) test was conducted in Test Facility No. 2 (TF-2). The postulated cause of failure of the System 80 design was flow induced vibration due to vortex shedding. The primary purpose of the TF-2 test was to characterize this phenomenon under controlled conditions.

This testing subjected each thermowell to flow velocities exceeding the range of field conditions. An accelerometer installed inside an RTD probe (internal accelerometer) was used to monitor movement of the thermowell tip. This accelerometer is limited to test temperatures below 250°F. A second (external) accelerometer was attached to the thermowell socket and was able to transmit information over all test temperatures. While direct measurement of thermowell tip motion is not possible over 250°F, the external accelerometer can monitor for impacts. The thermowell could impact against the nozzle if the initially specified thermowell preloading (or fit) in the well was insufficient or if wear of the nozzle and/or thermowell developed due to flow induced vibration. Two pressure transducers were mounted in line with, and downstream from, the thermowell to monitor local pressure fluctuations.

The test setup required installing the RTD nozzles in a test flange. Upstream and downstream flow tubes were bolted to a test flange and the entire assembly mounted in Test Facility No. 2.

A real time analyzer was used to
identify significant changes in energy density of the accelerometer
and pressure transmitter signals. Once a point of interest was
identified, the loop flow was held constant and data recorded. A
high speed chart recorder and photographs from the real time anal-
yzer or an oscilloscope was used to supplement tape recorded data.

Result from the flow loop tests are still being evaluated. Test
results will be used to demonstrate adequacy of the stress analysis
for the redesigned thermowell.

4.3.2   CE/KSB Pump Loop Tests

To more closely simulate actual cold leg conditions, a second test
was conducted at the C-E KSB (Pump Test Loop) facility. These tests
were conducted in the test loop used for testing the reactor coolant
pumps. This test focused on the determination of the flow environ-
ment downstream of the Reactor Coolant Pumps, where the thermowells
are installed on System 80 plants.

The exact thermowell locations could not be duplicated due to
differences in configuration between the pump test loop and System
80 reactor coolant loops. The thermowells were located four (4)
inches closer to the RC pump in the test loop because of a piping
transition. Locating the instruments closer to the pumps is con-
sidered conservative.

During the initial phase of testing, three thermowells were install-
ed to simulate the cold leg thermowells on System 80 plants.
Thermowells, modified with pitot probe instrumentation, were in-
stalled in the nozzles. A typical pitot probe is shown on Figures

4- 12

4.3-1 and 4.3-2. The three pitot probes were calibrated individually for velocities and temperatures ranging from   to   ft/sec. and   to   F, respectively. During the second phase of testing, the 10 o'clock and 12 o'clock pitot probe modified thermowells were replaced with two redesigned thermowells and pressure transducers were installed downstream of each thermowell. This instrumentation was installed to monitor pressure pulsations as a result of vortex shedding and fluid disturbances introduced by the reactor coolant pumps. The redesigned thermowells which were installed were instrumented with internal and external accelerometers to detect the response to structural vibration.

Results from the pump loop tests are still being evaluated. Test results will be used to demonstrate adequacy of the stress analysis for the redesigned thermowell.

PITOT TUBE INSTALLATION FOR THE
PRECISION TAPERED NOZZLE

FIGURE 4.3 - 1

PITOT TUBE PROBE PORT DESIGNATIONS
(TYPICAL ALL PROBE)

FIGURE 4.3 - 2

4-15

5.0 DESIGN MODIFICATIONS

5.1 DESCRIPTION OF THE REDESIGNED THERMOWELL AND A DETAILED DISCUSSION OF FIELD INSTALLATION

The original thermowell and nozzle assembly is shown on Figure 5.0-1. A small radial gap (.001 to .006") existed for the last 2.13" at the lower end of the nozzle. Relative motion between the thermowell and the nozzle as a result of flow induced vibration and the close proximity of the natural frequency of the thermowell to the vortex shedding frequency caused wear on the nozzle and thermowell. The high cycle vibration of the thermowell also caused the thermowell to fail at the interface between the slender part of the thermowell and the enlarged part at the top of the thermowell.

The modified design of the thermowell and nozzle assembly is shown on Figure 5.0-2. A comparison of the original and redesigned thermowells is shown on Figure 5.0-3. The major objectives of the redesign were to:

1) Increase the natural frequency of the thermowell to move it away from the potential vortex shedding frequency.
2) Eliminate the clearance and, thus, the motion at the support between the thermowell and nozzle.
3) Reduce stress levels.
4) Decrease the effects of vortex shedding.

The stiffness of the thermowell and therefore the natural frequency was increased by increasing the basic diameter of the thermowell from .375 to .700 inch. It was possible to increase the thermowell diameter to this value without increasing the outside diameter of the nozzle. The diameter of the thermowell in the area adjacent to the inside of the pipe wall where the original thermowells failed was increased from .375 to .500 inch. The outside diameter of the thermowell was tapered down to the original thermowell diameter at the tip of the thermowell. The smaller diameter at the tip of the thermowell is required to maintain the temperature response time of the RTD instrument.

In order to eliminate the clearance at the support between the thermowell and nozzle, the thermowell was designed to be locked into the nozzle. An axial preload force is restrained by the taper on the thermowell and the mating taper on the nozzle ID. This preload is maintained by the thread at the top of the thermowell and mating thread on the nozzle.

Some of the original thermowells were shown to fatigue at the point where they intersect with the inside wall of the RC pipe. The part of the thermowell which is exposed to the reactor coolant flow performs like a cantilever beam, where the maximum bending is at the

The insertion length of the thermowell into the reactor coolant flow stream has been decreased from 2.5 inches to 2.125 inches. This also helps to reduce the bending load on the thermowell. Stresses at the intersection of the enlarged section at the top of the thermowell and the shank were reduced by increasing the cross-sectional area by 5.5 times and, also, adding a large chamfer to reduce stress concentration effects.

The transition taper, on the part of the thermowell which is inserted into the flow stream, has been shown to reduce the effects of vortex shedding. The tapered section prevents organized vortex shedding from occurring due to the changing diameter along the length of the thermowell. Ideally, the thermowell would have been tapered all the way to the tip. This was not feasible because of the adverse effect of the thicker section on the RTD instrument's capability to quickly sense changes in temperature.

A seal weld is provided at the top of the thermowell and nozzle to seal against reactor coolant pressure. Chromium plating on the support taper and thread on the thermowell provide a hard surface which serves to reduce friction of the thermowell during installation and prevents galling.

All of the original thermowell and nozzles on Palo Verde Units 1, 2 and 3 are being replaced with the modified design.

RTD/TW INSTALLATION ORIGINAL DESIGN

FIGURE 5.0 - 1

RTD LOCATION

THERMOWELL

PIPE NOZZLE

HOT LEG PIPE WALL

COLD LEG PIPE WALL

LOCATION
OF FAILURES

.001 - .006"
DIAMETRAL
CLEARANCE

2.13"

2½"

.375"

MODIFIED THERMOWELL & PIPE NOZZLE

FIGURE 5.0 - 2

RTD LOCATION

THREADED
TO FACILITATE
PRELOAD
ON TAPER

0.700"

CHROME PLATED
OVER THIS LENGTH

PIPE WALL

2.0"

.500" DIA.

2.125"

0.375"
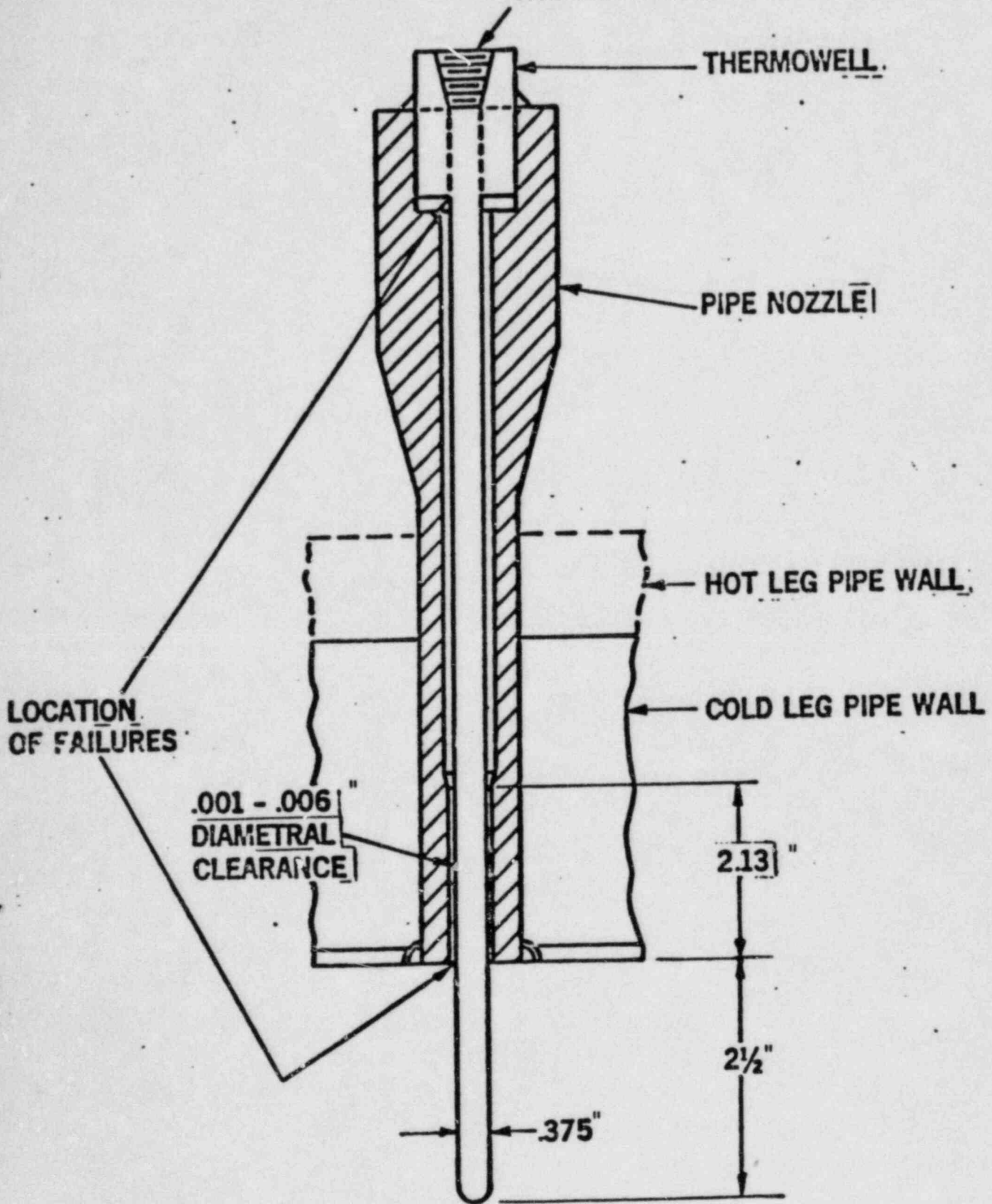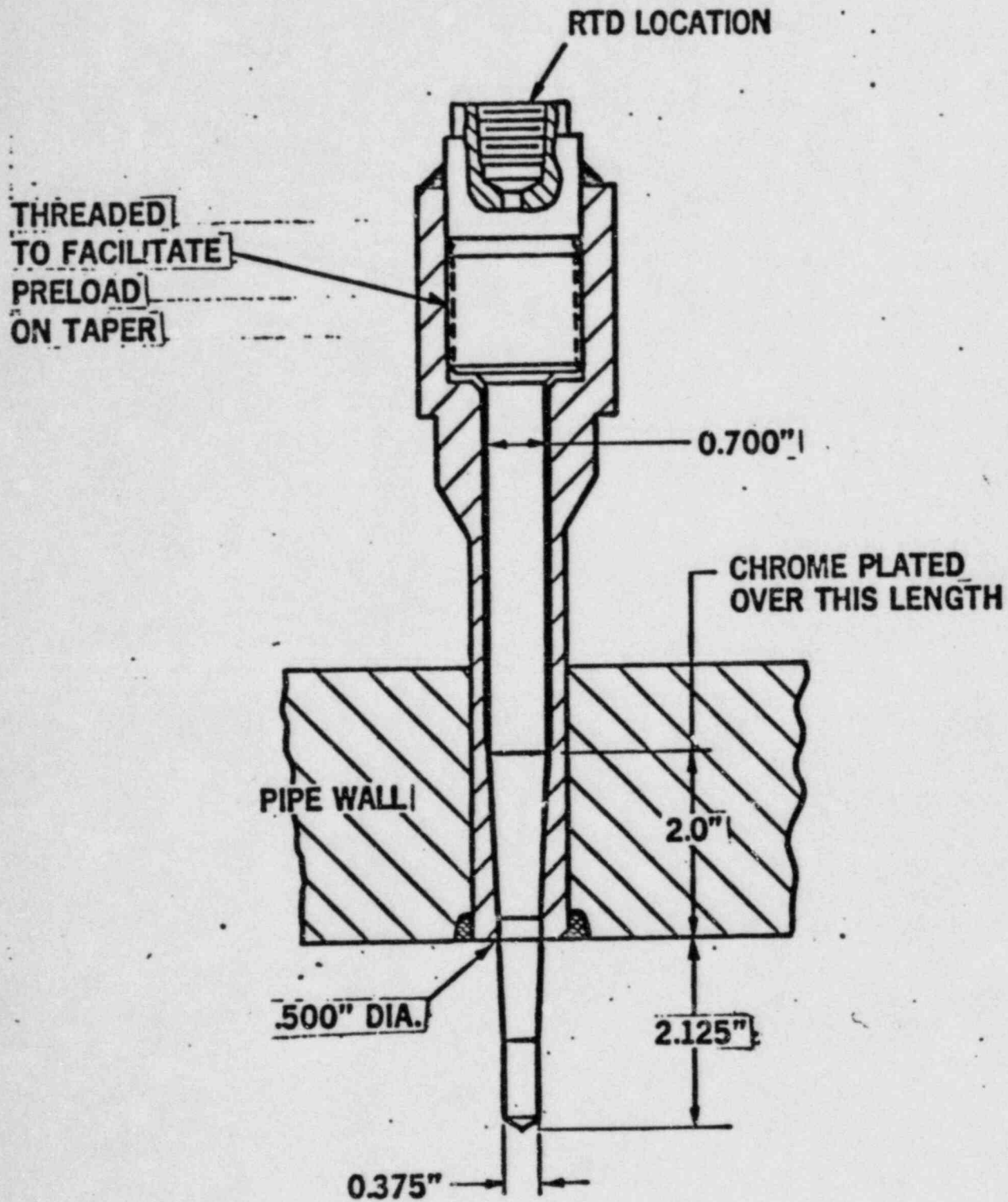
ANPP-1 THERMOWELL
DESIGN COMPARISON

FIGURE 5.0 - 3

(REDESIGNED)   (ORIGINAL DESIGN)

CHROMIUM
PLATED THREADS
TO FACILITATE
PRELOAD
ON TAPER

.700"

12.0"

8.375"

CHROMIUM PLATED
OVER THIS LENGTH

.500"

.375"

11.370"

9.870"

.375"
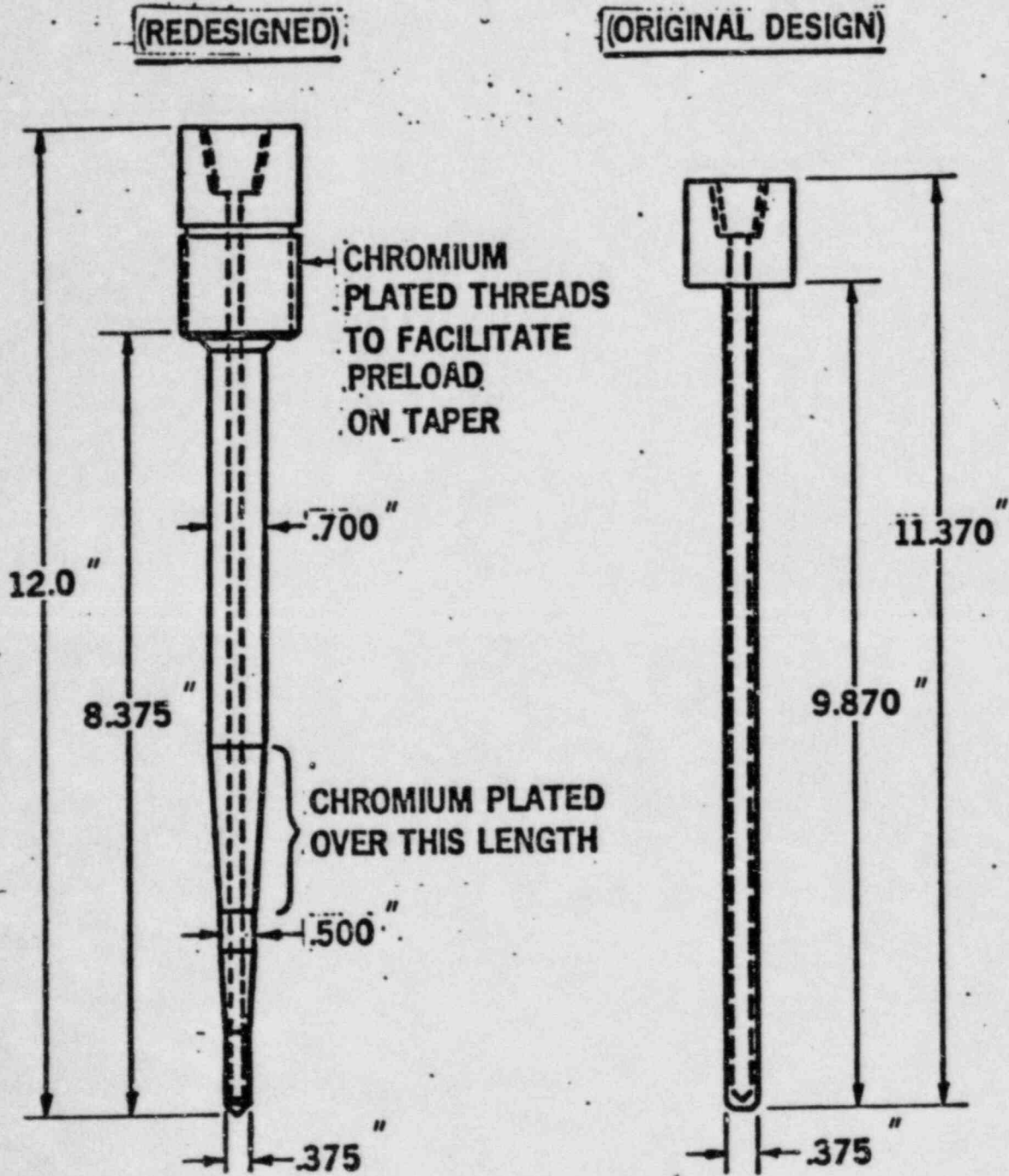
6.0 TESTS AND ANALYSIS (DESIGN VERIFICATION)

6.1 DESCRIPTION OF ANALYSIS AND TESTS WHICH VERIFY DESIGN ACCEPTABILITY AND RESULTS

6.1.1 Structural Analysis

The structural analysis performed to verify the new thermowell design considered the redesigned RTD nozzle and associated weld in addition to the redesigned thermowell and the thermowell to nozzle fillet weld. All stress results are satisfactory and meet the requirements from Section III of the ASME Boiler and Pressure Vessel Code.

The RTD nozzle is installed in the RC piping by means of a partial penetration (J-groove) weld. See Figure 6.1-1. The requirements for reinforcement area of the RC piping due to penetration holes were checked for the redesigned nozzle and found to be satisfactory.

A computer program was utilized to determine the discontinuity stresses in the nozzle, pipe and the attaching partial penetration weld by means of an interaction analysis. The computer program also established the cumulative damage ratios (fatigue factors) of the attaching weld. The finite element method of structural analysis, implemented in the ANSYS program, was used to model the upper section of the redesigned thermowell nozzle. Table 6.1-1 lists the maximum stresses for the RTD nozzle and attaching weld for various loading conditions. Allowable stresses for each loading condition are also listed.

The thermowell and the thermowell-to-nozzle fillet weld were analyzed for primary stress, primary-plus-secondary stresses, peak stresses and for fatigue usage factors. The stresses considered result from the external pressure loading, thermal loading, flow induced loading, seismic loading, preload and external mechanical loading which exist under design operating conditions of the RCS piping.

The analysis demonstrates the thermowell meets the requirements of Section III of the ASME Code. The thermowell was found to be capable of safely withstanding all transients specified for the ANPP Unit-1 Reactor Coolant piping system.

The thermowell was analyzed for minimum thickness requirements for externally pressurized cylinders per ASME Code Requirements and found acceptable. The minimum thickness required is   inch while the actual thickness is   inch.

A sketch of the thermowell and nozzle assembly shown on Figure 6.1-1 identified the cross-sections and locations where stresses were calculated. The calculated stress levels and allowables for the thermowell are listed in Table 6.1-2.

The thermowell natural frequency was calculated using ANSYS Finite Element Program. The computer model used simulated the entire thermowell assembly including, the thermowell, nozzle RTD and associated hardware including the cable. The nozzle was assumed fixed to the piping while the thermowell was assumed fixed to the nozzle at the top and pin connected to the nozzle at the support taper. The natural frequency and seismic response spectra were used to determine the seismic loads which act on the thermowell.

The flow induced vibration (at vortex shedding frequency) stresses in the thermowell were calculated based on published papers on the subject and standard structural analytical techniques. The flow induced loads consist of a steady drag force and an oscillating lift force. This lift force oscillates at the vortex shedding frequency

which is less than 50 percent of the natural frequency. Because of the contact fit at the support taper, all of the flow induced loads are reacted into the RTD nozzle tip at Cut A. Thus Cut A was analyzed for the full flow load.

Results from the Newington pump test loop will be used to demonstrate that loadings used in the analytical evaluation were conservatively assumed. In addition, local flow velocities and flow effects downstream of the RC pumps at the location of the cold leg thermowells are being observed as part of the Newington test.

The static pressure stresses in the hoop and radial directions are found by use of the LAME equations for thick-walled cylinders. The axial pressure stress is found using simple statics.

The mechanical load stresses due to dead weight, preload, externally applied loads and seismic forces are calculated using standard engineering formulas. The cold leg seismic forces are conservatively used in the analysis.

The thermal stresses at Cut A are calculated using an interaction analysis. The thermal stresses at Cut B are found using the equilibrium of forces and displacements in the "locked-in" condition which exists between the nozzle and thermowell.

The fatigue evaluation is based on a design fatigue curve for NI-CR-FE alloy 600 which provides stresses and cycles to failure up to 10^8 cycles. The ASME code endurance limit of 13.6 KSI is used in the fatigue evaluation. The endurance limit is defined as the stress value below which failure would not occur at any number of cycles.

6.1.2   Flow Loop Tests (TF-2)

The redesigned thermowell was tested in a flow test loop at the C-E
Nuclear Labs. This test facility is referred to as Test Facility
No. 2 (TF-2). The thermowell tested is shown on Figure 6.1-1.

The TF-2 test was conducted to observe the redesign under controlled
flow conditions and determine the effects of vortex shedding.
Testing subjected the thermowell to a range of flow velocities
exceeding those expected under field conditions. An accelerometer
installed inside an RTD probe (internal accelerometer) was used to
monitor movement of the thermowell tip. This accelerometer is
limited to test conditions up to 250°F. A second (external) accel-
erometer was affixed to the thermowell nozzle OD and transmitted
information over all test temperatures.. While no direct measurement
of thermowell tip motion is possible over 250°F, the external
accelerometer can monitor sympathetic response. Two pressure
transducers were also mounted in line with, and downstream from, the
thermowell to monitor local pressure fluctuations.

The test setup required installing the RTD nozzle in a test flange.
Upstream and downstream flow tubes were then bolted to the test
flange and the entire assembly mounted in Test Facility No. 2 of the
Engineering Development and Test Laboratory.

A real time analyzer was used to
identify significant changes in energy density of the accelerometer
and pressure transmitter signals. Once a point of interest was
identified, the loop flow was held constant and data recorded. A
high speed chart recorder and photographs from the real-time anal-
yzer or an oscilloscope was used to supplement tape recorded data.

The thermowell was removed after the six (6) hour test was completed and did not show any sign of wear.

6.1.3   Pump Loop Tests

The redesigned thermowell was tested in the C-E KSB pump loop simultaneously with the retesting of the reactor coolant pumps. The redesigned thermowell was installed during the second of two phases of testing. The test duration lasted over 180 hours. The purpose for the test was to verify that design objectives were met. The objective of this test was to test the redesigned thermowell against the influence of the flow from the reactor coolant pump.

The redesigned thermowell was installed in a 10 O'clock position to simulate the actual worst case field installation. Because of differences between the test loop and the actual loop, the thermowell had to be located 4 inches closer to the pump which is considered conservative because the pump will have more of an influence on the approach flow to the thermowell. The thermowell was equipped with an internal accelerometer, external accelerometer and pressure transducer similar to the TF-2 test.

The thermowell was removed after completion of 180 hours of testing and did not exhibit any signs of wear or other damage.

The test data for the tapered thermowell design tested in the Newington flow loops has not yet been reduced. This data will be evaluated to verify adequacy of the stress analysis previously discussed.

6-6

6.1.4   Shaker Table Tests

A shaker table test of the redesigned thermowell was performed. The configuration tested included the redesigned thermowell and nozzle with a mounting block to resemble the pipe wall, the actual cable and the RTD enclosure head. The objective of the test was to determine vibration characteristics for the assembly. A worst case installation orientation was considered. Accelerometers were used on the RTD head, the upper part of the nozzle, the external part of the tip of the thermowell and the internal part of the tip of the thermowell via a modified RTD probe (accelerometer mounted in tip of RTD).

TABLE 6.1-1

STRESS LEVELS AND ALLOWABLES
FOR REDESIGNED RTD NOZZLE

TABLE 6.1-2

STRESS LEVELS AND ALLOWABLES
FOR REDESIGNED THERMOWELL

MODIFIED THERMOWELL & PIPE NOZZLE

FIGURE 6.1 - 1

RTD LOCATION

SEAL WELD (FILLET)

THREADED TO FACILITATE PRELOAD ON TAPER

CUT B

0.700"

CHROME PLATED OVER THIS LENGTH

PIPE WALL

2.0"

TAPER

CUT A

J GROOVE WELD

.500" DIA.

2.125"

POINT 1

CUT C

TIP

0.375"
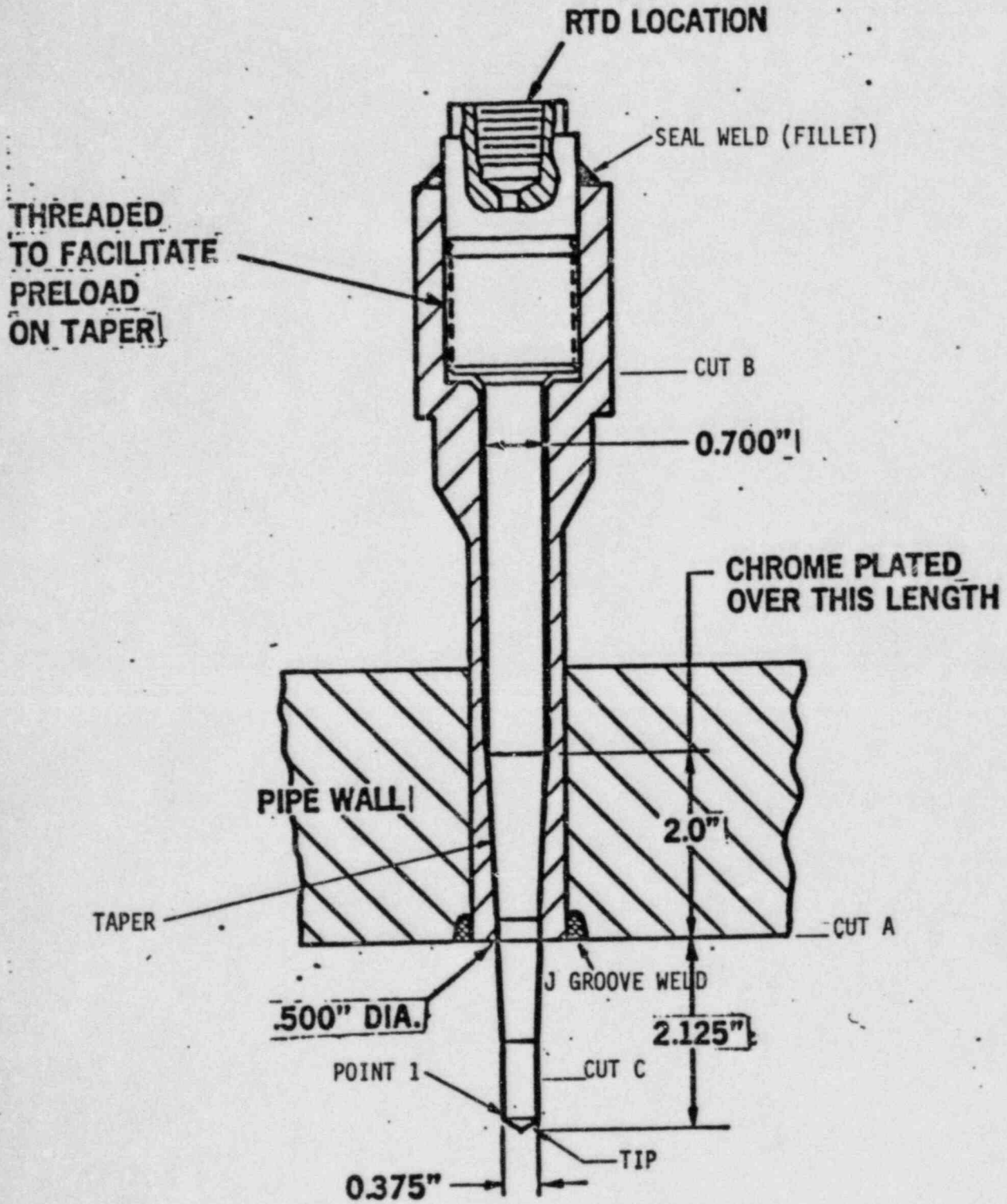
6.2   DESCRIPTION OF TEST PERFORMED DURING RESTART TESTING AND RESULTS

Restart testing of Palo Verde Unit-1 has not yet begun. The plan
for testing the redesigned thermowell during restart is limited to
establishing that the thermowell response is consistent with that
observed during other tests and by analysis. Inconsistencies, if
any, will be further evaluated. During restart testing, various
thermowells will be equipped with internal accelerometers, and three
triaxial accelerometers will be used to determine R C pipe motion at
the location where the RTD's are installed to verify the design
input to the analysis.

INTERIM REPORT ON THE PERFORMANCE EVALUATION OF THE PALO VERDE CONTROL ELEMENT ASSEMBLY SHROUD

January, 1984

POWER SYSTEMS

COMBUSTION ENGINEERING INC

LEGAL NOTICE

ABSTRACT

An investigative program is described to evaluate the nature and extent of cracks which were seen in the Control Element Assembly (CEA) shroud following the pre-core hot functional tests on Palo Verde Unit 1 in July, 1983. A combination of experimental and analytical results to date indicate that vibration caused the fatigue cracks in localized regions with high stress concentration. A modified design minimizes this stress concentration and limits the maximum possible amplitude of the likely damaging mode of vibration.

This is an interim report. It will be reissued with final results after the completion of a demonstration test with the modified shroud in Palo Verde Unit 1. Extensive temporary instrumentation in the reactor test will help to confirm the conclusion from the prior testing and analyses.

Table of Contents

Table of Contents

List of Figures

List of Figures

List of Tables

1.0   INTRODUCTION

1.1   DESCRIPTION OF PROBLEM

Inspection of the Palo Verde Unit 1 reactor internals subsequent to
Pre-Core Hot Functional Testing (PCHFT) revealed damage to the Control
Element Assembly shroud (CEA shroud). The CEA shroud is part of the
Upper Guide Structure (UGS) assembly (see Figures 1-1 and 1-2). The
CEA shroud consists of an array of vertical round tubes 9 in O.D. which
are arranged in a square grid pattern with 16 in pitch. The tubes are
joined by welding vertical plates called webs between adjacent tubes.
Tubes and webs are made from 3/16 in type 304 stainless steel. The
purpose of the CEA shroud is to provide separation of the CEA assemblies.
The CEA shroud is mounted on eight pads on the UGS base plate and is held
in position by eight tie rods which are threaded into the UGS base
plate at their lower end. At their upper end, the pre-tensioned tie
rods are held by nuts which bear on eight plugs in the tops of eight
of the CEA shroud tubes. Guides for the 4-finger CEA extension shafts
are attached to the top of the tubes and guides for the 12-finger CEA
extension shafts are attached to the webs (see Figure 1-3). These
guides serve the purpose of aligning CEA extension shafts for entry
into the closure head nozzles during closure head installation and into
the internals lift rig during attachment.

The damage, revealed by visual and dye penetrant examination consisted
of the following:
1. A total of 13 cracks in eleven 4-finger CEA shroud tubes. In most
    instances, these cracks start in the welds at the attachment of the
    4-finger CEA guides to the shroud tubes.
2. Two cracks involving the welds at the attachment of the 12-finger
    CEA extension shaft guides to the webs.
3. Three cracks involving the welds between 4-finger CEA shroud tubes
    and webs; two at the top of the shroud and one at the bottom.
4. One crack in the base metal of a web.
5. Three wear marks on the shroud at the 45° location.
6. One ductile break, one half inch long, located in a web at the
    bottom.

The locations of the above described damage are shown on Figure 1-4.

1.2 SAFETY IMPLICATIONS

The CEA shroud is a feature first used in the C-E System 80 reactor. The design is not used on other C-E NSSSs. In addition to Palo Verde Unit 1, similar CEA shrouds are part of the UGS delivered to Palo Verde Units 2 and 3, and other S80 plants under construction. The Palo Verde Unit 1 and all of the other units are in the construction phase and, therefore, the problem described herein does not affect any operating reactor.

The CEA shroud is not a core support structure under the definition of the ASME code, Section NG, and does not in itself perform a safety function. The assemblage of long tubes and webs serves to provide separation of the CEAs. Flow is restricted within the CEA shroud region and, therefore, the shroud is not subjected to significant operating loads. On previous C-E NSSS designs, the same function of providing separation of the CEAs is provided by heavier tubes, also called shrouds, which are designed as part of the support structure of the UGS and are exposed to the flow forces in the upper plenum.

The extension shaft guides located at the top of the shroud are provided to align CEA extension shafts for entry into the closure head nozzles during closure head installation. They have no function during reactor operation. Although not observed, a hypothetical, complete failure in CEA shroud tubes or webs particularly to the extent that extension shaft guides loosen or become detached, would have potential adverse safety implications in that the inser- tion of CEAs could be impeded or prevented by interference with the loose components. The damage which was observed on the Palo Verde Unit 1 shroud would not have prevented reactor trip had it been present in an operating reactor. The repair described in Section 5.0 includes removal of the CEA guides, thereby eliminating the potential for interference with CEA inser- tion.
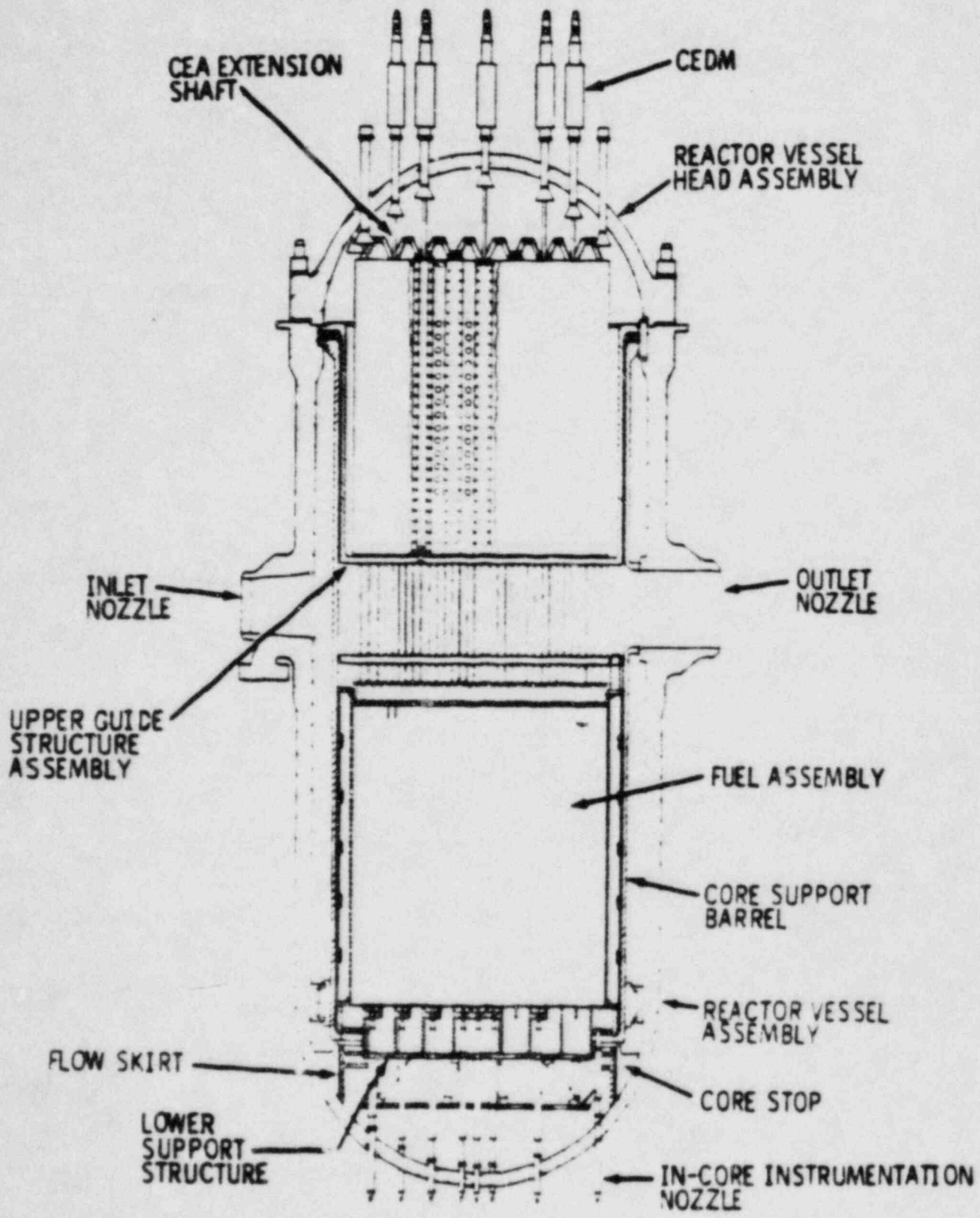
FIGURE 1-1

REACTOR VERTICAL ARRANGEMENT
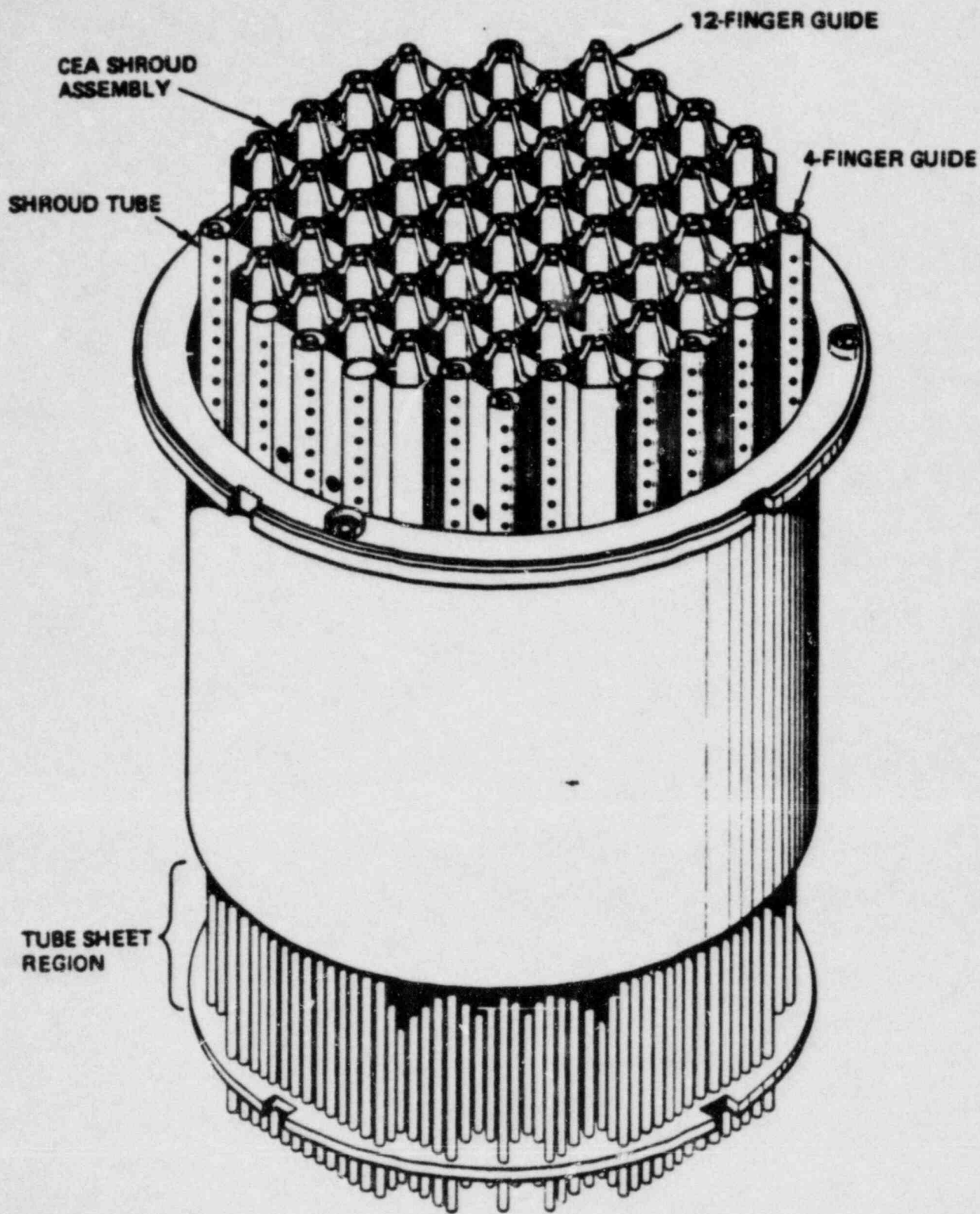
FIGURE 1-2

UPPER GUIDE STRUCTURE
ASSEMBLY

1-4

FIGURE 1-3
CEA EXTENSION SHAFT GUIDES

TWELVE FINGER
EXTENSION SHAFT
GUIDE

4 FINGER EXTENSION
SHAFT GUIDE

BACKING
PLATE

SHROUD WEB

SHROUD TUBE
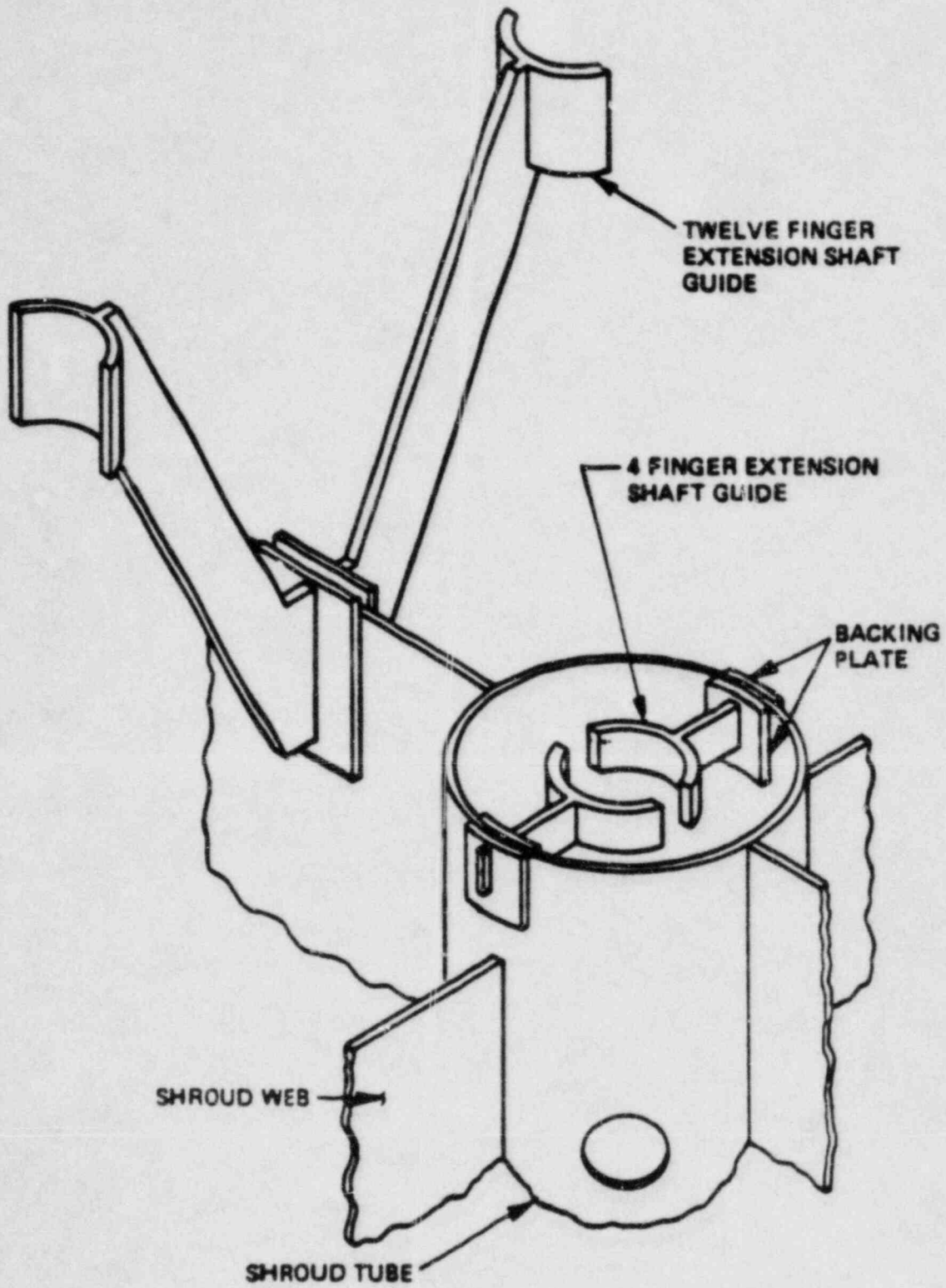
FIGURE 1-4
CEA SHROUD ASSEMBLY
CRACK LOCATIONS
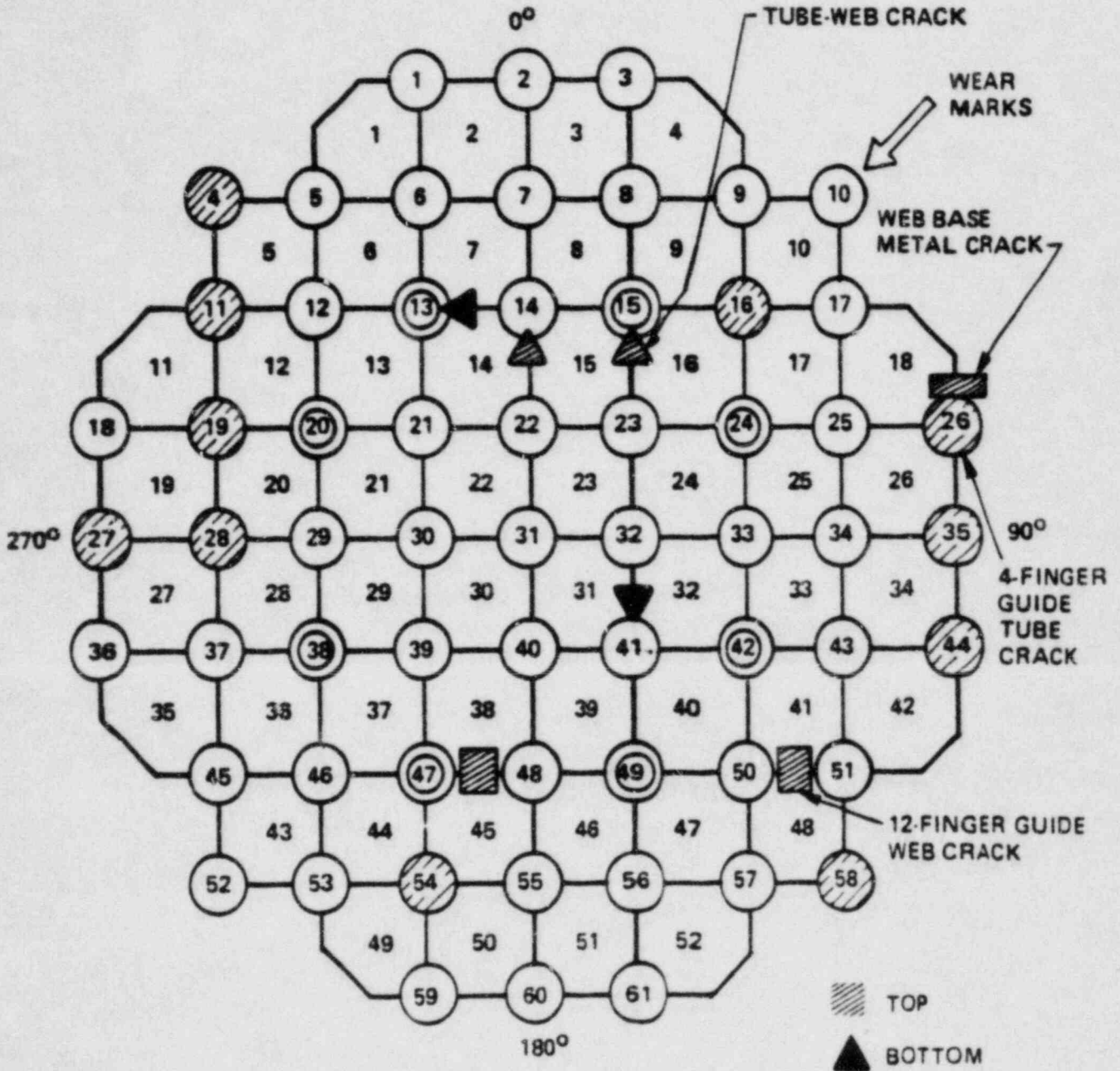
2.0 SUMMARY

2.1 DESCRIPTION OF INSPECTION, TESTING AND ANALYSIS RESULTS

2.1.1 Inspection Results

Visual inspection of the shroud following the Pre-Core Hot Functional Test (PCHFT) was conducted as part of the Comprehensive Vibration Assessment Program (CVAP) required by Reg Guide 1.20 for Palo Verde Unit 1, which is the first System 80 NSSS. During the inspection, seven cracks were observed at the tops of CEA shroud tubes. Subsequent dye penetrant inspection over the top and bottom of the shroud revealed a total of 19 indications. Of the 17 at the top, 14 were in the weld heat affected zone adjacent to the location of attachment of the CEA extension shaft guides.

A metallurgical program was established to identify the nature of the failures. Samples of the shroud were removed and examined. Metallography and chemistry confirmed that the shroud material was as specified. Fractography of the fractured surfaces showed that the failures occurred by high cycle fatigue; i.e., by induced cyclic stresses of a magnitude at or near the endurance limit of the material. This result led to the investigation of sources and modes of vibration of the shroud and of the CEA guides.

2.1.2 Testing To Identify Hydraulic Forcing Functions

The investigation includes testing to identify hydraulic forcing functions. A shroud tube with 4-finger CEA guides was subjected to a range of flow velocities which encompassed those calculated to exist in the shroud region of the reactor during the pre-core tests. The experiment (See Section 4.1.1) could not identify direct hydraulic forces on the shroud which could make a significant contribution to shroud failure.

2.1.3 Vibration Testing

This phase of investigation consists of three vibration tests. In the first test (Section 4.1.2), an extra CEA shroud assembly identical to the Palo Verde Unit 1 shroud and located in the manufacturer's shop was instrumented with accelerometers to identify modes of vibration. Excitation by impacting identified resonance frequencies for the CEA guides and for single shroud tubes in the assembly. These frequencies are generally higher than those typically associated with internals vibration, but are in the range of the reactor coolant pump blade passing frequency and its first harmonic and are in the range of the resonant frequency of the tubes of the upper plenum tube sheet (See Figure 1-2). With appropriate forcing functions to induce it, vibration at these frequencies is a potential cause of the failures.

The second vibration test was performed by a consultant (Section 4.1.3) on the Palo Verde Unit 1 CEA shroud after its return to the shop. This test included modal testing in both air and water. It confirmed the earlier results for the resonant frequencies of the CEA guides and the shroud tubes in air, and in addition, identified modes of vibration of the overall shroud assembly. The frequencies of the assembly modes were much lower than frequencies of the shell modes of the tubes. If the assembly modes are excited, they are another potential cause of the observed failures through bending deformations of the shroud assembly.

The third vibration test (Section 4.1.4) was performed on a single CEA shroud tube with three attached webs. Resonant frequencies for the tube and CEA guides were again identified and were approximately the same as from previous tests. Extensive instrumentation combined with excitation by a controlled load electro-magnetic exciter placed at three different elevations provided a thorough characterization of the modes of vibration of the CEA guides and shroud tube. Also, known boundary conditions for the tube and web supports enable an analytical model of a shroud tube to be experimentally correlated. This analytical model of a single tube is then used to calculate stresses in tubes for normal operating loading conditions.

This mechanical excitation test also provided some confirmation of the nature of the structural failures by deliberately inducing failure in the test shroud tube. At the resonant frequency of the CEA guides, the exciter load was fixed to give a specified measured strain or local stress in the tube adjacent to the CEA guides and excitation was continued until failure. A comparison of the measured stress with the material fatigue stress at the observed number of cycles to failure yields an estimate of the stress concentration caused by the welded configuration of the attachment of the CEA guides to the shroud tube. The validity of this estimate is is supported by the fact that the crack produced experimentally is similar to most of the cracks in the reactor shroud tubes.

This test was continued after removal of the top three inches to simulate the shroud modification summarized in Section 2.2.. Results of the tests on the modified tube will be presented in the final CEA shroud report. Preliminary results from testing to date show that the natural frequency associated with the CEA guide is eliminated.

2.1.4 Analytical Modeling

This portion of the investigation is the analyses of the shroud failure (Section 4.2). Three stages of successively more detailed analytical modeling are employed. In the first stage, the entire upper guide structure assembly is modeled (Figure 1-2). The analytical model is subjected to the loading from random pressure acting on the tube bank. The pressures were obtained from the data taken during the pre-core hot functioinal test. The result of this stage of analysis is the lateral acceleration of the UGS support plate to which the CEA shroud is connected.

The second stage of analyses models the CEA shroud assembly. The resultant calculated assembly modes of shroud response are partially verified by the modal testing described in Section 4.1.3. Input loading to this global model is the acceleration of the Upper Guide Structure Support Plate (UGSSP)obtained from the first stage. Output includes the lateral displacement and moments which are transmitted by the connecting webs to individual shroud tubes.

The third stage is a detailed finite element model of a single tube, including the CEA guides and the webs. This detailed model is verified by the experiments described previously. Moments and displacements at the web-to-tube junctions as obtained from the second stage are input to the single tube model. The result is stresses in the tube as a consequence of deformation induced by the over all shroud global motion. Stiffening of the shell locally by the CEA guide attachment increases the local stress in the tube wall near the location of the observed failures.

Results of this three stage analysis identify a near coincidence of the beam mode frequency of the UGS barrel and one of the assembly modes of the CEA shroud. These frequencies are below the resonant frequencies of the CEA guides and tubes. Calculated displacements of the outermost shroud tubes are larger than the minimum measured clearance at one corner between the UGS barrel and the CEA shroud. This result is supported by the observed impact marks on the shroud tube and barrel at one location. The displacement amplitude calculated with this mode is sufficient to cause local tube stresses larger than the fatigue stress. These analyses are continuing, to try to identify additional global or overall assembly modes which can induce stresses sufficient for failure.

The impacting of the CEA shroud against the UGS barrel at the flange elevation was evident from wear marks on one tube. Mechanical excitation tests show that impact can excite the resonant frequency of the CEA guides. Hence, impacting might have been a contributor to failure.

The hydraulic test did not identify direct hydraulic forces within the CEA shroud as a cause of failure. However, the normal flow through the upper plenum does contain random and periodic dynamic pressure pulsations which could be mechanically transmitted through the structure to the CEA shroud. The frequency content of these pulsations encompasses the resonant frequencies of the CEA guides and shroud tubes. It is questionable, at present, whether sufficient energy can be transmitted to the shroud at these frequencies to cause the observed failures.

2.2   DESCRIPTION OF DESIGN MODIFICATION

Two design modifications eliminate potential causes of the failures which were identified by test and by analysis. First, the top three inches of the CEA shroud is removed along with all the CEA guides. This has two effects. It eliminates the potential resonance failure caused by vibration of the CEA guides. It also eliminates the high stress concentration at the top of the web-to-tube junctions and thereby reduces the local stresses induced by global shroud vibration. The function of the CEA guides is provided by a separate tool which is utilized only during refueling operations. It is removed during reactor operation.

The second modification is the addition of snubbers which limit the lateral displacement of the CEA shroud in the global modes of vibration. Snubbers are located on the shroud at the UGS flange elevation and transmit the loading to the UGS flange.

Additionally, welds at the web-to-tube junctions near the top and at the tie rod locations on the bottom of the shroud are upgraded to full penetration welds and are fully dye penetrant inspected. Thus, potential crack initiators resulting after cutoff of the shroud are minimized.

2.3 DESCRIPTION OF TEST, ANALYSES AND RESULTS OF MODIFICATION

Mechanical excitation tests of a modified CEA shroud tube will be performed as an extension of the test with the CEA guides which was taken to failure. The test with the modification will confirm the detailed analytical model of a modified shroud tube. Results of this test will be presented in the final shroud report.

The modifications do not substantially alter the overall shroud configuration. Consequently, the same analytical models used to describe the failure modes are used to describe the shroud performance after the modification (Section 5.1.2). The most significant effect is caused by the snubber. It introduces a load path between the CEA shroud and the UGS flange. Preliminary analytical results indicate that the load on the flange is acceptable and that the overall dynamic response of the UGS is improved. Complete analytical results will be included in the final report.

Results from the demonstration test on the reactor (Section 6.2) will be presented in the final report. This test complements the component testing and the analytical results for shroud performance. It will be used to confirm the acceptability of the UGS performance with the modified CEA shroud, to verify the hydraulic loading on the UGS, to determine the hydraulic loading directly on the CEA shroud and to verify the structural integrity of the CEA shroud assembly.

3.0 INSPECTIONS AND EXAMINATIONS

Visual inspection of the Palo Verde Unit 1 shroud following the precore hot functional tests revealed cracks at the tops of seven of the CEA shroud tubes. A program of metallurgical examinations was immediately begun to determine the nature and extent of the cracking. This section describes that program and the results obtained.

3.1 Description of Cracks

Initial visual inspection showed cracks at the tops of seven of the shroud tubes. The cracks were adjacent to the bracket plates to which the CEA extension shaft guides are welded. Figures 3-1 and 3-2 show two of these cracks. Subsequently, dye penetrant inspection of the upper and lower twelve inches of the shroud identified additional cracks in various locations. Figures 3-3 and 3-4 show all the locations and the configurations of the cracks. These are categorized and described in the following.

3.1.1 Cracks near 4-Finger CEA Guide Brackets

These cracks include the seven initially seen visually during post-test inspection. They run vertically along the toe of the fillet weld joining the bracket to the tube. Additional cracks were also located in the weld bead, having initiated from the weld root. Figures 3-1, 3-2 and 3-5 are representative.

3.1.2 Cracks near 12-Finger CEA Guide Brackets

The 12-Finger brackets are welded to the webs which join the tubes. The cracks run vertically along the weld which joins the brackets to the webs. Figure 3-6 is representative of the two such cracks found.

3.1.3 Tube to Web Cracks

These cracks were found near the welds which join the tubes and webs. They occur on both the web side and the tube side of welds. Figure 3-7 is representative of these cracks.

3.1.4 Web Base Metal Cracks

Only one crack was found which was not associated with a weld. The crack initiated at the corner of the rectangular cut-out of a web. Figure 3-8 shows this crack.

3.1.5 Bottom Cracks

Two cracks were found at the bottom of the shroud. They run vertically near the welds joining tubes and webs.

3.2 Shroud Construction and Material

3.2.1 Construction

The CEA shroud tubes were constructed of SA240, Type 304 S.S. plate material. The tubes were cold formed from 3/16" plate. The webs were 3/16" and 1/4" plate with the 1/4" plate existing at all web locations around the assembly OD. The webs were welded to the shroud tubes by 1/4" fillets using one of the following processes; shielded metal arc, gas tungsten arc or gas metal arc (MIG). The 4 and 12-finger extension shaft guides were SA-351, Grade CF-8 material. The guides were welded to inner and outer brackets made of Type 304 plate. The brackets were then welded to the ID and OD of the shroud tube with 4-finger guides and to both sides of a web with 12-finger guides. All welds were 3/16" fillets.

3.2.2 Material Examination

Chemical analyses and hardness tests were performed on samples of material taken from the failed shroud. Results of the chemical analyses show that the elemental composition is within the allowable tolerances for chemical requirements per ASTM A480. In the basic material, nothing was found which is considered as a contributing factor to the failures.

Hardness tests were conducted on the tube wall, backing plate and CEA guide. The bracket and shroud tube values are typical for 304 S.S. plate material. The values for the 4-finger CEA guide were as expected for casting material. In conclusion, the failures were not caused by the use of improper materials.

3.2.3 Residual Stresses

Residual stresses are present in the structure prior to operation due to the fabrication processes such as clamping, welding and cold working. Alternating stress imposed on the structure during operation will attempt to raise the maximum stress above the yield point. However, austenitic material will not sustain a mean stress when the alternating stress exceeds the yield strength because yielding occurs. After a few cycles of operation beyond the yield point, the mean residual stress will shake down. Residual stress below the yield point are taken into account by the ASME Code fatigue design curves which are used to design the shroud. The conclusion is that residual stresses were not a significant factor in the shroud vibration cracking.

3.3 Metallographic Examination

Upon receipt of samples cut from the shroud, visual and dye penetrant examinations were performed. Fracture surfaces were visually examined to provide evidence of possible initiation sites. Metallographic samples were prepared to study weld and base metal microstructure. The significant observations associated with the various groups of samples are provided below. The tube numbers referred to below are shown on Figure 1-4.

3.3.1 Top End of the Shroud

3.3.1.1 Finger-Guide Assembly Samples

Visual examination of the cracks showed all were at one time associated with a weld. All cracks were transgranular with no preferential attack or evidence of ductile tearing

The major cracks associated with 4 or 12-finger guides were toe cracks traveling in a longitudinal direction with respect to the welds. Once past the guide assembly region, in most cases the cracks branched off in other directions. Weld and base metal microstructure in the areas of these cracks are typical of type 304 S.S. and indicate no material defects.

Crack initiation near 4-finger guide assemblies probably occured on the ID of the shroud tube because: (a) the cracks were closely associated with the bracket to tube weld fusion line on the ID (see Figure 3-9), and (b) the center lip between the ID and OD crack fronts seen on tube 26 trails back to the OD side (see Figure 3-10).

Weld bead cracks were also identified in several welds and in many cases adjacent to major cracks in both shroud tube 26 and 44 guide assemblies. Figure 3-11 shows a weld bead crack in a tube to bracket weld. Note the close proximity with a major crack at the toe of the same weld. Welds on shroud tube 44, 180° side assembly were completely cracked at both the ID bracket to tube weld and the finger-to-bracket weld (see Figures 3-12 and 3-13).

Cross-sectional mounts of the 4-finger and 12-finger guide assemblies were made to observe weld and base metal microstructure (see Figure 3-14). Weld microstructure indicates lack of penetration in several welds, undercutting in over half the welds and minimum throat dimensions of less than 2/3 of the bracket plate thickness in almost half the welds. The weld shapes produced severe stress concentrations at the root of these fillet welds. Cracks in several of the welds originated at the root of the weld (see Figure 3-15). One crack starting from the root of the bracket to guide weld propagated transversely through a 4-finger guide casting. The crack had reached a depth of approximately 20% of the wall thickness extending along the entire guide to bracket weld area (see Figure 3-16).

3.3.1.2 Shroud Tube to Web Weld Samples

Two samples of tube to web weld locations were removed. Both were located near tube to web welds, however, the crack from tie-rod tube 15 was located on the tube (see Figure 3-7 or 3-17) while the other crack near shroud tube 14 existed on the web (see Figure 3-18).

3-4

The crack on tie-rod tube 15 was approximately 80% through the wall. The uniform crack front indicates compressive stresses probably prevented further propagation. The crack was transgranular with no evidence of corrosion or ductile tearing. The crack propagated away from the web-to-tube weld junction indicating a higher stress condition existed in the base material than at the weld. Crack initiation occured near the top of the web to tube junction based on chevron mark indications which were evident on the fracture surface of the crack shown in Figures 3-7 and 3-17.

An additional observation was also made on tube 15 with regard to a linear indication evident on the right hand side of the tie-rod shroud tube web weld following dye penetrant examination (see Figure 3-17). During field dye penetrant examinations, these indications were widespread. However, the indications were not interpreted as cracks but rather weld discontinuities. As proof, the indication on tube 15 was examined cross-sectionally and no cracks were identified.

The web crack fracture surface near shroud tube 14, as shown in Figure 3-19 provides evidence that the web was experiencing reverse bending loads. Two crack fronts at the crack tip can be seen which is indicative of such a phenomena. Crack initiation location is clearly distinguishable by characteristic beach marks (like the ripples in the sand on a beach) near the top of the web along the toe of the weld.

3.3.1.3 Web Base Metal Sample

The web base metal crack within cavity #18 (see Figure 3-8) was transgranular, propagating from a corner cut-out in a web. Metallographic examination of the fracture surface showed the crack propagated in a reverse bending mode with the appearance of two crack fronts as seen previously in other samples. The sharp angle apparent at the corner of the cut-out induces a high stress concentration upon loading, contributing to crack initiation.

3.3.2 Bottom End of Shroud

Examination of two samples from the bottom end of the assembly was performed. The 1/2" crack from shroud tube 41-to-web weld showed ductile tearing and not fatigue. While impossible to distinguish whether the crack occured prior to or during the pre-core testing, the mode of failure would indicate it was probably an isolated, pre-test failure.

The 2 1/2" crack along the web to shroud tube 13 weld was again a transgranular crack. Initiation, however, did not appear to have occured on the bottom of the tube to web weld but up 2" (see Figure 3-20). In addition, additional cracks were found running normal to the 2 1/2" crack as shown in the center of the fracture surface in Figure 3-20. A cross-sectional view of this area shows transgranular cracks with extensive branching indicative of stress corrosion cracking (see Figure 3-21). An ongoing investigation has identified the causative species as a hydroxide not present on the Palo Verde Unit 1 replacement CEA shroud. Further discussion of these cracks will follow in the final report.

3.4 Scanning Electron Microscopy (SEM)

Fracture surfaces from CEA guide assembly cracks, tube to web weld cracks, (top and bottom), and cavity #18 web base metal were examined. In all cases, the failure mode was identified as high cycle, low stress fatigue (with the exception of the stress corrosion cracks identified previously). Figures 3-22 to 3-24 show fatigue striations found in the vicinity of crack fronts from various fracture surfaces.

Distances between striations were approximated to provide an estimate of the crack propagation rate. These measured values were then used to calculate the number of cycles during crack propagation. By dividing the distance the crack traveled by the crack propagation rate (assumes crack starts at one of its ends), a value for the number of cycles was derived. This estimate of the number of cycles is only useful in classifying the type of fatigue as high cycle and providing a lower limit estimate. Actual cycles to failure are probably higher and potentially much higher because: (a) the number of cycles is inversely proportional to the distance between striations which becomes greater as the crack propagates, and (b) the greater portion of high cycle fatigue is spent in the initiation stage versus the propagation stage. The values for the crack propagation rate ranged from[   ] inches/cycle.

3.5 Metallurgy Summary

The cracks identified and examined had similar crack morphologies, with the exception of the stress corrosion cracks. The failure mechanism in all cases was identified as high cycle fatigue. Crack initiation was typcially at weld toe locations. Chemical and metallurgical conditions of base material were acceptable. Cracks near 4-finger guides were more predominant and generally found on the outer shroud tubes. Shroud tube-to-web cracks were less numerous and closer to tie rod shroud tubes.

The welds showed undercutting, misalignment, incomplete penetration, voids, and rough and serrated weld toes upon visual and metallographic examination. These conditions were acceptable based on a visual examination only. In the original shroud design, the weld specification allowed acceptance based on only visual inspection, which was adequate for the anticipated operating conditions and shroud function. Weld quality appears to have been a factor only with regard to weld bead cracks found on 4-finger guide welds. In fact, cracks associated with CEA guides or tube to web weld areas in some cases propagate away from welds indicating higher stresses exist at the base material. Additionally, the existence of cracks along a variety of welds suggests that other factors including joint configuration were of greater significance to crack location than weld quality.
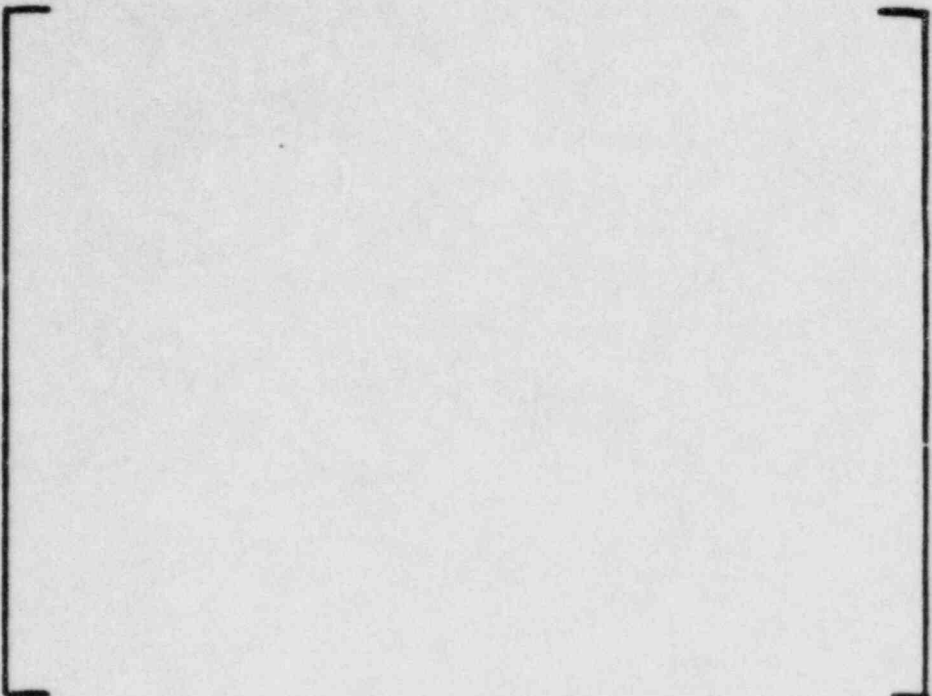
62380-10

Figure 3-1. Crack Near 4-finger Guide on
Shroud Tube 28
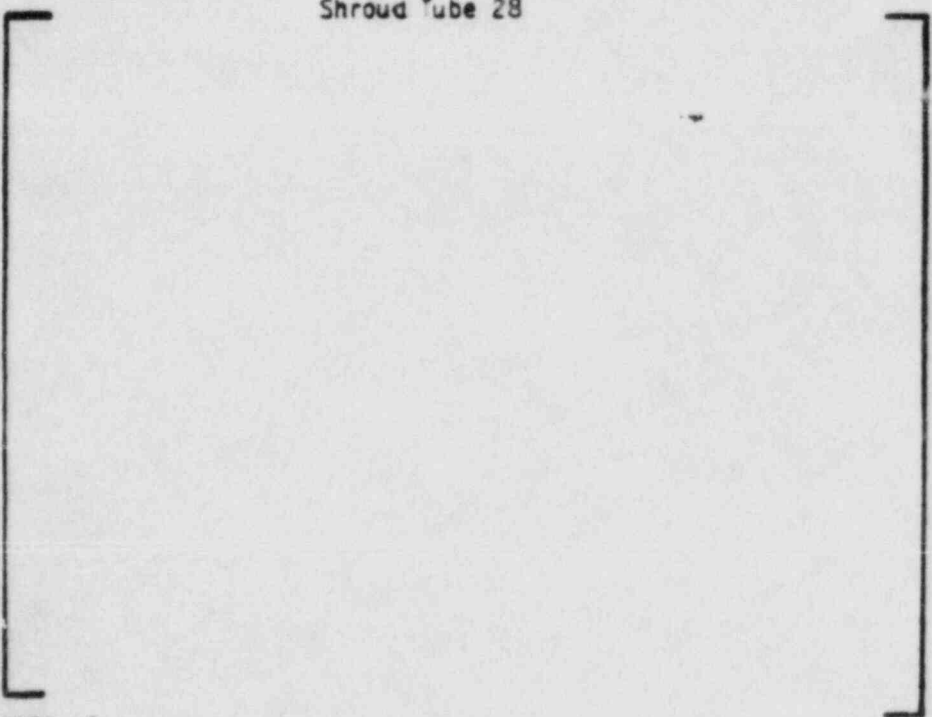
62380-17

Figure 3-2: Crack Near 4-finger Guide on Shroud Tube 44
(180° side)

3-7

FIGURE 3-3
TOP CRACK SUMMARY

Wear Marks

0°

270°

90°

180°

TYPICAL CRACK
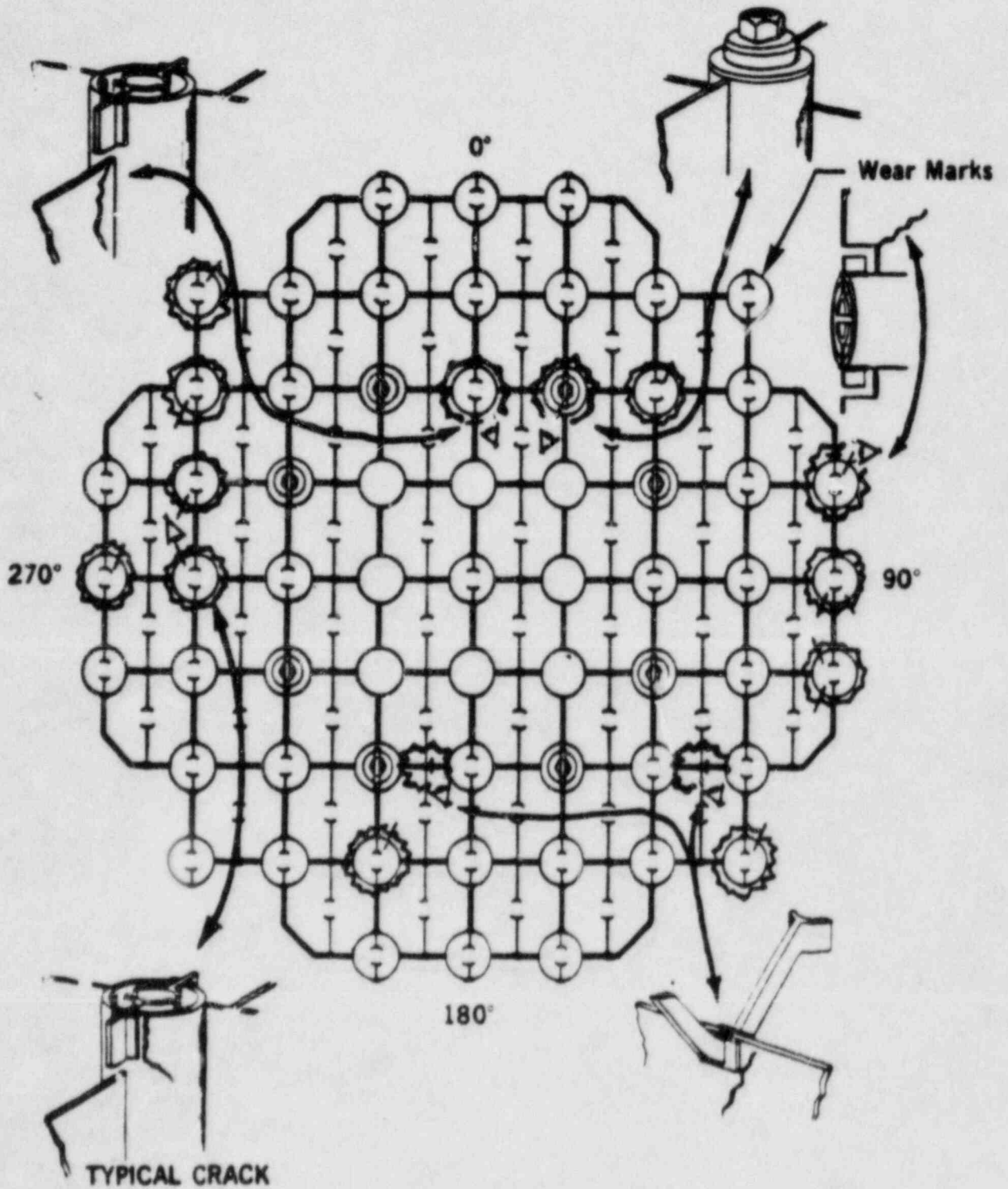
FIGURE 3-4
BOTTOM CRACK SUMMARY
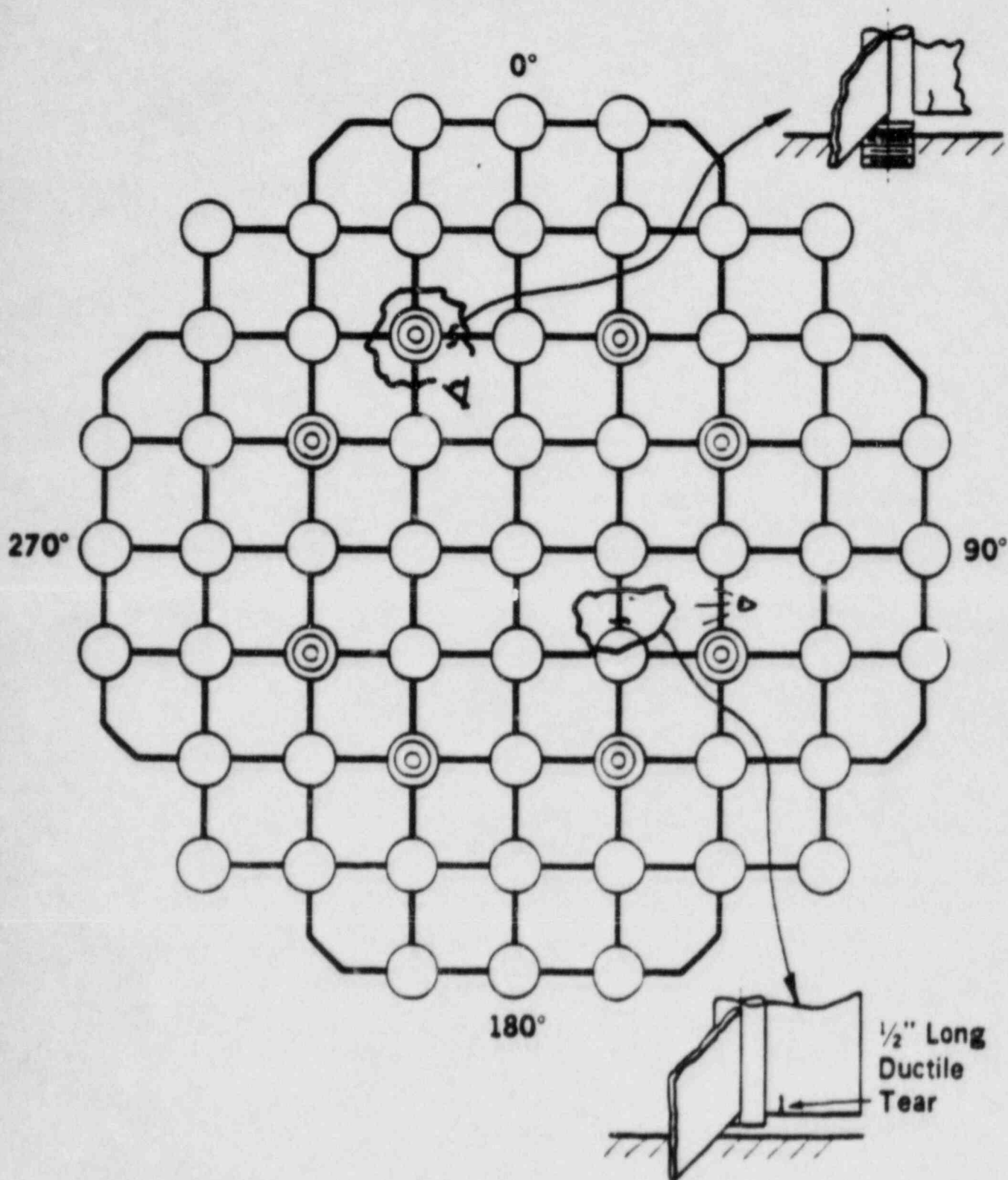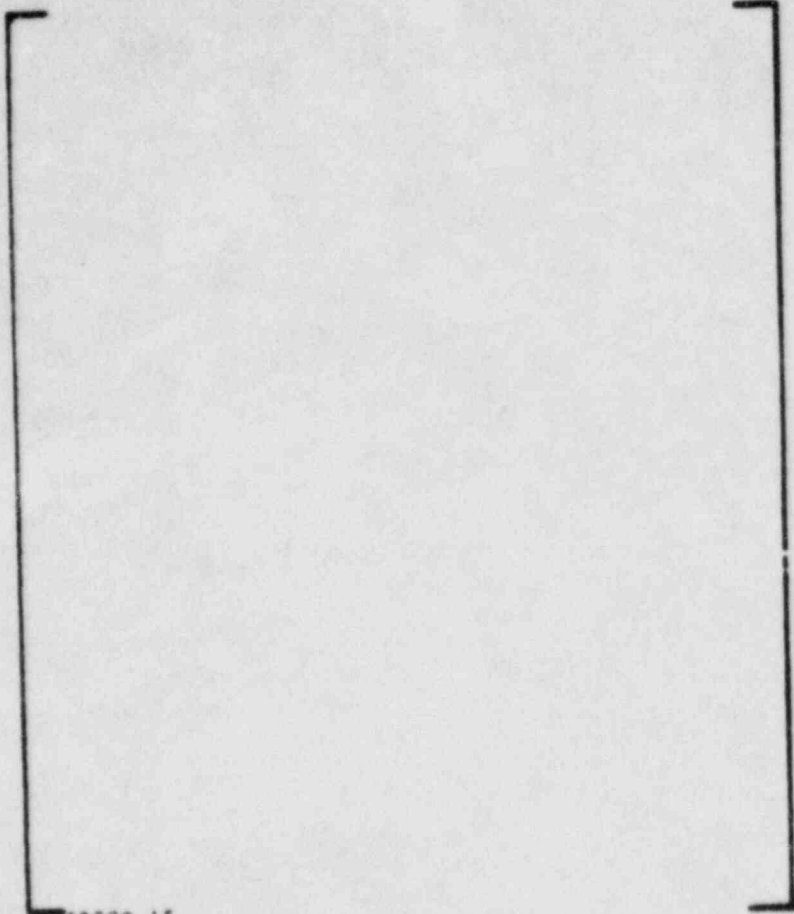
62380-15

Figure 3-5: Crack on 4-finger Guide on
Shroud Tube 26 (0° side)
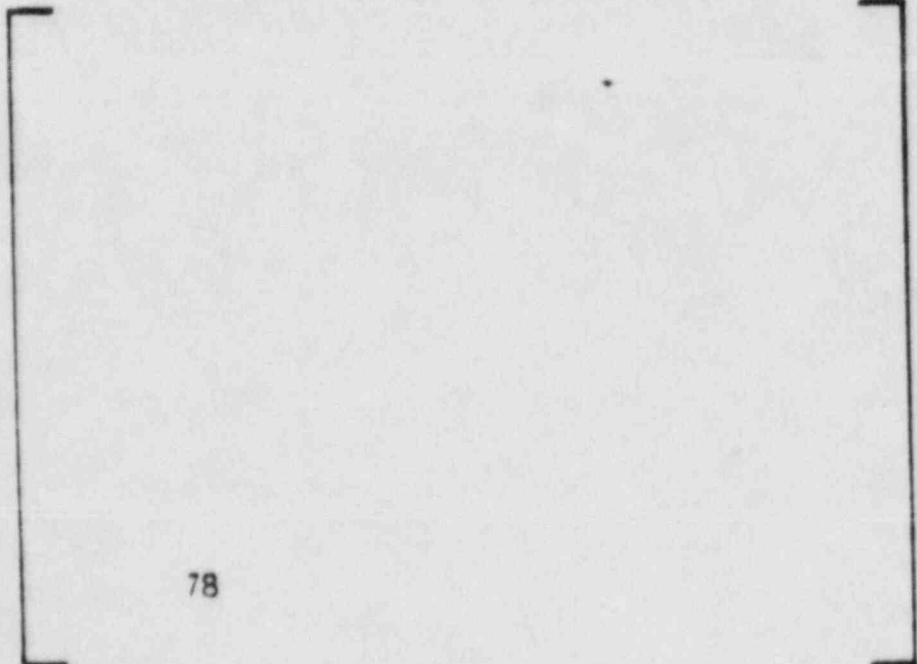
78

63702-11

Figure 3-6: Crack Near 12-finger Guide on Web Between
Tubes 50 & 51

3-10
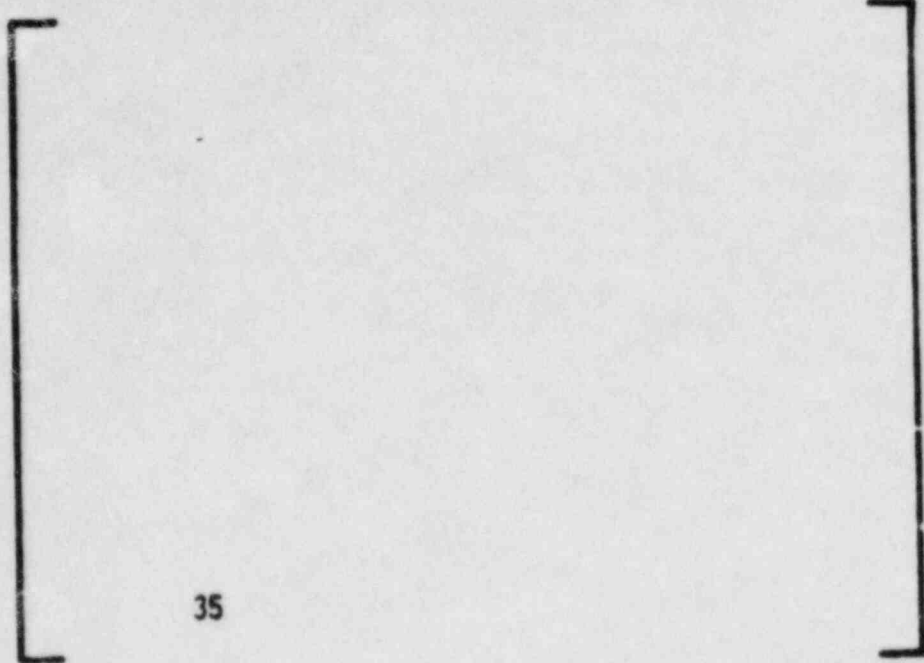
35

63703-3

Figure 3-7: Crack Near Shroud Tube to Web Weld on
Shroud Tube 15
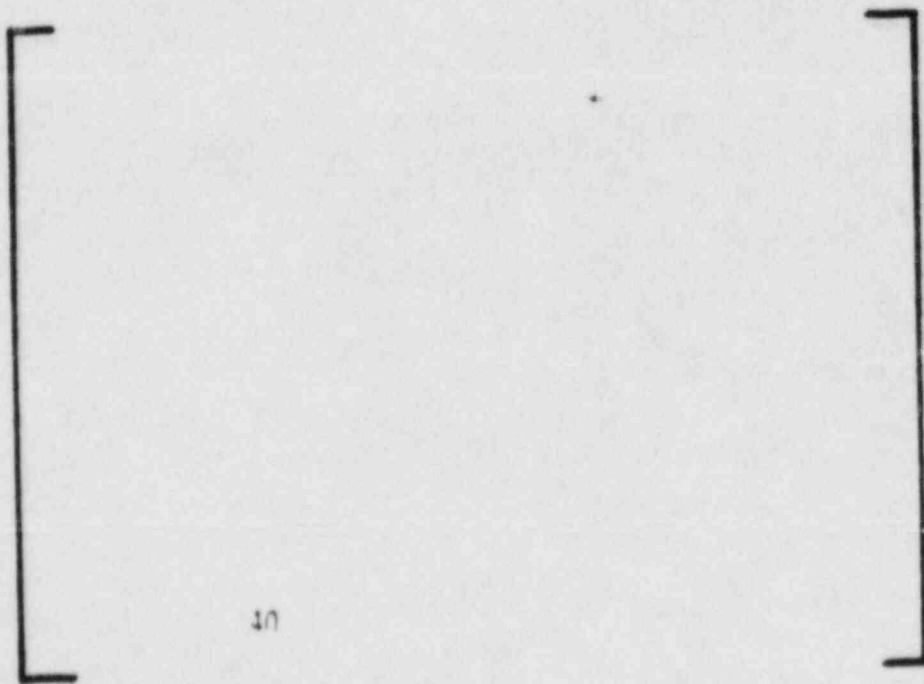
40

63704-7

Figure 3-8: Web Cavity #18 Base Metal Crack near Shroud
Tube 26

3-11

Figure 3-9: Fracture Surface of Crack
Near 4-Finger Guide (180°)
on Shroud Tube 44

62917

ID   OD
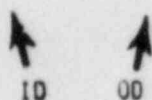
Figure 3-10: Fracture Surface of Crack
Near 4-Finger Guide (0°)
on Shroud Tube 26

Opposing
Halves

Center Lip

Crack Tip

62979

Figure 3-11: Weld Bead Crack on Shroud
Tube 26 4-Finger Guide

62962

Weld Bead Crack

Figure 3-12: Weld Bead Crack at ID
Bracket to Shroud Tube
44 Weld

62916

Figure 3-13: 4-Finger Guide to Bracket Weld Crack on Shroud Tube 44

62915

incomplete penetration

Figure 3-14: Cross Section of 4-Finger Guide Assembly on Shroud Tube 44 (0° side)

undercutting

63271
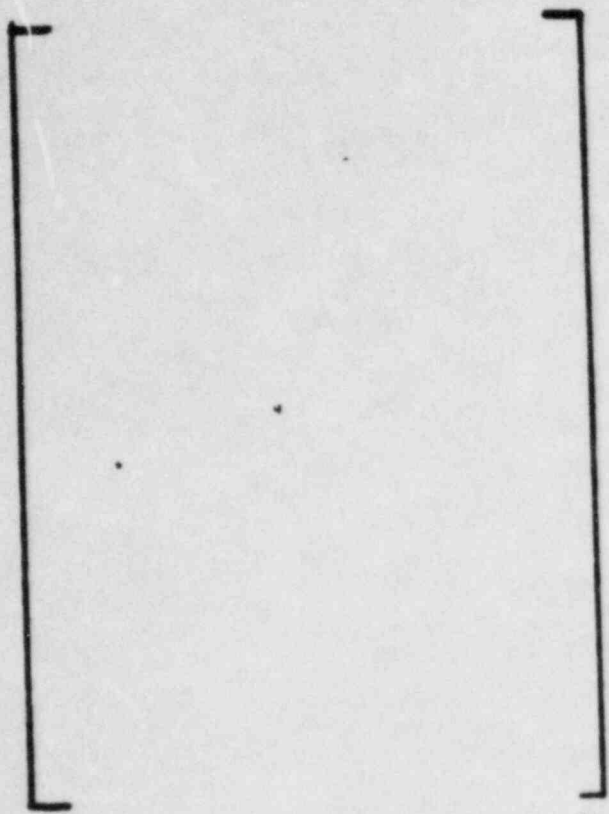
Figure 3-15:   Cross Sectional View of
Weld Bead Crack Through
the Guide to OD Bracket
Weld on Shroud Tube 26

63444   11.5x

4-Finger
Casting

Figure 3-16:   Cross Sectional View of
Crack Propagating Through
a 4-Finger Guide on Shroud
Tube 44 from the ID Bracket
to Guide Weld
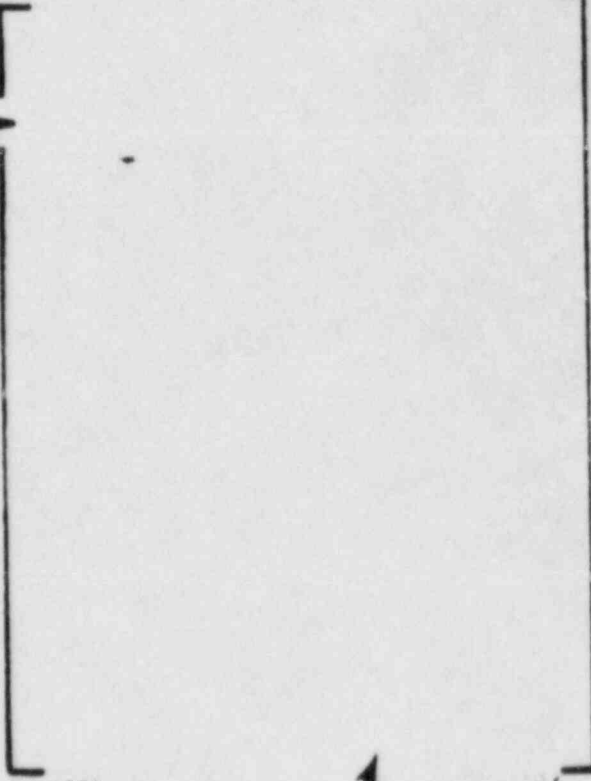
63231

Bracket

3-15
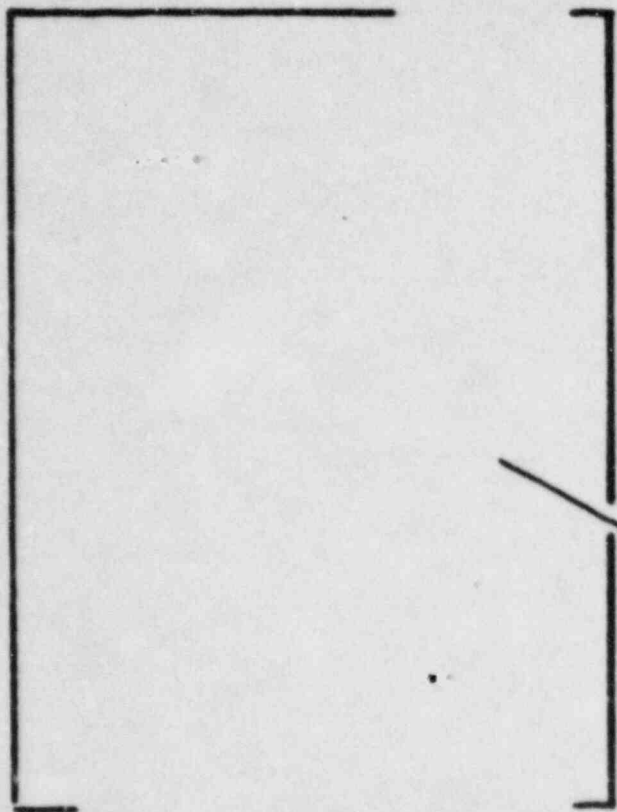
Figure 3-17: Dye Penetrant Examination Showing Crack at web to Shroud Tube 15 Weld, As Received. Crack is Located on the Shroud Tube.

Linear
Indications

63446

Figure 3-18: Dye Penetrant Examination Showing Crack at web to Shroud Tube 14 weld, As Received. Crack is Located on the web.

Shroud
Tube

54459
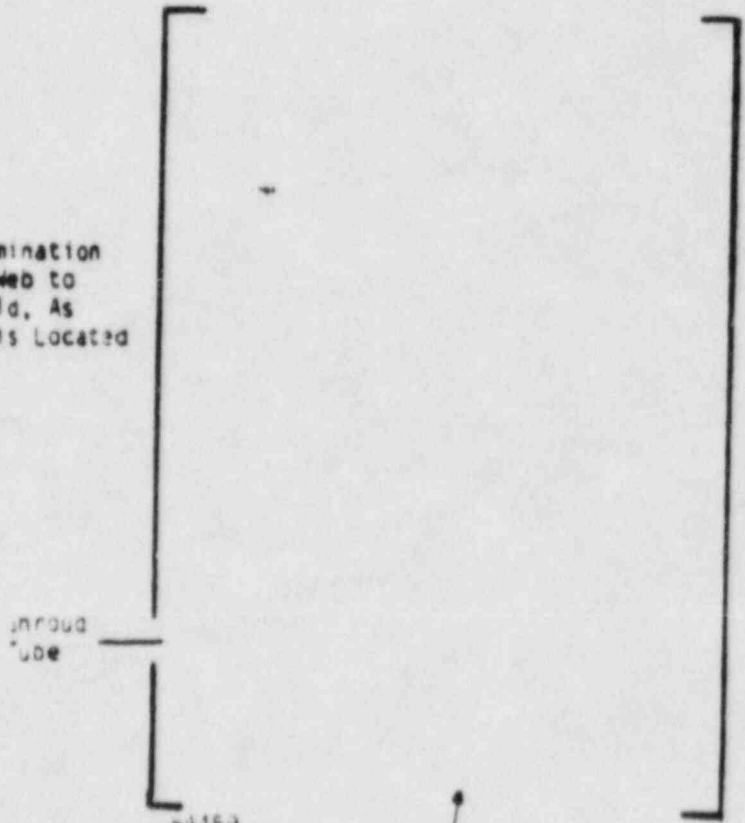
web

Figure 3-19: Web Crack Fracture
Surface Near Tube 14
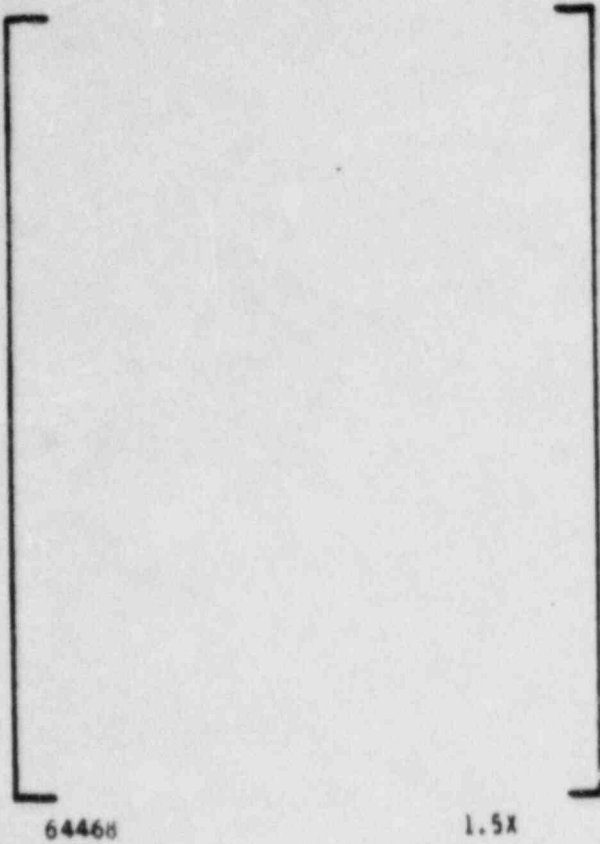
64468   1.5X

Figure 3-20: Fracture surface of crack
on tube 13 near bottom of
shroud.

636d7   2X
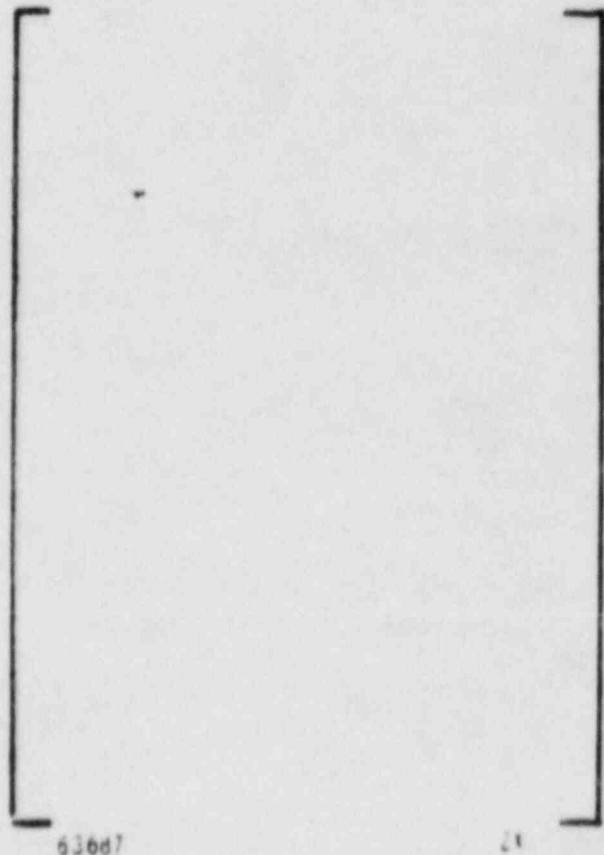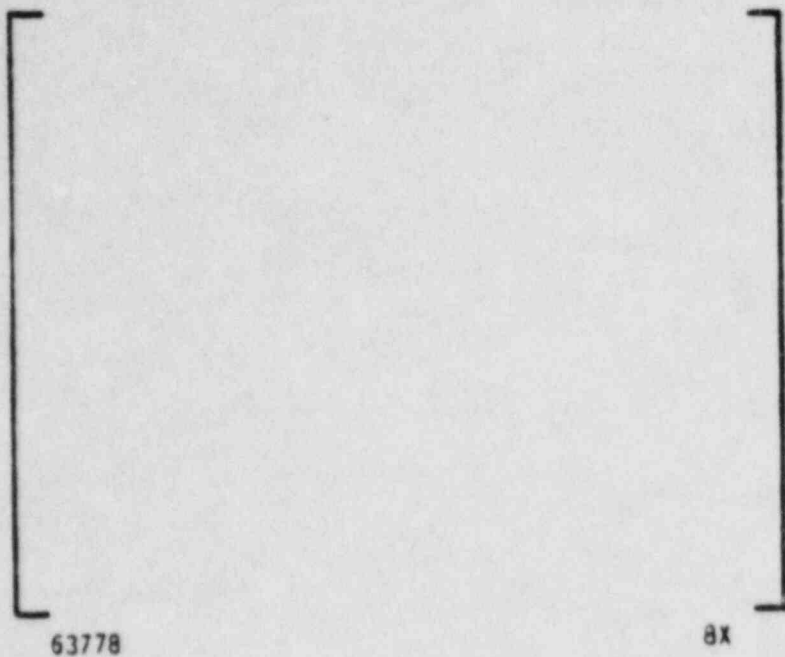
63778   8X

Figure 3-21:   Cross-sectional view of crack showing
               additional stress corrosion cracks.

igure 3-22:   Fatigue Striations Near
              Crack Tip on Shroud Tube
              26
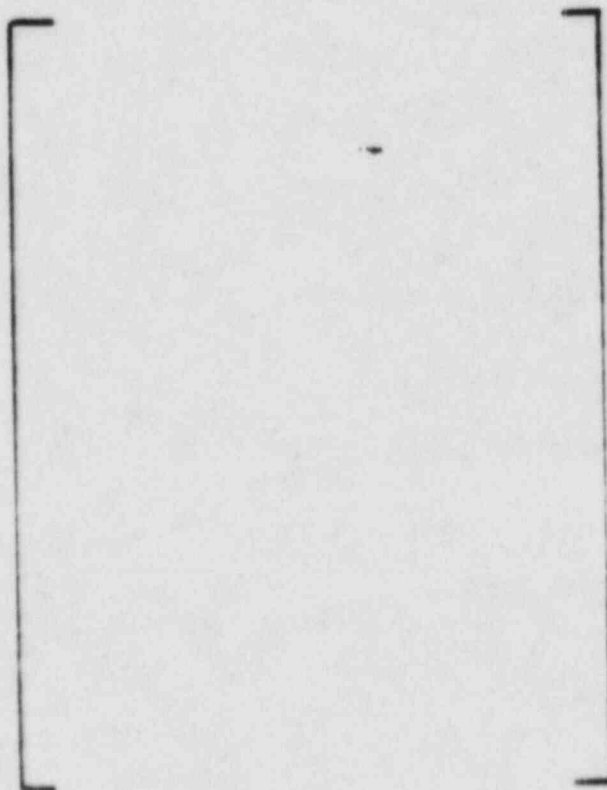
                              52825   1000X
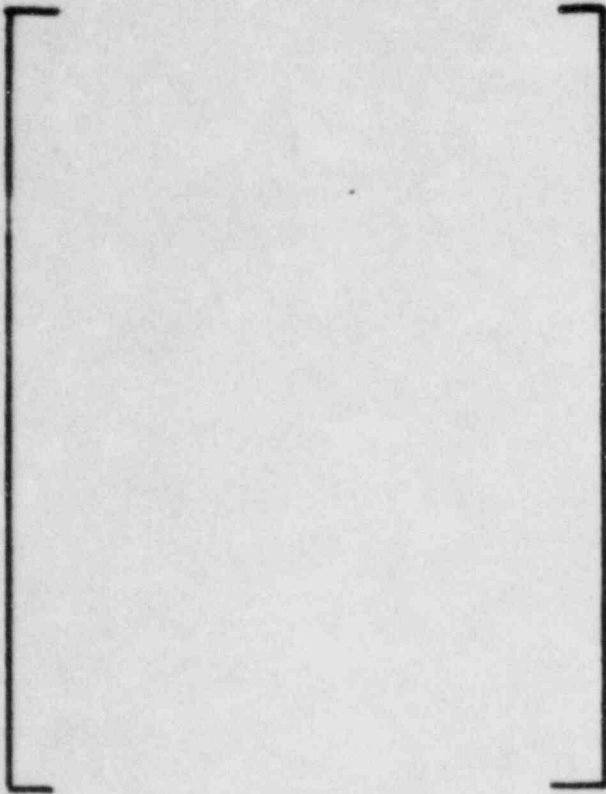
Figure 3-23: Fatigue Striations Near
Crack Tip on Tube 15

63542   1500X

Figure 3-24: Fatigue Striations Near
Crack Tip on Web Between
Shroud Tubes 50 and 51.
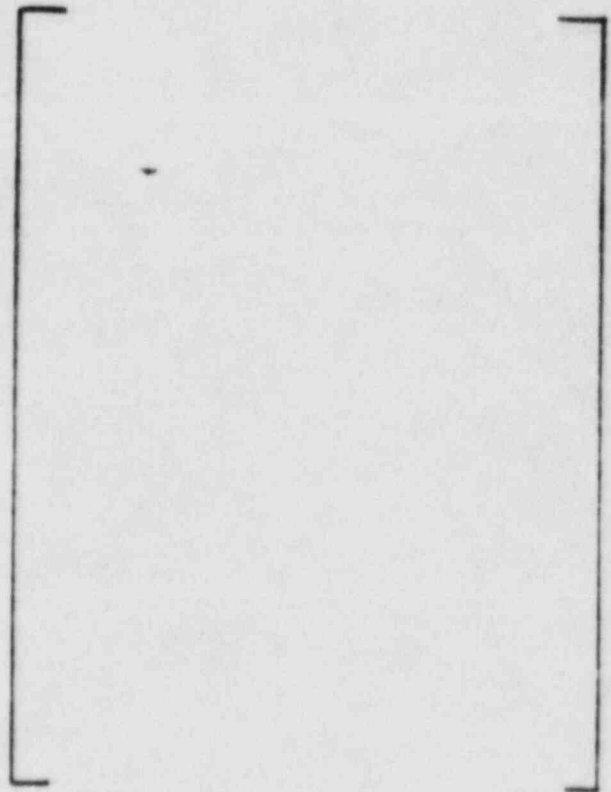
63472   1500X

4.1 TESTING

A series of hydraulic and mechanical tests were performed to identify potential forcing functions which might induce shroud vibrations and to characterize the modes of vibration of the CEA shroud assembly and of individual CEA shroud tubes before and after modification.

4.1.1 Hydraulic Test

The purpose of the test was to investigate the response of the CEA shroud tube to excitation attributable to flow and/or acoustic phenomena. Of primary concern were mechanisms which can induce fluctuating stress levels high enough to cause fatigue failure.

A four-finger CEA shroud tube was instrumented with two piezoelectric pressure transducers and twelve strain gauges. The tube was installed in a flow test facility which simulates the flow paths entering the bottom of a tube and the induced lateral cross flow under the tube. Figure 4.1-1 shows the various reactor flow paths with the core in place, including the flow into the CEA shroud region. Without the core, the circulating flow into the CEA shroud region is increased from [   ] of the total flow. Analyses of the distribution of this flow within the shroud yield very low velocity over the CEA guides at the top (Figure 4.1-2). Even without the core, the velocity is too low to induce vortex she   off the guides at high enough frequency to cause resonant vibration of the   des from a vortex phenomena. This test examines the region of turbulent jets at the bottom of the shroud tube as shown in Figure 4.1-2. Figure 4.1-3 shows the test equipment schematic. Strain gages were distributed at the top of the tube to monitor strain near the observed crack locations and to provide the tube mode shapes of the vibrations. Figure 4.1-4 shows the strain gage locations.

Two test sequences were performed. In the first, the axial and lateral coolant velocities were varied up to [   ] respectively. This range of velocities encompasses the velocities in the pre-core reactor tests. In the second test sequence, acoustic pressures, which simulate, for example, periodic pressure fluctuations originating at the reactor coolant pumps, were induced by placing a tunable underwater sound generator (SONAR) a few inches above the top of the shroud tube.

coherences and phase angles among the transducers were calculated for selected test conditions and then plotted. Periodic excitation frequencies due to flow were determined from comparisons of test-run PSDs with PSDs obtained with the pump running but no loop flow. Periodic excitation frequencies due to structural response were determined with comparisons with rap tests. Analysis was carried out in the frequency range 0 - 500 Hz.

In the flow tests, two shell mode resonant frequencies were observed. At 132 Hz, the lowest resonance frequency, the extension shaft guides move out of phase with each other. At 180 Hz, the next higher resonance frequency, the guides move in phase. The mode shapes agree well with the mode shapes obtained in the mechanical excitation test (Section 4.1.4) in air at about 192 Hz, and 275 Hz, respectively. The RMS magnitude of the stress fluctuations is about $\pm$ 100 psi. These stress fluctuations by themselves are too small to cause fatigue failure.

In the acoustically excited test, excitation was induced over the range of 100 to 300 Hz. At 130 Hz excitation, the tube response frequency was 132 Hz with a maximum RMS stress of $\pm$ 11 psi. At 177 Hz excitation, the tube response is at 180 Hz with a maximum RMS stress about $\pm$ 25 psi. Mode shapes agree with those obtained from the flow test. Figure 4.1-5 shows the measured strain distributions at 132 Hz for both tests and Figure 4.1-6 shows the strain distributions at 180 Hz.

The acoustic pressure induced by the SONAR was about 0.1 psi. Maximum measured periodic coolant pressure fluctuations in the CVAP were [   ] psi at 240 Hz under the UGS plate which supports the CEA shroud assembly. Even if these fluctuations propogated undiminished through the flow holes in this plate and into the shroud region, the resulting induced stress is too small to cause fatigue failure.

In conclusion, the hydraulic tests were unable to identify a direct hydraulic forcing function acting on the CEA shroud which could cause fatigue failures in the shroud during pre-core testing. On the basis of this conclusion, it was decided that there is no need to provide temporary devices to restrict the flow into the shroud during pre-core testing. Post-core hydraulic forcing functions are smaller because, when the core is in place, the total reactor flow is smaller and also the fraction of the total which enters the shroud region is smaller. Therefore, the same conclusion applies for the hydraulic forcing functions during normal reactor operation.

4.1.2 Modal Vibration Tests by C-E

4.1.2.1 Shroud Assembly Test by C-E

The purpose of the test was to identify the modes and frequencies of vibration for the four finger and twelve finger CEA guides as installed on the CEA shroud assembly and to determine the interaction behavior among guides on the shroud. Testing was performed in air on a new CEA shroud at the C-E manufacturing facility in Newington, NH. A number of accelerometers were mounted on the guides, shroud tubes, and webs. These sensors were moved about according to the particular component or phenomenon being measured. Similar data analyses and recording and display equipment as mentioned in Section 4.1.1 were utilized. Excitation was by manual impact hammer.

When impacted horizontally, the four finger guides had resonance peaks in the range from 178 to 196 Hz in air. The twelve finger guides had resonant peaks at about 57 Hz when impacted perpendicular to the web and at about 182 Hz parallel to the web. Damping was very small; less than 0.1% of critical for the guide vibration.

When the tube is impacted, rather than the guide directly, the resonant peaks for the guides are seen along with many other resonant peaks. The relative amplitude of response at the various resonant frequencies depends on the location of the impacting along the tube and on the locations in the shroud assembly of the tube which is observed and the tube which is impacted. For example, impacting a tube at the top showed the strongest response peak at 196 Hz, the frequency of the guides. Impacting at the bottom still excites a response at 196 Hz but other frequencies have stronger response. Just below the guides near the top, the maximum response occurs at 276 Hz. At higher elevations, more resonance frequencies occur with comparable amplitude of response.

The peripheral web was impacted in the direction of the outer row of tubes. Maximum response occurred at 196 Hz in the closest tube and at 240 Hz in the other two tubes in the row. Other response peaks were also observed from about 80 Hz and up.

mode is a shell mode of the tube which is determined in part by the mass of the guides and their attachment. Second, there are many modes of vibration for the tube shell away from the guides, depending on excitation location.

4.1.2.2 Single Tube Test by C-E

To further characterize the vibration modes and to determine the effect of water on resonant frequency, a single shroud tube with guides was suspended in air and then in water. Accelerometers were mounted on the guides at the top and on the tube at the bottom. Impacting the guides in air gave a dominant frequency of the guides of 204 Hz for this particular tube and is equivalent to 196 Hz measued on the shroud assembly. A combination of variations in the tubes, their test configurations, and the instrumentation cause the difference in frequency..

Impacting the tube at the top or bottom gave the same 204 Hz response of the guides and, in addition, gave other frequencies. In water, the 204 Hz frequency dropped to approximately 130 Hz. Other groups of frequencies showed similar decreases in water.

4.1.2.3 Summary of C-E Modal Tests

The overall result of these scoping vibration tests is that the CEA shroud has several characteristic resonant frequencies corresponding to the CEA guides and the tube shell modes. It also has numerous other weaker resonant frequencies. The dominant frequencies are associated with the four finger guides and round tubes and are evident both in a single tube and in tubes which are an integral part of the shroud assembly. In conclusion, the investigation of the cause of the observed cracks should include resonant vibration of the tubes and guides as a potential contributor.

4.1.3 Modal Vibration Test by SDRC

This test was performed for C-E by Structura' Dynamics Research Corporation who has the capability for dynamic video displays of vibrating structures. The purpose of the test was to identify local and overall assembly of vibration of the CEA shroud in air and in water. Testing was performed on the original Palo Verde Unit 1 CEA shroud after it was returned to the C-E manufacturing facility in Newington, NH. The shroud was fastened down with tie rod assemblies which are employed in the reactor. It was located inside a barrel which was filled with water for some of the testing.

of sensors on the shroud and the geometry of the shroud were incorporated into computer software which enabled dynamic video output of the overall global mode shapes of the vibrating shroud. Testing has been completed and reduction and interpretation of the data are underway.

A summary of this test will be included in the final CEA shroud report.

4.1.4 Mechanical Excitation Test

This test was initiated by C-E after the previously described modal tests by C-E identified the need for a thorough laboratory characterization of tube vibrations. The purpose of this test is to determine the dynamic vibration response characteristics in air of a single CEA shroud tube with CEA guides and of a single tube as modified by cutting off the top three inches including the guides. Also, the test provides a means of producing a crack in the shroud tube similar to the cracks observed in Palo Verde Unit 1.

A single shroud tube with guides and with three webs, simulating a peripheral tube in the shroud assembly, was mounted in air as shown in Figure 4.1-7. Rigid mounting of the webs as shown provides a known boundary condition which can be represented in an analytical structural model of the same tube for correlation with the test (See Section 4.2).. The tube was excited at a point on its circumference by an electromagnetic exciter. Excitation was applied at one of three elevations: 8 inches up from the bottom, 8 inches down from the top, or 42 inches down from the top which is the elevation of the UGS barrel flange. Tube response is monitored by 15 strain gages at the top and by 5 at the bottom, as shown in Figure 4.1-8. In addition, an accelerometer was placed at various locations to map the axial and circumferential distributions of the acceleration, from which displacement is obtained.

Resonant frequencies were identified from 93 Hz to 420 Hz. The relative amplitude of response depended on the location of the exciter and the axial elevation which is monitored. Generally, there were two dominant frequencies. They are 192 Hz which is the resonant frequency in air of the guides and tube at the top, and a group of frequencies from about 250 Hz to 300 Hz which are resonant frequencies in air of the shell modes of the shroud tube.

strain at this frequency is more than twice as great as the strain at
the top for any other frequency and is more than three times greater
than the concurrent maximum strain at the bottom.

When the exciter is located at the bottom, the maximum strains at top and
bottom occur at a shell mode resonant frequency near about 284 Hz in air.
The strain at the top is almost as large as for the guide resonant frequency
when the exciter is at the top, but occurs at the higher frequency. The strain
at the guide resonant frequency of 192 Hz is less than one tenth of the value
it had when the exciter was at the top. The strain at the bottom when the exciter
is at the bottom is less than the strain at the top.

When the exciter is located at 42 inches down from the top, at the UGS flange
elevation, the maximum strain occurs at the top but at a higher frequency of about
418 Hz. Strains at 192 Hz and near 284 Hz are 70% or less of the strain at 418 Hz.

The axial distribution of displacement amplitude was obtained from hand held
accelerometers. Generally, the axial mode shapes at the guide frequency of
192 Hz indicate very large amplitude at the top, smaller amplitude at the
bottom, and much smaller along the intermediate lower length. At most higher
resonant frequencies, the bottom displacement is larger than the top and the
axial distribution has two nodes. These displacement distributions correspond
to the overall observations of location and relative amplitude of the strains.

Measurements of strain amplitude as a function of the peak magnitude of
the sinusoidal exciting force were made at the various resonant frequencies.
Using these data, a frequency and force were selected for a long term test at
constant frequency, or a dwell test, to induce failure. The resonant frequency
of the guides was selected and the force adjusted to give a maximum measured
local strain equivalent to a stress which was below the fatigue stress at 10^6
cycles. For top excitation at the guide resonant frequency, the maximum measured
strain occurs on the gage adjacent to the welded attachment plates for the guides
(See Figure 4.1-8). Because of the finite size of the strain gages, they
necessarily indicate the strains in the tube wall adjacent to the welds.
Taking account of the stress concentration caused by the welds and the
local change in tube wall thickness at the guide attachment, failure will
occur at measured values which are below the fatigue limit for the material.
Dwell excitation at 192 Hz succeeded in cracking the tube at [   ] cycles.
The crack was similar to those cracks visually observed at Palo Verde 1.

The fact that a crack could be induced is not, in itself, significant since any welded steel structure can be cracked by applying an appropriate force at a resonant frequency. In this case, the force was applied at a point on the tube circumference and such a force does not exist in the reactor. The significant fact here is that a different loading condition produced a crack similar to the reactor cracks. It is postulated that bending of the tube wall by moments and displacements transmitted through the attached webs near the CEA guides, even if not at the resonant frequency, would also cause similar cracks because of the restraint provided by the double welded plates and the related local stress concentration. An approximation of the stress concentration factor is obtained from the test by determining the ratio of the material fatigue stress at the number of cycles to failure to the measured stress near the guide attachment. Calculated stresses in the tube wall for various postulated exciting forces in the reactor are multiplied by the stress factor and compared to fatigue limits to evaluate the potential for those postulated forces to have been the cause of the reactor failures. Analytical models used in this comparison (See Section 4.2) are confirmed using the detailed modal shapes and frequencies obtained from this test.

Following the test to failure, the top three inches of the tube along with the guides was cut off and the cut surface was prepared in the same manner as in the shroud modification discussed in Section 5.0. New strain gages were installed at the top and characterization of the tube vibration is underway. Complete results will be given in Section 6.1.1 of the final shroud report. Preliminary data indicate that the guide resonant frequency is eliminated.

FIGURE 4.1-1
REACTOR FLOW PATHS
POST - CORE CONDITIONS

FLOW THROUGH UGS
SUPPORT PLATE

TOTAL FLOW

→ MAIN FLOW

∿ BYPASS FLOW

1 THRU OUTLET NOZZLE
   CLEARANCE
2 THRU INSTRUMENTED
   CENTER G.T.
3 THRU SHROUD-BARREL
   ANNULUS
4 THRU CENTER GUIDE TUBES
5 THRU OUTER GUIDE TUBES
6 THRU ALIGNMENT KEY-WAYS
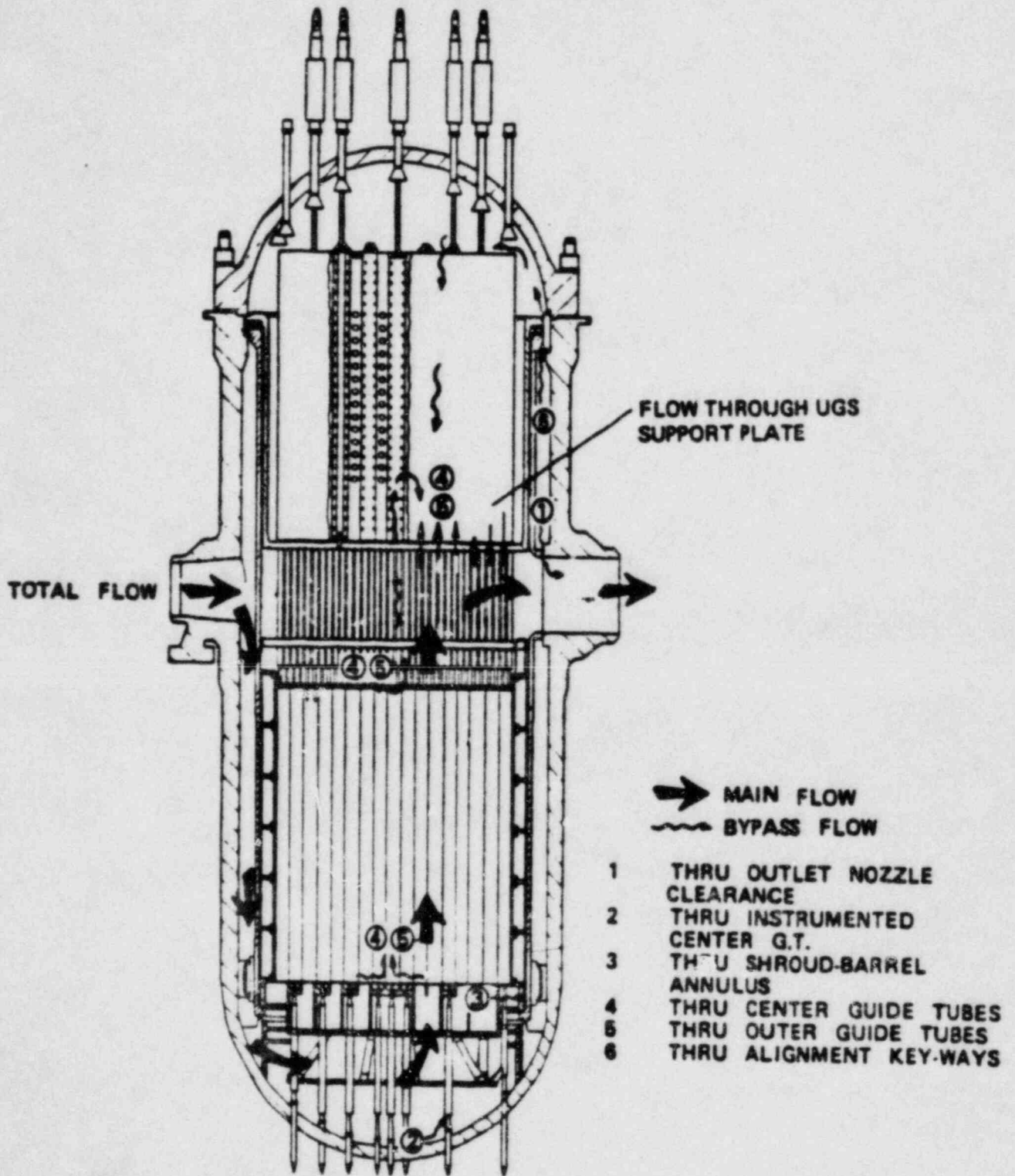
FIGURE 4.1-2

TURBULENT
JET PRESSURE
FLUCTUATIONS

CEA Shaft Guides

Typical Circular
CEA Shroud Tube

Axial Jets

Turbulent Fluctuating
Pressure

Lateral Jet

UGSSP

Tie Tube

FIGURE 4.1-3
HYDRAULIC EXCITATION TEST
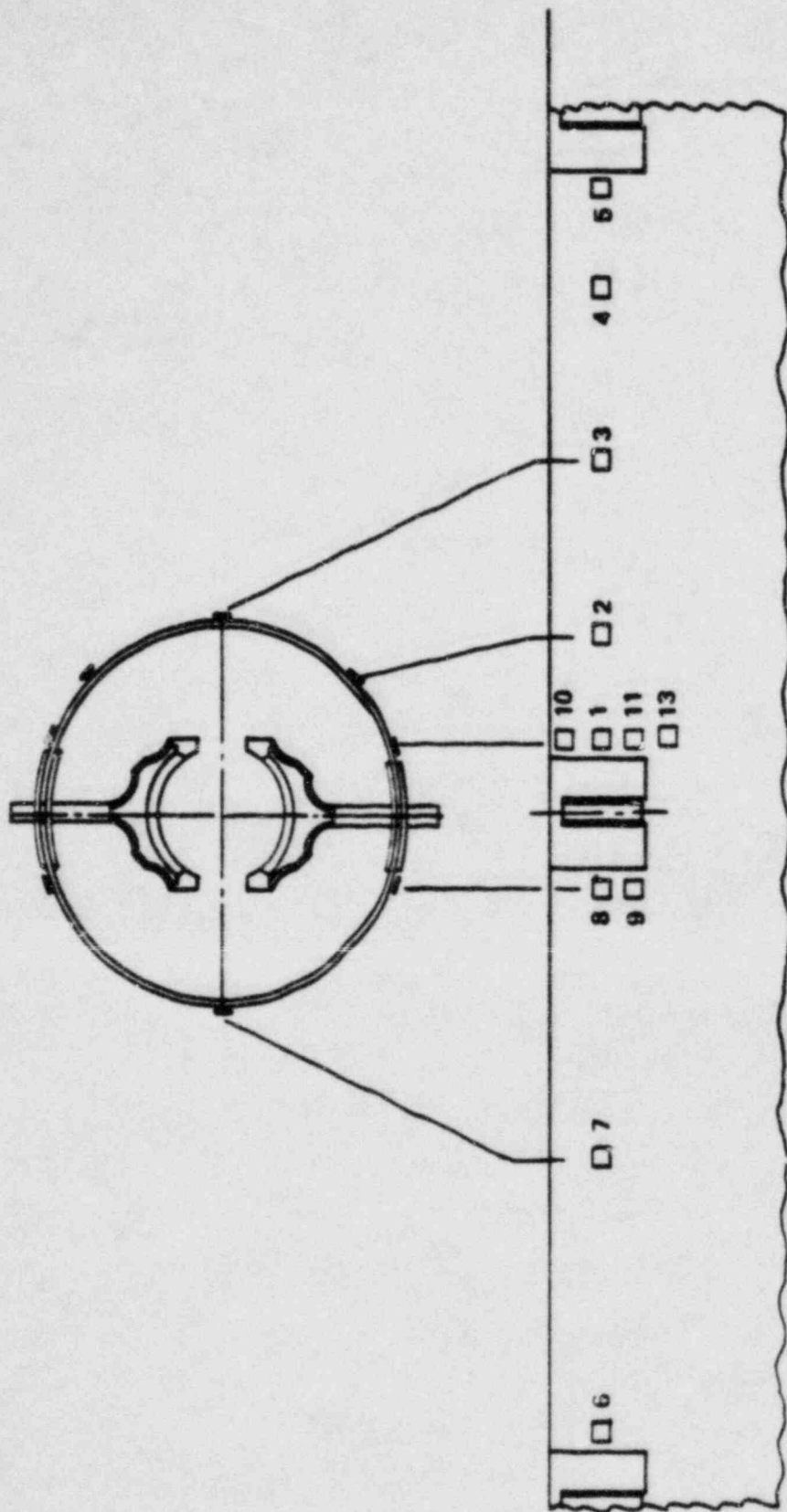
FIGURE 4.1-4
STRAIN GAGE LOCATIONS

FIGURE 4.1-5
SHROUD TUBE STRAIN DISTRIBUTION
AT 130 HZ IN HYDRAULIC TEST

EXCITED BY FLOW

EXCITED BY SONAR

FIGURE 4.1-6
SHROUD TUBE STRAIN DISTRIBUTION
AT 180 HZ IN HYDRAULIC TEST

EXCITED BY FLOW

EXCITED BY SONAR

FIGURE 4.1-7

SINGLE TUBE MECHANICAL EXCITATION TEST

FIGURE 4.1-8
STRAIN GAGE LOCATIONS

4.2 Analyses

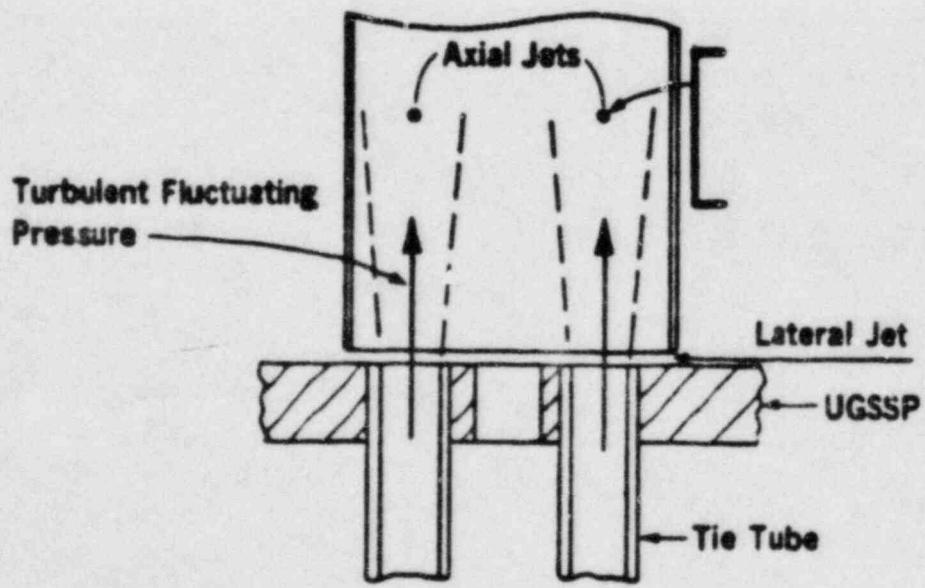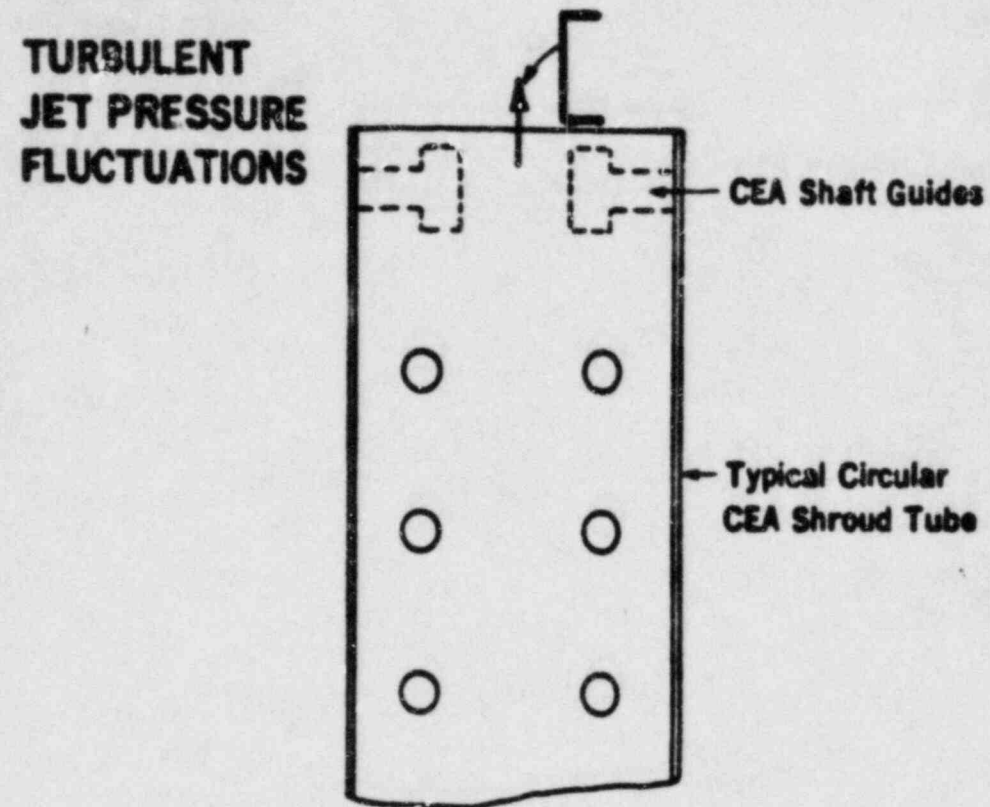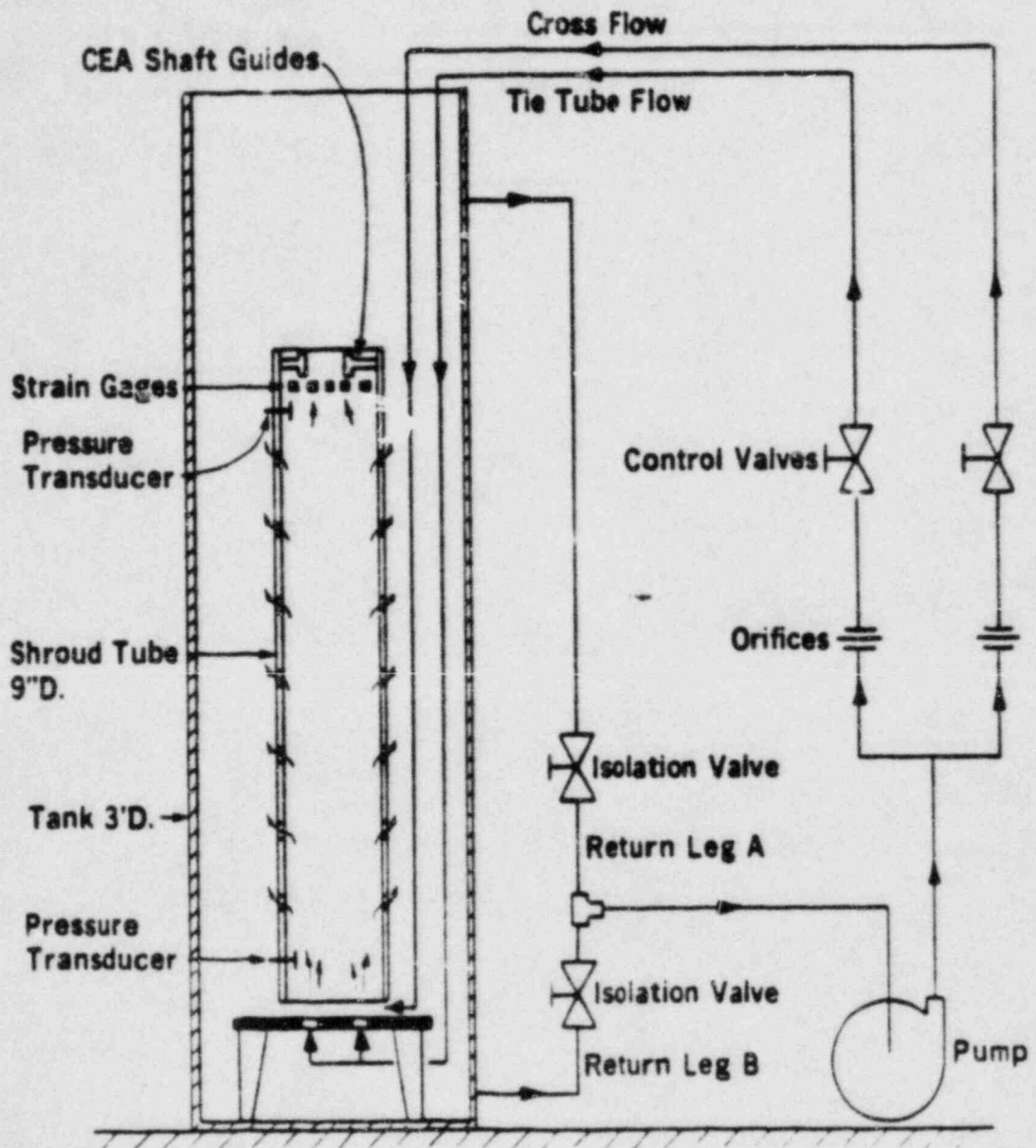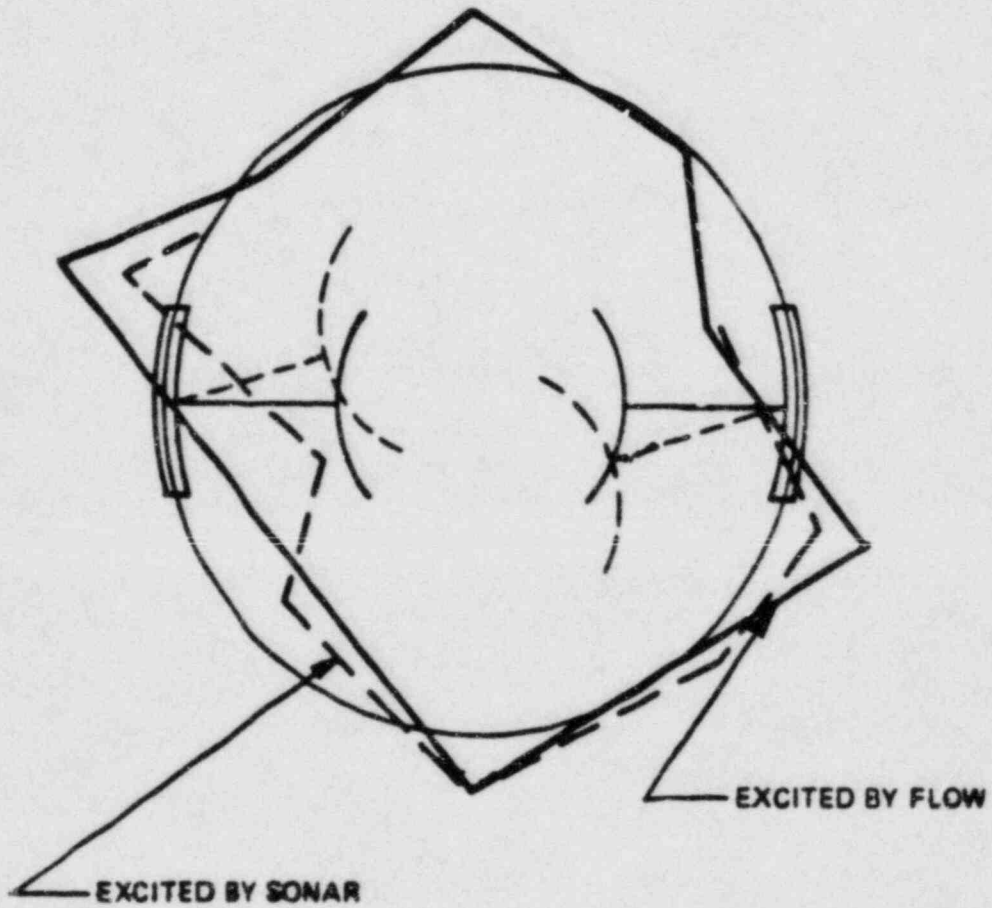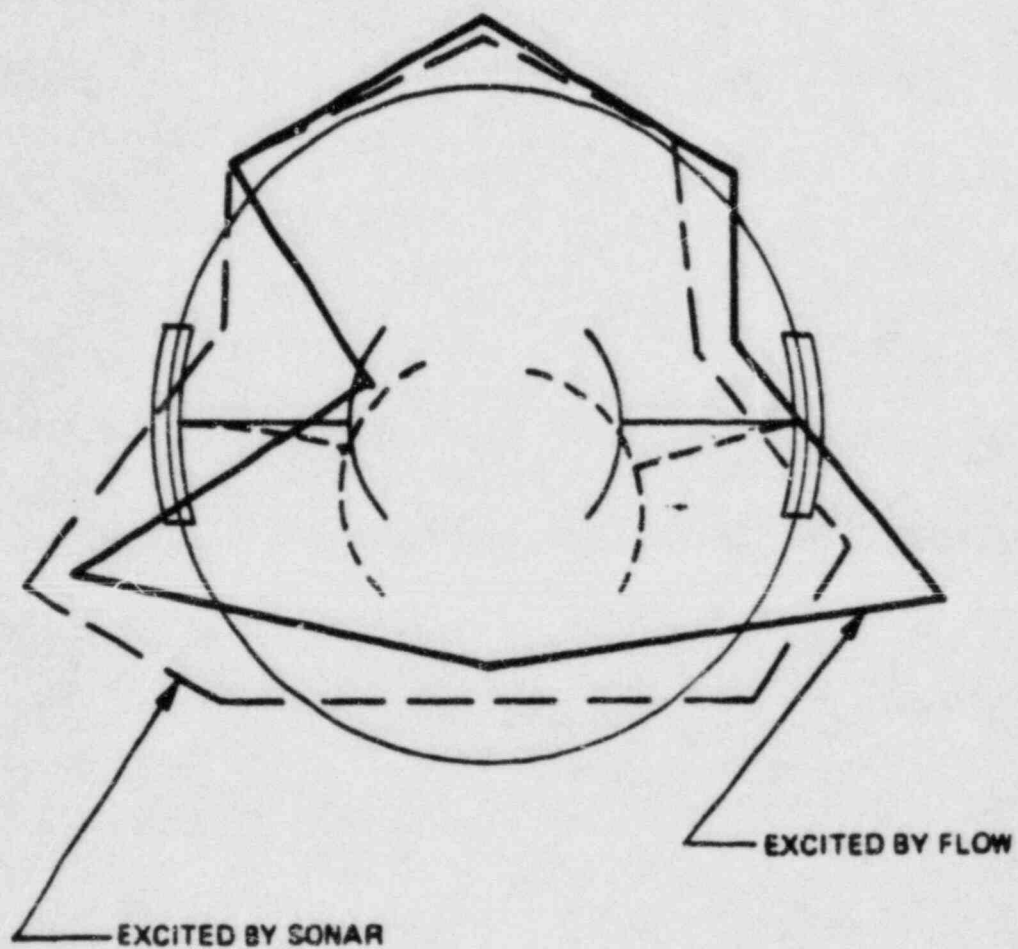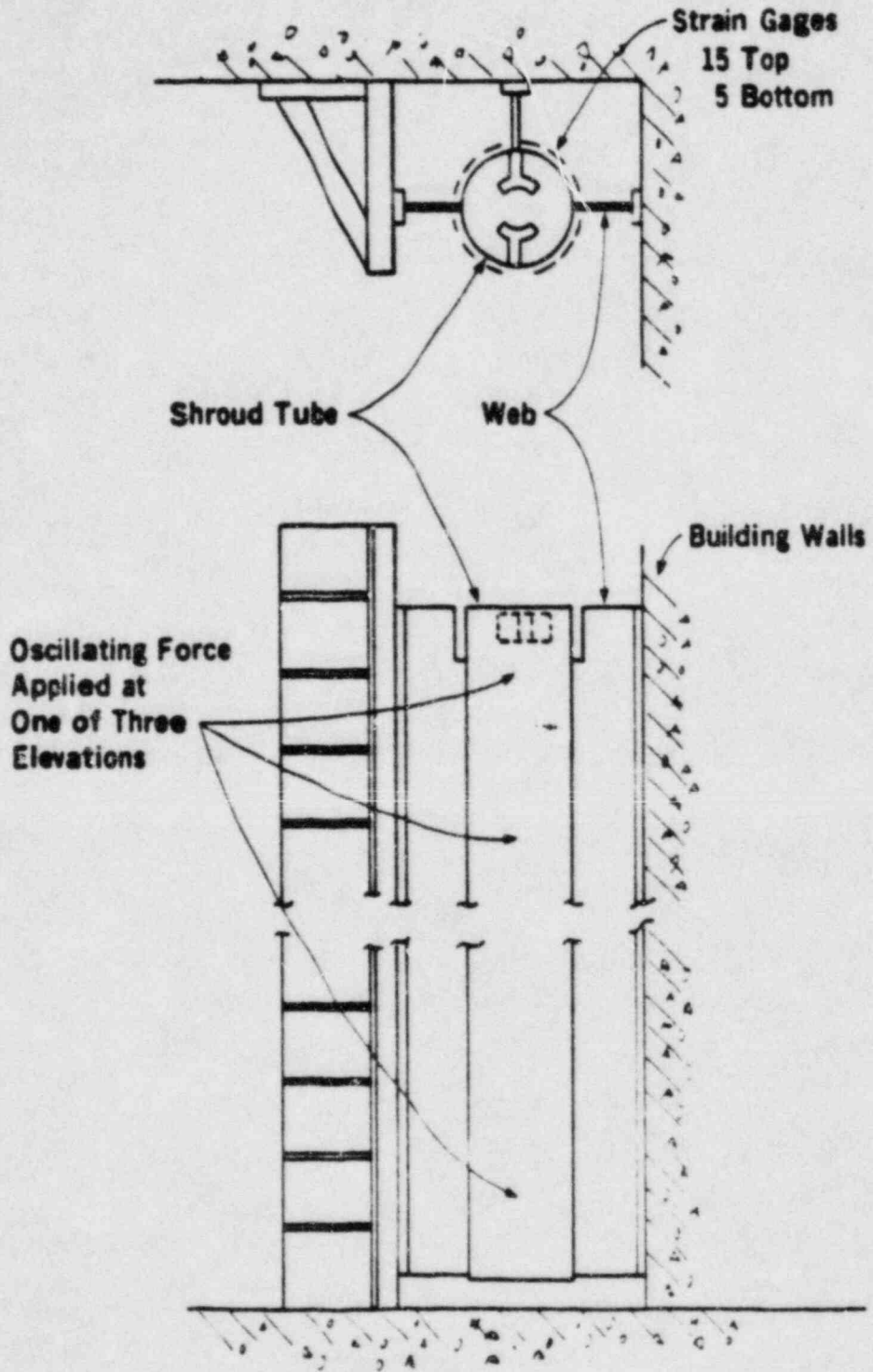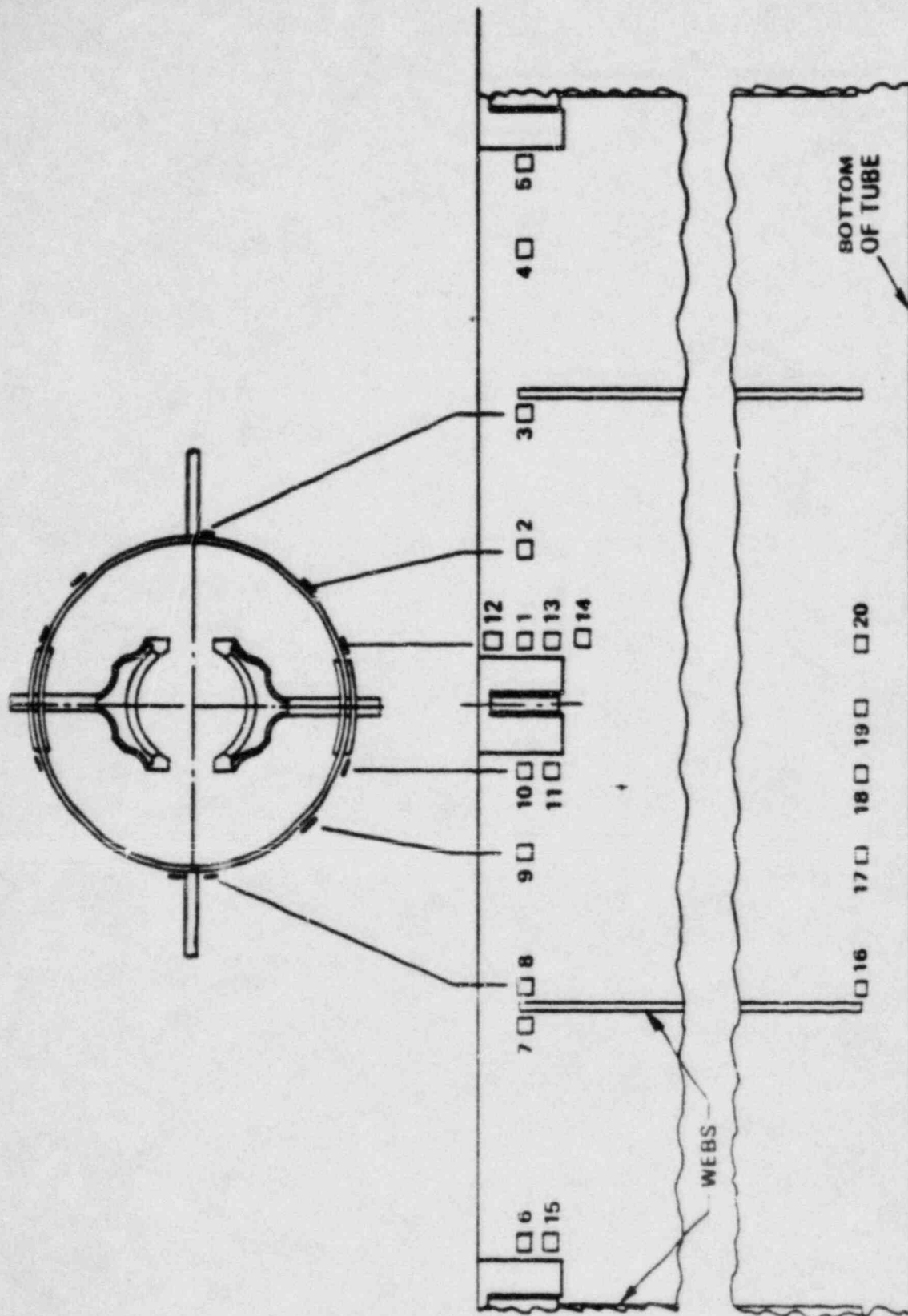The purpose of the analyses is to demonstrate the structural integrity of the CEA shroud under the usual design loading conditions. These conditions include the normal operating loading including that which existed during the pre-core testing and the Safe Shutdown Earthquake, Operating Basis Earthquake and Loss of Coolant Accident blowdown loadings. The shroud assembly as originally designed was shown to be a strong structure which is adequate for the large and relatively short duration loading of the non-normal conditions. Further, during normal operation the original shroud was not subjected to significant direct loads from flowing coolant. This fact was confirmed by the testing described in Section 4.1.1. The conclusion reached, based on results from the examinations in Section 3.0 and the various tests described in Section 4.1, is that the failures occurred not from large static loads, but from high cycle fatigue induced by vibration. Therefore, the primary emphasis of the analyses is to identify the potential forcing functions and consequent modes of vibration during normal operation.

4.2.1 Structural Response of the Upper Guide Structure

The methodology used to calculate the dynamic response of the upper guide structure assembly is divided into three major areas; the calculation of the forcing function due to hydraulic loading, the development of structural models which characterize the vibratory modes, and the calculation of the structural response. The purpose of this section is to describe the analyses which were used to assess the failure mechanisms which occurred during the pre-core hot functional testing. These results are used as the basis for demonstrating the structural integrity of the modified structure. The structural assessment of the modified design is discussed in Section 6.1.2.

4.2.1.1 Calculation of the Forcing Function

The forcing functions which were used to excite the various structural models were obtained from the hot functional test program. During this program, the tube sheet region of the upper guide structure assembly was instrumented with accelerometers, pressure transducers,

4-16

outlet nozzles where the flow loadings are the most severe. Data were obtained for different pump combinations and the results of four pump operation, which are indicative of normal operating conditions, were used as the upper guide structure assembly input forcing function. This loading was then used in a dynamic response analysis and resulted in a set of RMS acceleration levels and forcing frequencies of the upper guide structure support plate. The details of this and other analyses are described in the following sections.

4.2.1.2 Random Vibration Response Analysis

A lumped mass model of the upper guide structure (Figure 4.2-1) was developed to determine the structural response of the CEA shroud assembly, upper guide structure cylinder, tube sheet region, and fuel alignment plate with measured random loading as the input forcing function. The masses used in the model account for the weight of the structure and the effects of both contained and displaced water. Beam elements were used to represent the structural stiffness and shear deformations were included in the development of the stiffness matrix.

The model was subjected to two loading conditions which were obtained from the hot functional test program:

1) Random pressure acting on the tube sheet region (Figure 4.2-2) for four-pump operation at 565°F. This loading was among the highest recorded and represents conditions most typical of normal operation. These flow loadings are also conservative because the fuel was not present during the pre-core testing.

2) Random upper guide structure flange acceleration (Figure 4.2-3). The data were obtained from an external CEDM accelerometer. This loading is considered representative of the actual conditions at the UGS flange since the flange is clamped between the reactor vessel head ledge and a holddown ring.

Response power spectral densities (PSD) were calculated at various points in the model and used as input for more detailed structural models of the shroud assembly. These models, which will be described

4-17

in subsequent sections of this report, were developed to calculate the three-dimensional responses of the upper guide structure with and without the proposed structural modifications. The calculated PSD for the response of the upper guide structure support plate to measured random pressure loading using the lumped mass model is shown in Figure 4.2-4, and was used as the loading for the detailed models. Another PSD was calculated for the center of the tube sheet and was compared to a measured PSD at the same location (Figure 4.2-5). As can be seen, the agreement is very good and gives confidence in the results of the model.

In order to more fully assess the effect of this random loading on the tangential response of the CEA shroud assembly, a more detailed lumped mass beam model of the assembly was developed (Figure 4.2-6). A correction factor of $(1-V^2)$, where V is Poisson's ratio, was used to modify the beam properties to more accurately represent the plate bending behavior of the connecting webs. The purpose of this model was to determine the dynamic responses of the outer rows of CEA shroud tubes where most of the cracks occurred. The tie rods were assumed rigid since they are stiff relative to the connecting plates in the shroud assembly. An analysis was performed using forcing functions determined from the calculated PSD of the upper guide structure support plate response and the results indicated that structural failures could occur.

4.2.1.3 CEA Shroud Assembly Dynamic Response Analysis

A three-dimensional finite-element model of the shroud assembly was developed for the purpose of determining the natural frequencies and mode shapes of the structure and the response of the structure to a vibratory motion of the upper guide structure support plate (UGSSP).

The half symmetry model was constructed using a thin plate/shell element for both the tubes and interconnecting webs. The bases of four shroud tubes were fixed to simulate the tie rods. All of the other shrouds were allowed to move laterally and vertically. Seven axial levels were used to define the nodal coordinates.

4-18

The modal analysis resulted in a first mode frequency, in water, of about [ ] Hz. The frequencies of the first 15 modes were under [ ] Hz. In-water frequencies were determined by using both contained and displaced water.

Most of the resulting mode shapes indicate lateral motion of the shrouds with the peripheral rows exhibiting the most motion in the lower modes. Figures 4.2-7 and 4.2-8 show mode shapes for modes 1 and 3 which clearly indicate this behavior. In addition, the highest participation factors which are a guide to determine which modes contribute to the overall structural response, were found in the lower modes with in-water frequencies of less than [ ] Hz and in several higher modes with frequences near [ ] Hz.

The model was subjected to a base excitation frequency of [ ] Hz which determined from the random vibration response analysis described in Section 4.2.1.2. Even though other base excitation frequencies at [ ] and [ ] Hz were also identified, these were not used in the dynamic analysis because the magnitudes of the excitation are lower at these higher frequencies and the response levels would also be less. The [ ] Hz forcing frequency was found to be close to an in-water frequency of the unmodified upper guide structure assembly.

The model was subjected to a base excitation frequency of [ ] Hz which determined from the random vibration response analysis described in Section 4.2.1.2. Even though other base excitation frequencies at [ ] and [ ] Hz were also identified, these were not used in the dynamic analysis because the magnitudes of the excitation are lower at these higher frequencies and the response levels would also be less. The [ ] Hz forcing frequency was found to be close to an in-water frequency of the unmodified upper guide structure assembly.

The results of the base excitation analyses performed for the original CEA shroud assembly have shown a potential for failure if the forcing frequency is close to an in-water natural frequency of the structure. The resulting deflections, when applied to a detailed finite element model of a single CEA shroud tube with webs (Section 4.2.1.4), are severe enough to cause fatigue failures in the vicinity of the four finger guides.

In addition, the results of the visual inspection of the upper guide structure after the hot functional test revealed that one of the CEA shroud tubes had impacted the UGS flange. Because of this finding, analyses are being performed to determine the effect of this impact on the dynamic responses and whether it was a contributor to the observed cracks. The results of these analyses will be presented in the final report.

4.2.1.4 CEA Shroud Tube Analyses

Various single CEA shroud tube finite element models which included the four finger guides and backing plates were developed and used for modal, static, and dynamic response analyses. The models represented shroud tubes with both three and four webs to account for the various locations, loading conditions and response interactions. These models were constructed with lengths of 10, 20, and 160 inches (full length). The shorter models, such as the one shown in Figure 4.2-9 were used to determine the effects of the CEA guides on the tube response and to quickly determine the sensitivity to various static and dynamic loading conditions. The full length model was used to calculate mode shapes and stresses using deflections obtained from a three-dimensional model of the CEA shroud assembly (Section 4.2.1.3). These stresses were obtained for the unmodified structure (failure analysis) and for the modified structure (prediction analysis).

The models were constructed with a thin shell quadrilateral element of arbitrary geometry formed from four compatible triangles. The element accounts for both membrane and bending behavior and has twenty four degrees of freedom, i.e., six degrees of freedom per node in the global coordinate system.

The results of a full-scale forced vibration tube test, which is described in Section 4.1.4, were used to correlate the full length model. This test determined the in-air frequencies and resulting stress levels for various input loadings and points of load application. Analytical and test comparisons at both ends of the tube were determined to be very good with regard to frequency and mode shape and excellent with regard to strain and stress. A typical result of the stress/strain correlation is shown in Figure 4.2-10.

The model was also used as a means of estimating the damping levels in the structure. This estimate was obtained by comparing the calculated stresses with an assumed damping to those obtained from the test for various loading conditions. By ratioing the stress levels, the amount of structural damping was obtained for each loading condition. The resulting damping levels were approximately [ ] percent of critical for the comparisons which were made and agree well with single tube stress results.

In addition, the four web full length model was used to predict the number of cycles to produce a structural failure in the tested shroud with the exciter located near the top of the tube. Test results had indicated that the highest stress levels were in the top of the tube near the four finger guides at a forcing frequency of 190 Hz. With a force input of 12 pounds, the measured strain levels near the welds were approximately [ ] in/in [ ]. These findings agreed well with the analytical predictions of loading and stress. Also, using a fatigue curve for SS304 which is based on raw data and an estimate of the stress concentration factor, the predicted number of cycles to failure is of the order [ ] cycles and represents approximately three hours of test time. The test results agreed well with this prediction and the estimates of required loading giving confidence in the accuracy of the model.

As mentioned previously, the single CEA shroud tube models were used to calculate stresses using deflections obtained from a random vibration analysis (Section 4.2.1.2) and a base excitation analysis (Section 4.2.1.3). These latter analyses were performed using detailed finite element models of the CEA shroud assembly which account for the structural interactions between the various tubes and connecting webs. Preliminary results of these investigations using the single tube shroud models have indicated that the bending stresses are most severe near the four finger guide attachment plates where most of the actual failures occurred. The stresses are generally higher in the first interior row of tubes and most of the response is attributable to the first mode which is possible when snubbers are not used. The findings from a failure analysis of the original structure can be summarized by the following:

1) The CEA shroud tube stress levels are well below the fatigue allowables when the horizontal displacement in the first interior row is [ ] mils. At this displacement, impacting occurred as evidenced by the marks observed on the outer most shroud tube at 45° (Figure 3-3).

2) At the maximum allowable horizontal displacement of [ ] mils in the 180 -
270° quadrant, the maximum stresses in the outer row are close to the
allowables in some cases and fatigue damage defined by the usage factor
is about [ ]. The inner tube stresses are higher than the allowables
in some locations and failures will occur.

The above findings do not include the effects of single tube impacting or the
presence of snubbers on the structural responses. The effects of snubbers are
addressed in Section 6.1.2. The effects of impacting on the dynamic response are
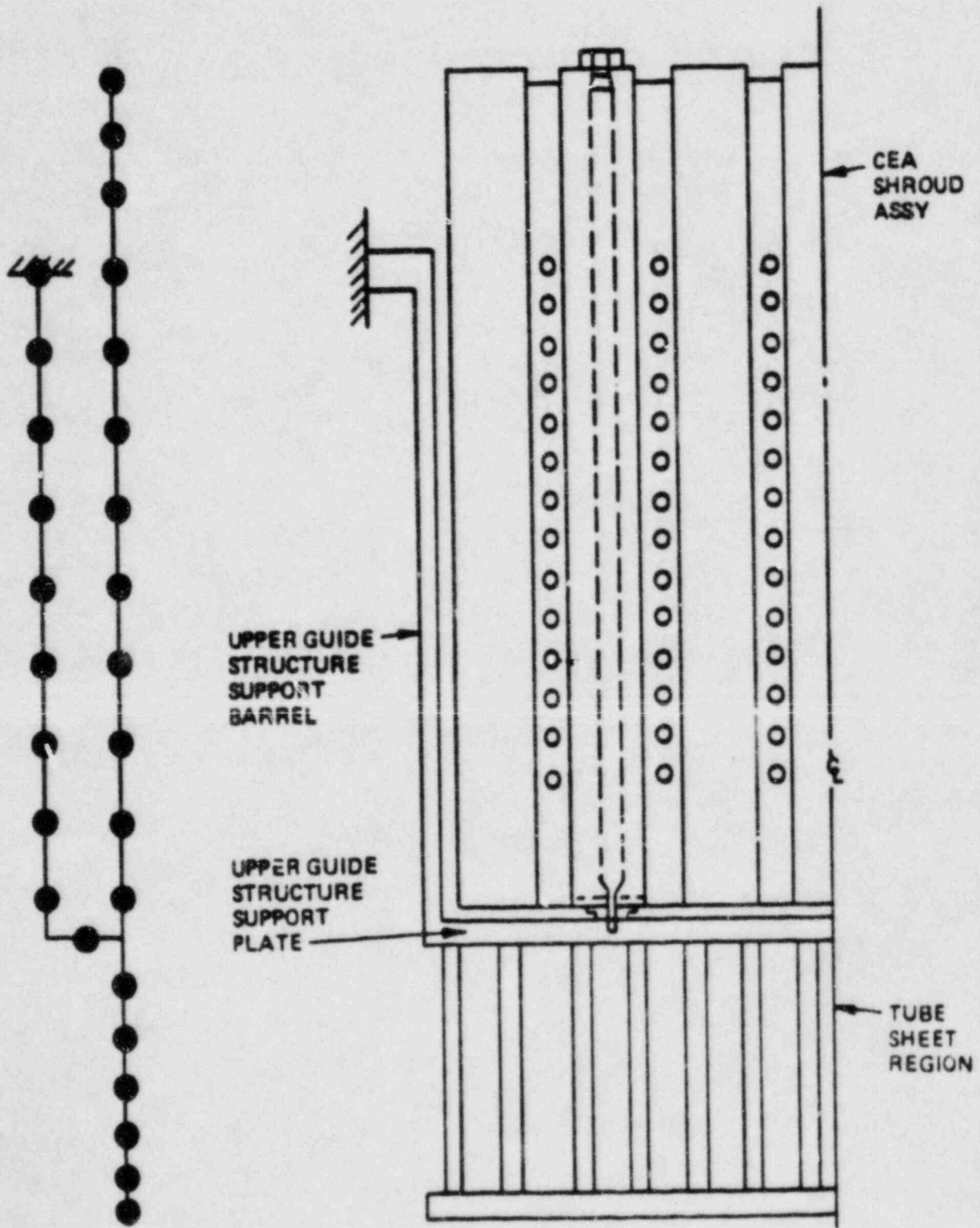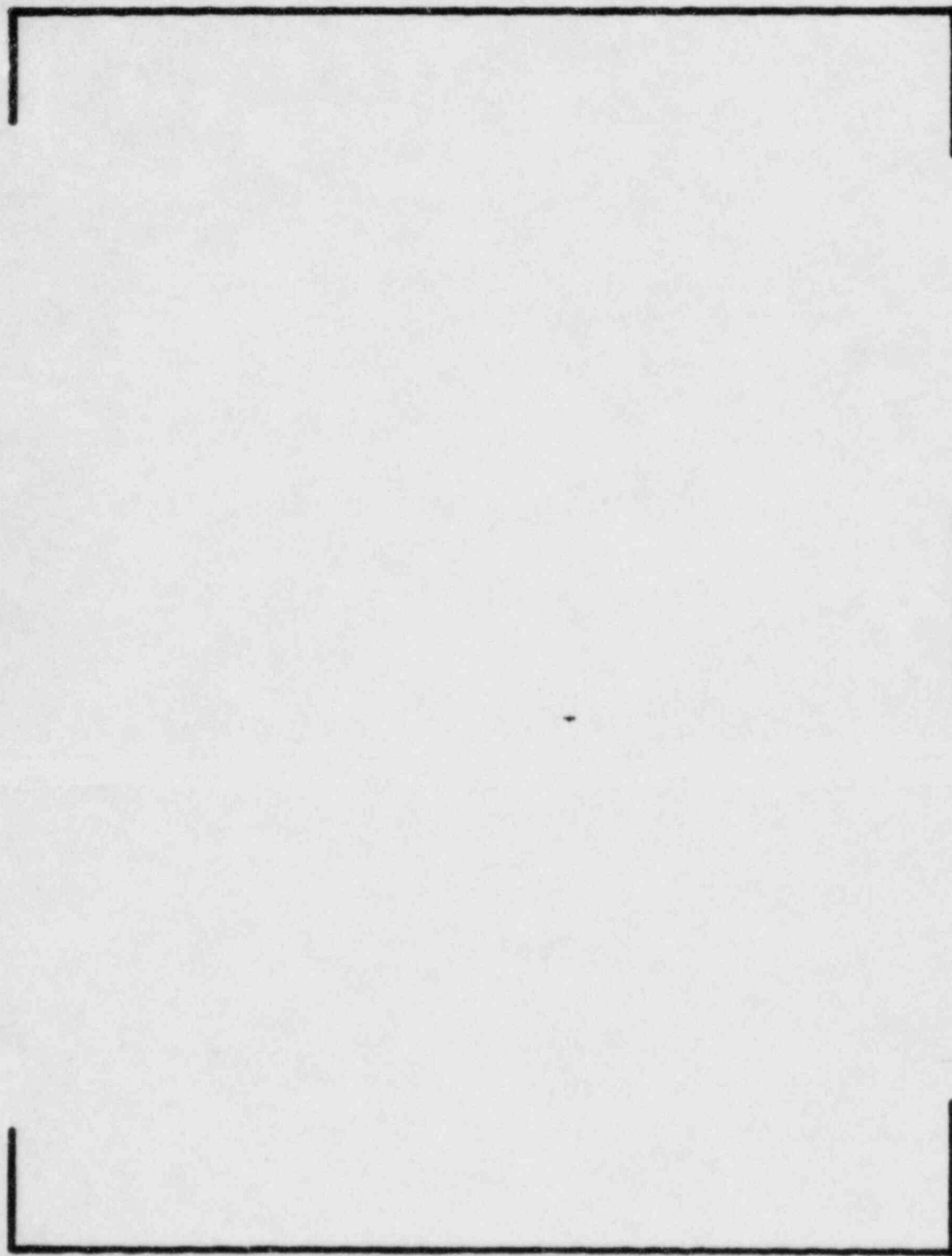presently being determined.

FIGURE 4.2-1

TUBE BANK RANDOM PRESSURE LOADING
FOUR PUMP OPERATION AT 565°F

(PSI)²/HZ

FREQUENCY, HZ

FIGURE 4.2-2

4-24

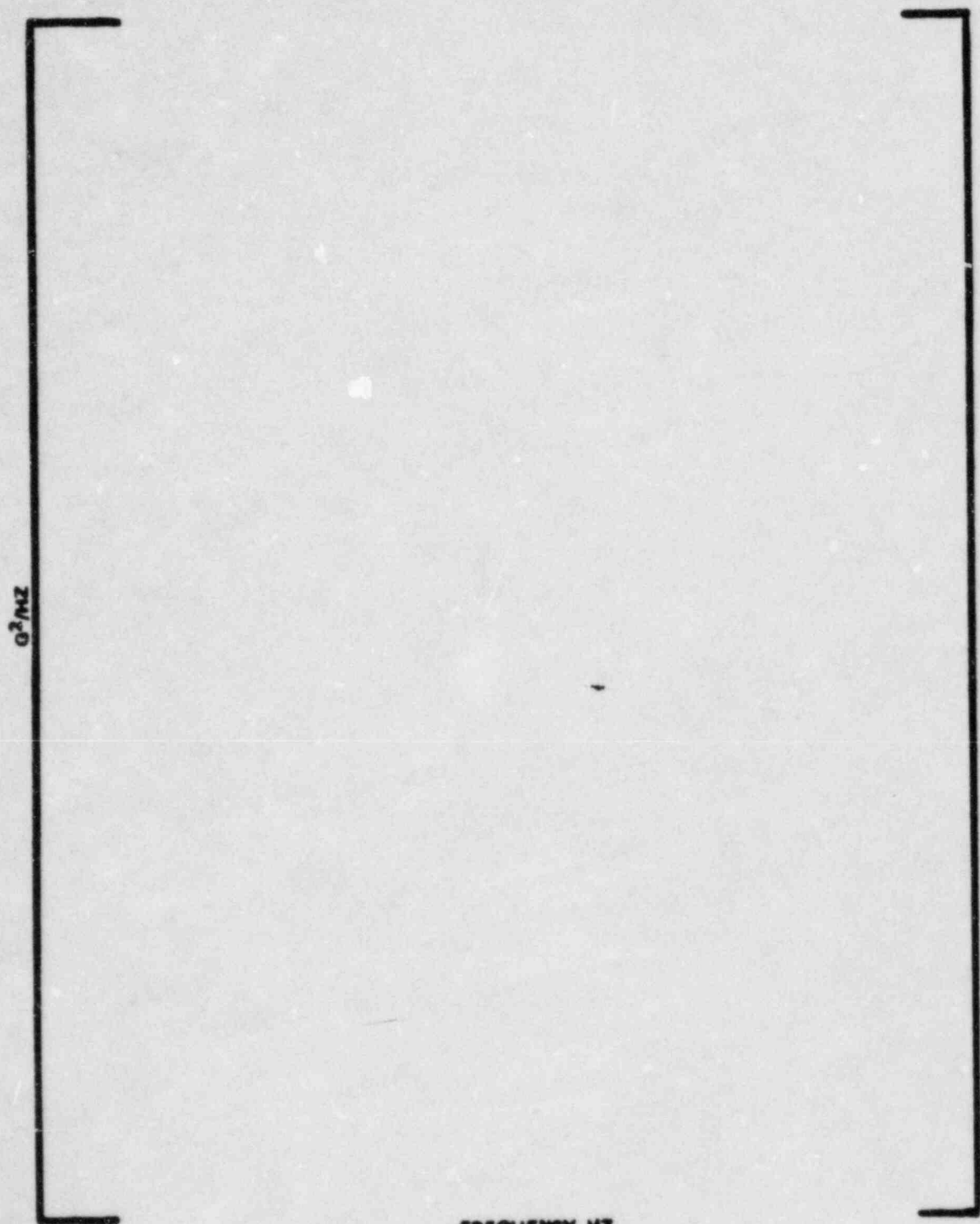CEDM ACCELERATIONS MEASURED DURING
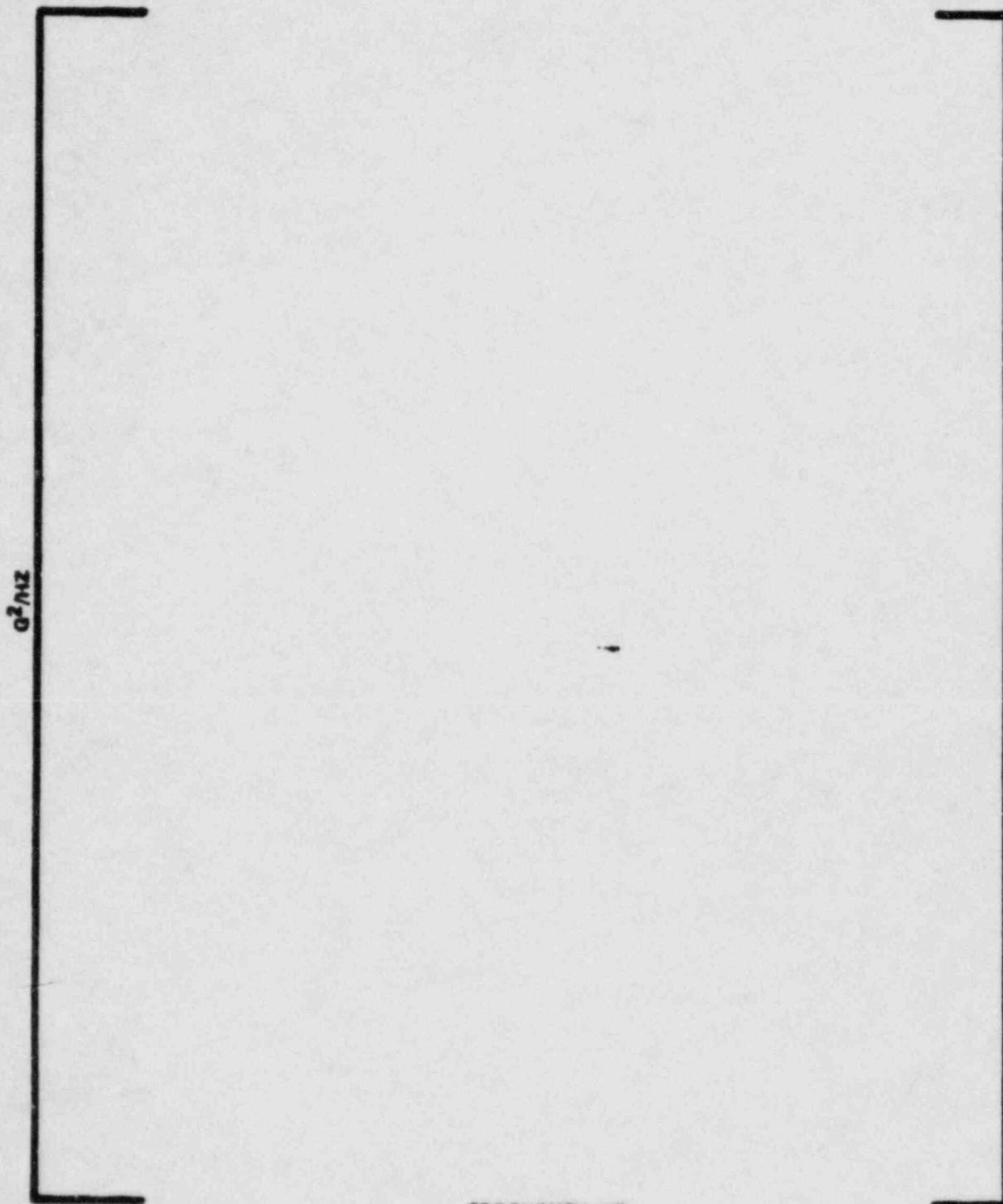PRE-CORE HOT FUNCTIONAL TEST

G^2/HZ

FREQUENCY, HZ

FIGURE 4.2-3

CALCULATED POWER SPECTRAL DENSITY AT
UPPER GUIDE STRUCTURE SUPPORT PLATE

G²/HZ

FREQUENCY, HZ

FIGURE 4.2-4

COMPARISON OF MEASURED AND CALCULATED
PSD AT CENTER OF TUBE BANK

a^2/Hz

FREQUENCY, HZ

FIGURE 4.2-6

CEA SHROUD ASSEMBLY
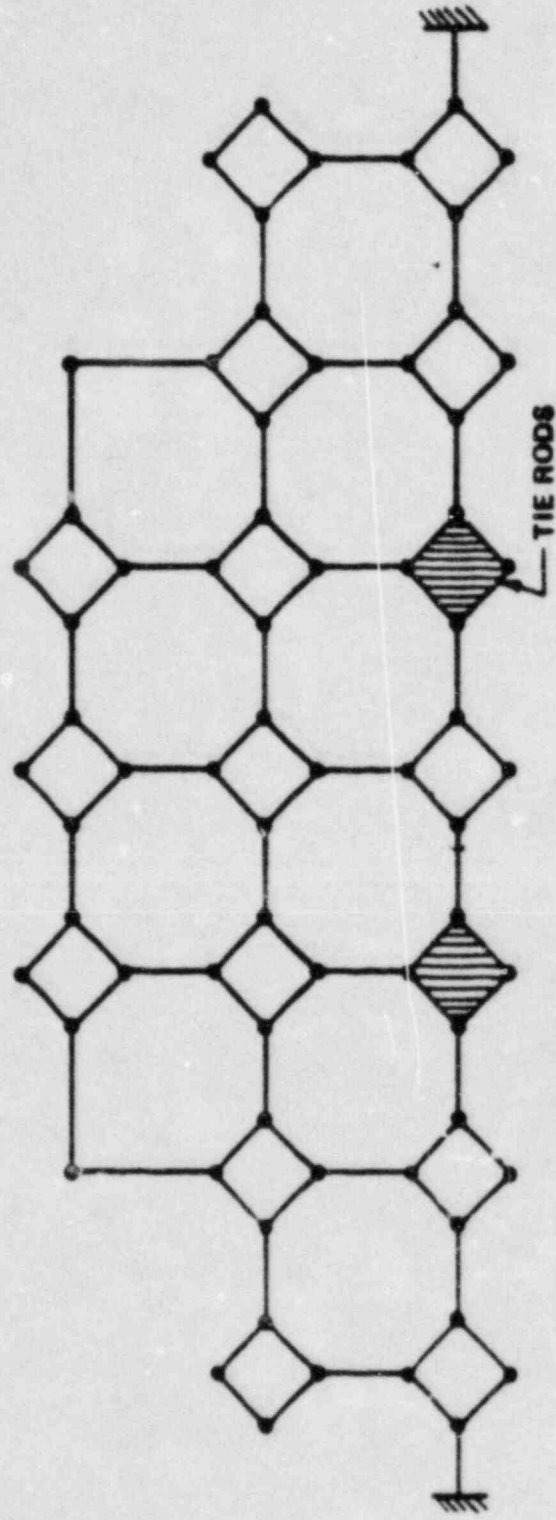
MODEL USED IN RANDOM VIBRATION RESPONSE ANALYSIS

TIE RODS

FIGURE 4.2-8

CEA SHROUD ASSEMBLY
FIRST MODE SHAPE
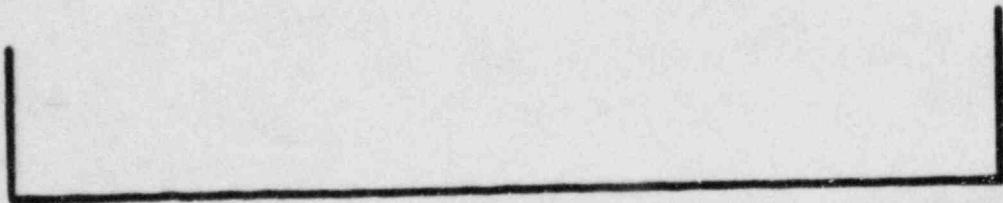(ORIGINAL STRUCTURE)

DISPLACEMENTS OF SELECTED TUBES

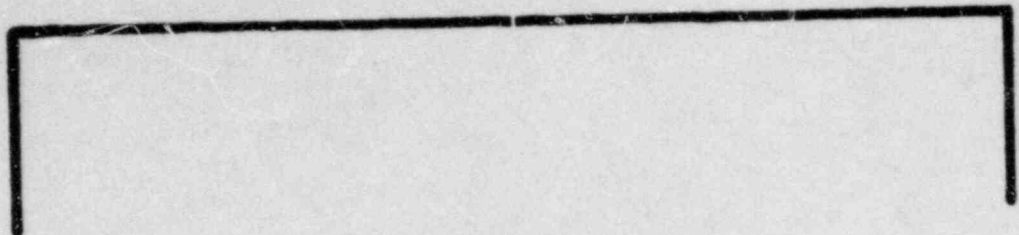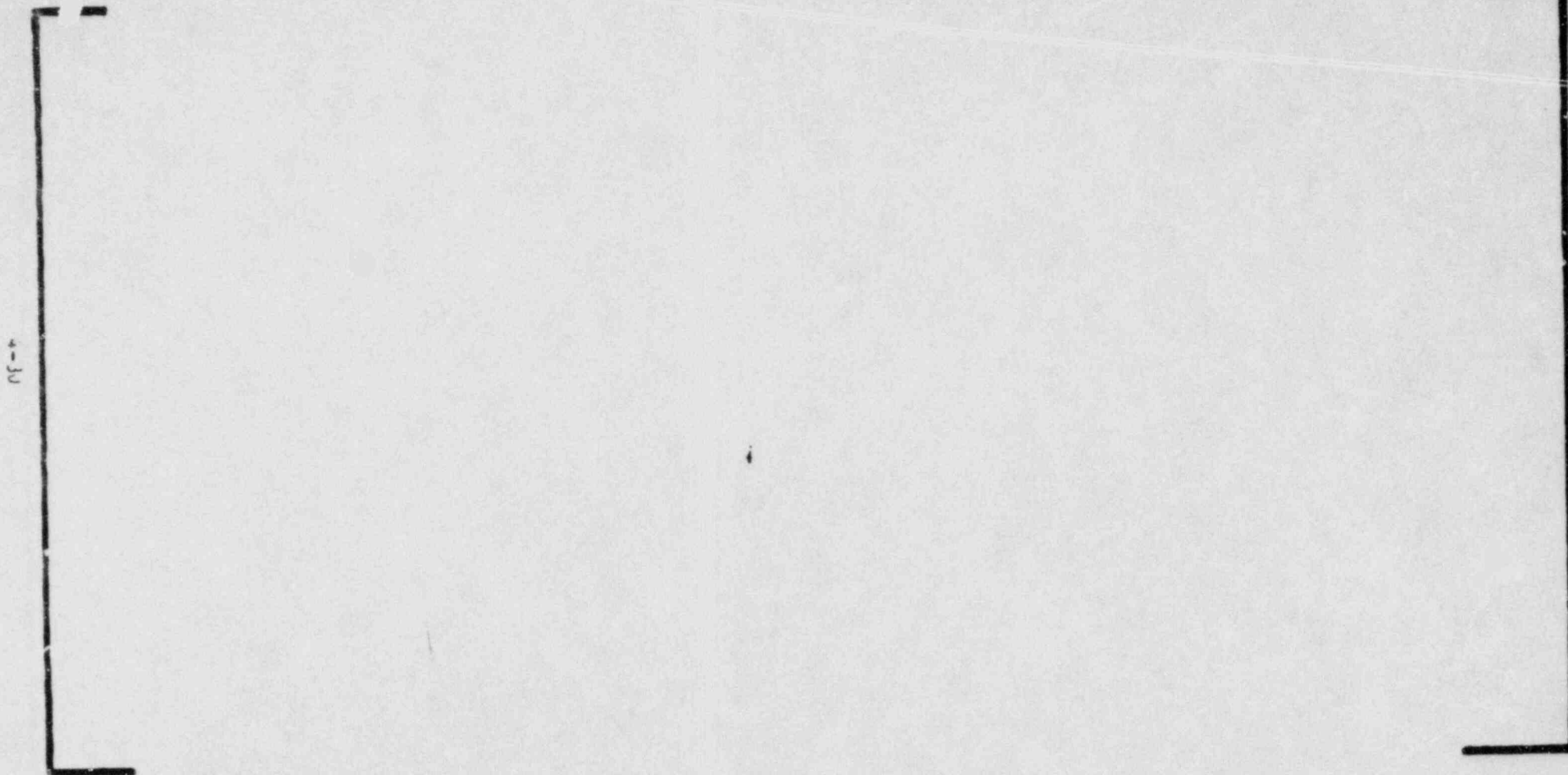FIGURE 4.2-7

CEA SHROUD ASSEMBLY
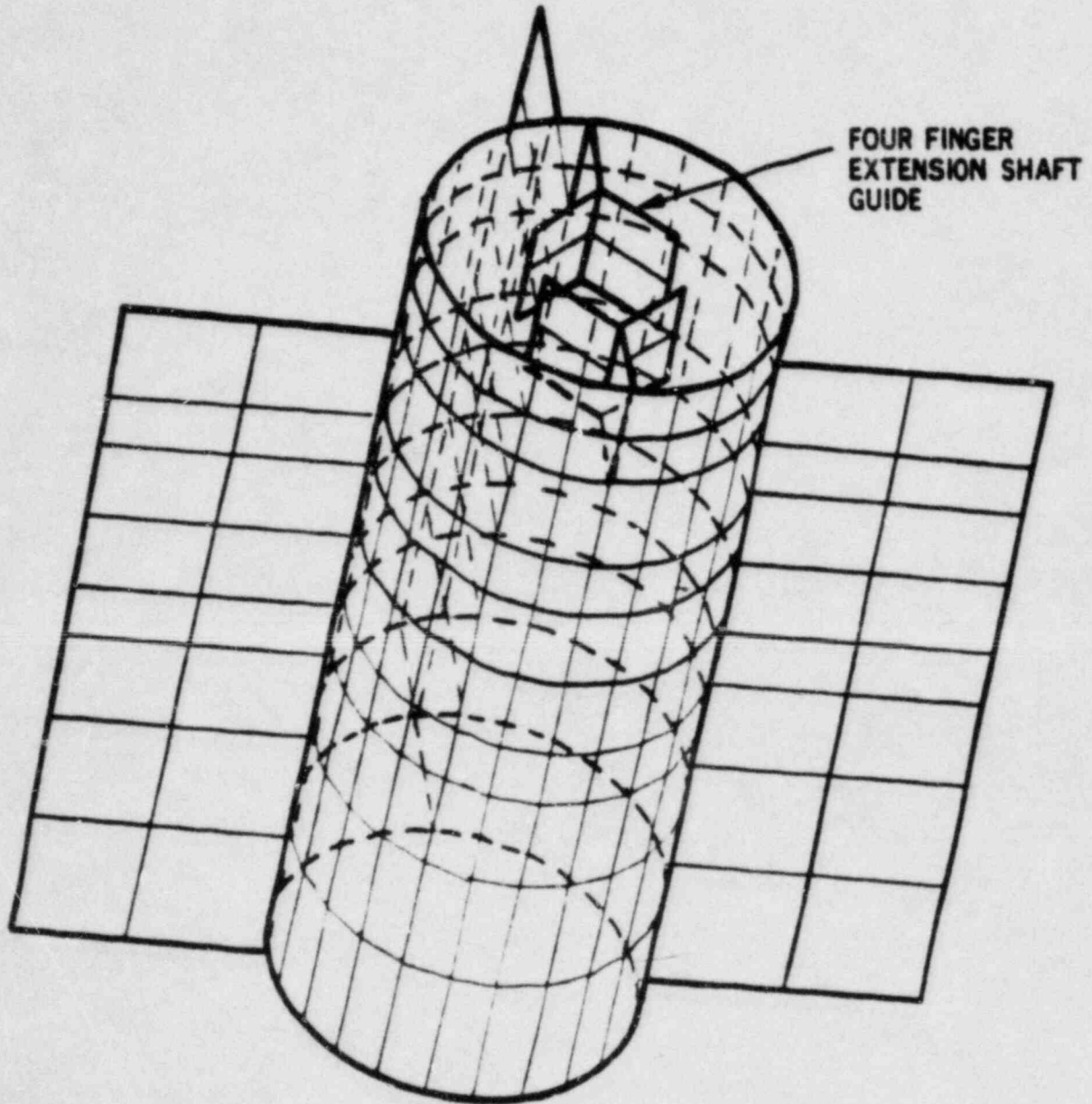THIRD MODE SHAPE
(ORIGINAL STRUCTURE)

DISPLACEMENTS OF SELECTED TUBES

NOTES: "T" INDICATES TOP OF TUBE.
BOTTOM OF TUBE SHOWN DOTTED.
"R" INDICATES TIE ROD TUBE.

FIGURE 4.2-8

FIGURE 4.2-9

FINITE ELEMENT MODEL
OF CEA SHROUD TUBE

FOUR FINGER
EXTENSION SHAFT
GUIDE

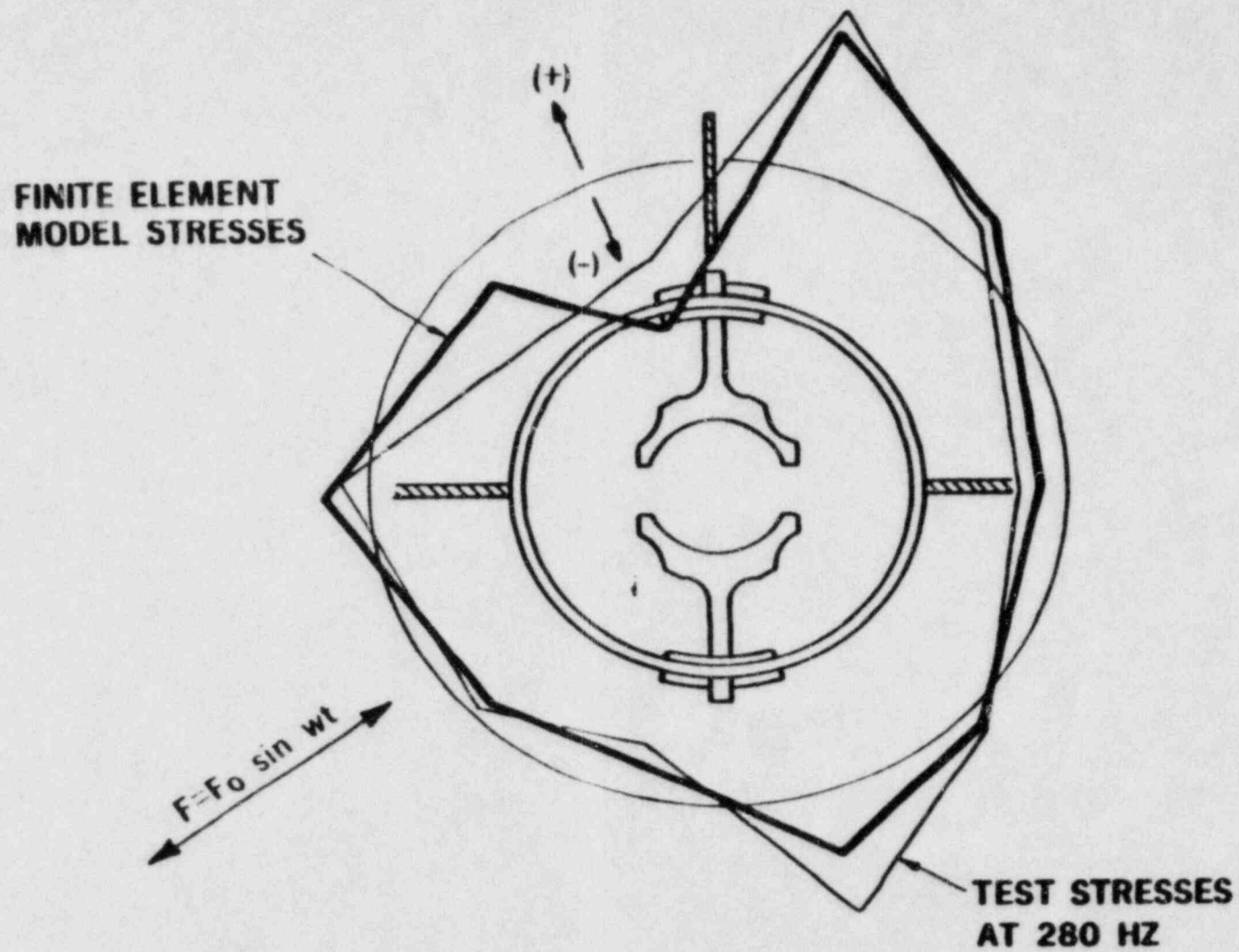# COMPARISON OF TEST AND FINITE ELEMENT STRESSES FOR FORCED EXCITATION

FIGURE 4.2-10

5.0 CORRECTIVE ACTIONS

The problem described in Section 1.1 was corrected by taking the actions described below.

5.1 CEA GUIDE MODIFICATION

The configuration of the attachment of the CEA guides to the top of the shroud contributes to local stress concentrations. This is evident from the observed crack locations (Section 3.0), from the experimental test results (Section 4.1.4), and from the analytical results (Section 4.2). The modification consists of removing the top three inches of the CEA shroud and all the 4-finger and 12-finger CEA guides. Thereby, the locations for crack initiation are eliminated. Since the guides have no function during normal operation, their function is provided by a separate tool which is not a permanent part of the vessel or the internals. The tool is utilized only during refueling operations.

Cutting a length of three inches from the top of the CEA shroud assures that effects of the original welding of the guides is removed. This length is cut off everywhere except at the eight tie rod locations and two locations for Reactor Vessel Level Monitoring System (RVLMS) probes. Those shroud tubes remain full length to eliminate the need for changes to the tie rod assembly and to the Heated Junction Thermocouple RVLMS. The maximum allowable cutoff length is greater than three inches. It is based on the requirement that the CEA spiders remain within the shroud when the CEAs are in the fully withdrawn position. Figures 5-1 and 5-2 show the modified CEA shroud.

After cutoff, a minimum of three inches of the welds at the top between webs and shroud tubes are ground out and replaced with full penetration welds. An additional fillet weld is applied over this to minimize the stress concentration at the junctions. The bottom welds at the tie rod locations are also similarly prepared. Liquid penetrant inspection according to the ASME code requirements is imposed for these weld repairs.

5-1

5.2   CEA SHROUD LATERAL SUPPORT MODIFICATIONS

The CEA shroud is held down to the Upper Guide Structure Support Plate
(UGSSP) by the eight tie rods.   Stiffness of the shroud assembly
provides the restraint against lateral forces in the original design.
Analyses in Section 4.2 indicate that global modes of vibration of the
shroud may cause lateral deflection of the outer tubes and webs and may
contribute to high stresses.   To limit such lateral deflection, four
snubbers are added to the CEA shroud as shown in Figures 5-1 and 5-3.

The snubber consists of three pieces.   A snubber block assembly is
shop welded into the three outermost shroud tubes on each of four sides
of the shroud.   A flange block assembly is field installed on the UGS
barrel flange by pins and bolts.   A hard shim is field fitted to the
snubber block to provide controlled clearance with the sides of the slot
in the flange block.   The completed snubber assembly allows radial and
axial differential motion between the CEA shroud and the UGS barrel but
restricts lateral or tangential motion to the amount of clearance at the
shims (maximum [ ] mils).

Vibratory lateral displacements of the CEA shroud are limited by the
snubber.   The lateral load is transmitted into the barrel flange which in
turn is clamped by the reactor vessel flanges.   The hard snubber shims
and their hardened mating surfaces on the flange block provide wear
surfaces to allow for normal radial and axial differential movement.

5-2

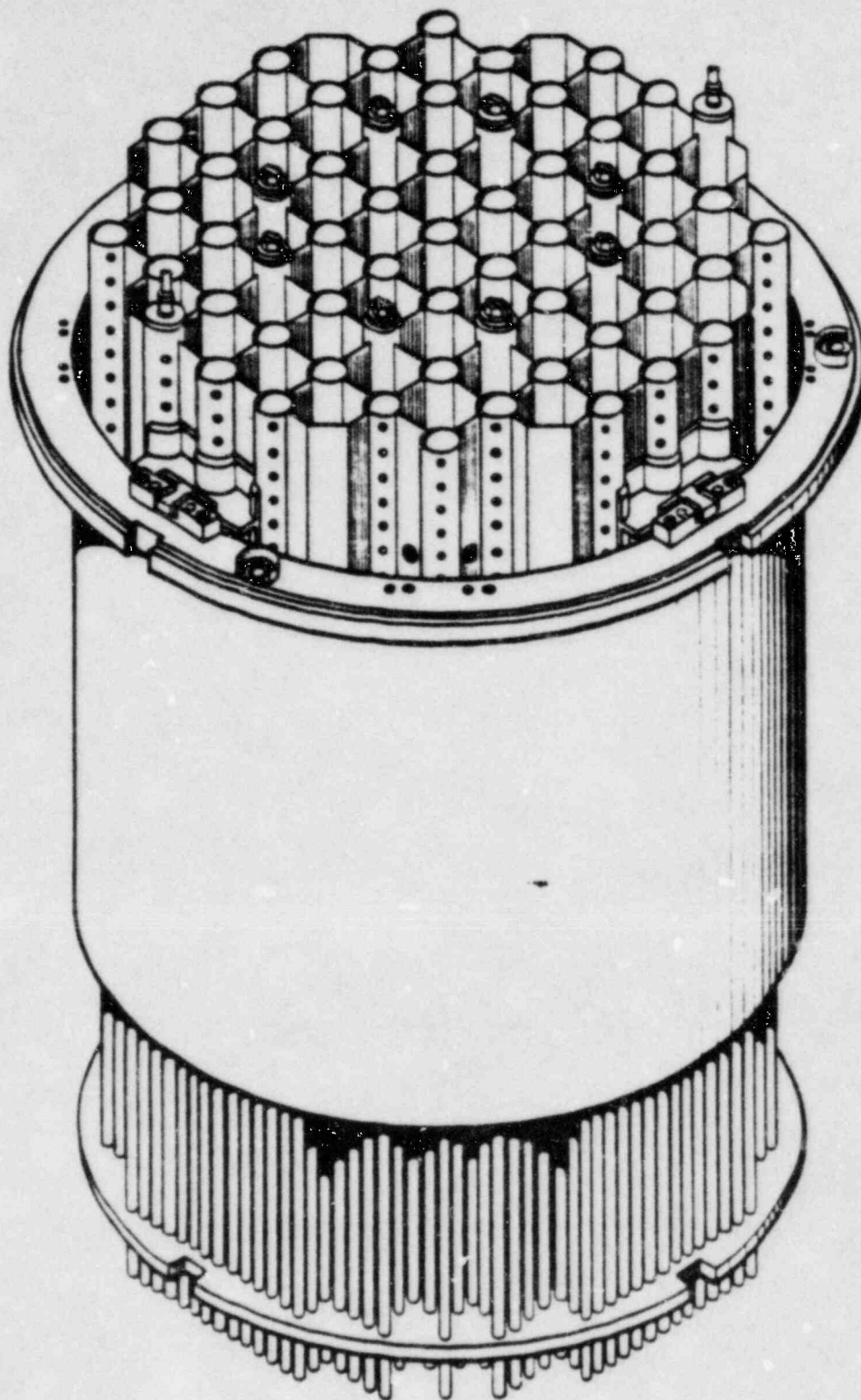FIGURE 5-1

MODIFIED
UPPER GUIDE STRUCTURE
ASSEMBLY

5-3

FIGURE 5-2

MODIFIED UPPER GUIDE STRUCTURE ASSEMBLY

Cut Off Top
3" and CEA
Shaft Guides
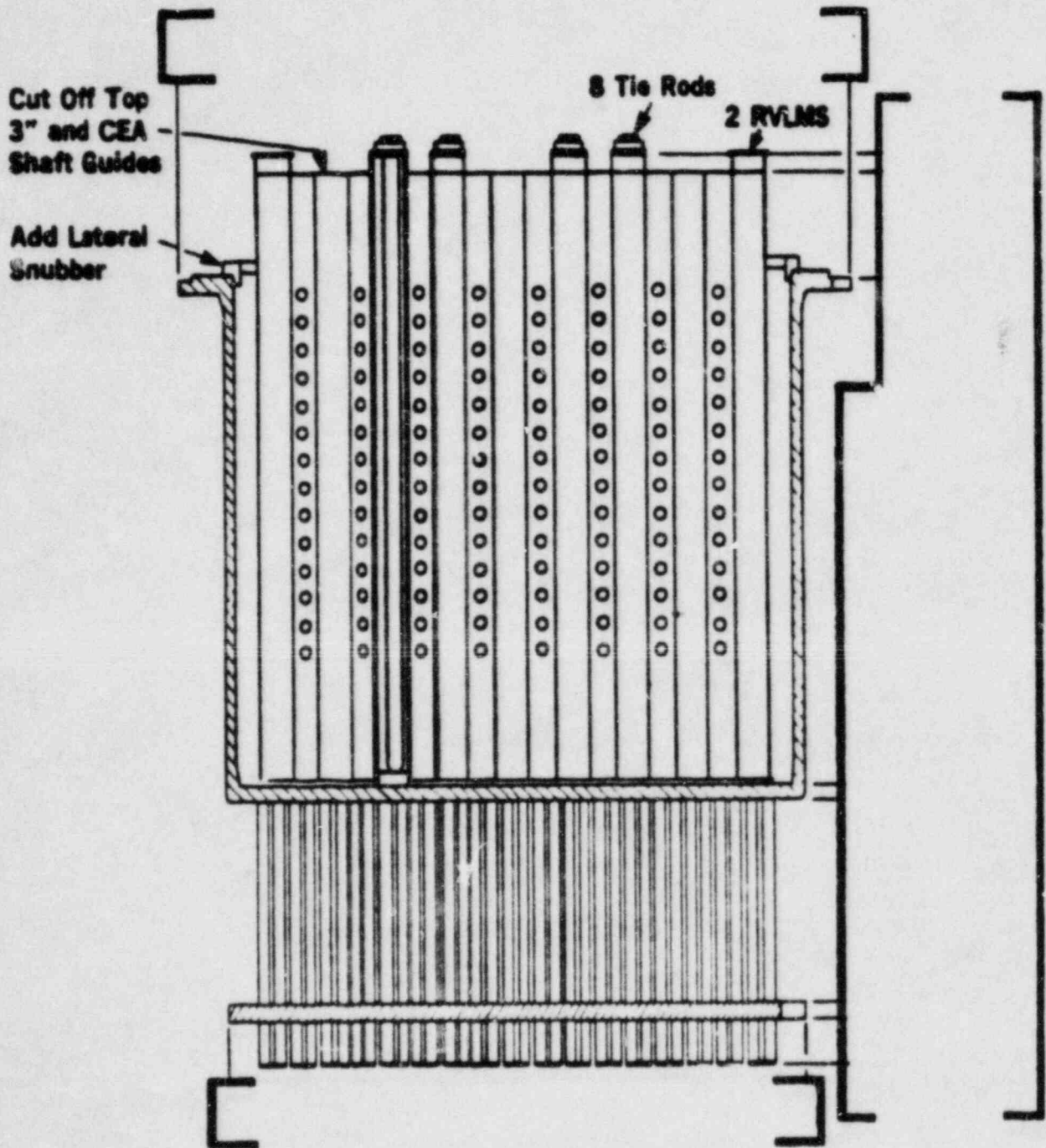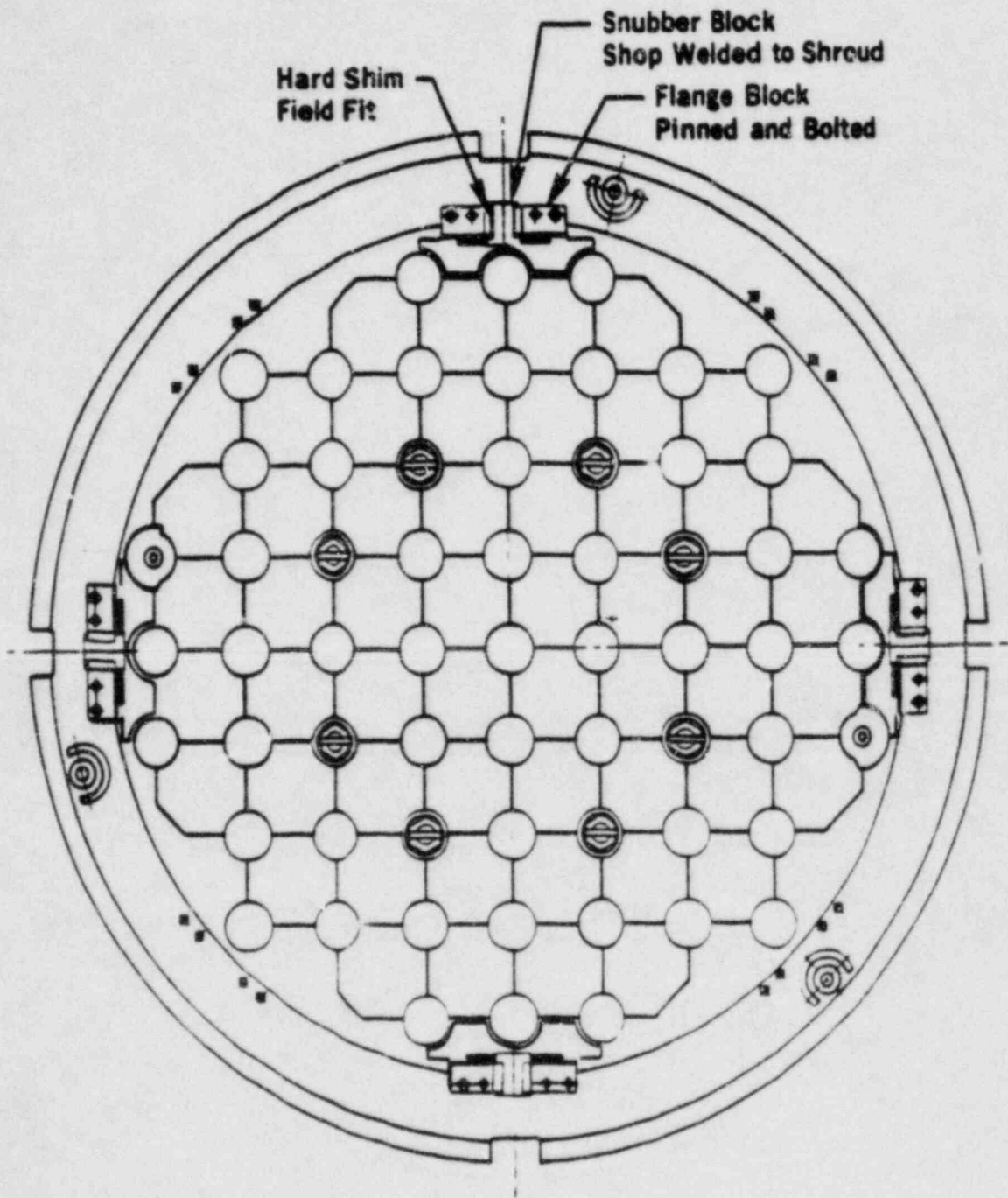
8 Tie Rods

2 RVLMS

Add Lateral
Snubber

FIGURE 5-3

MODIFIED UPPER GUIDE STRUCTURE ASSEMBLY

6.0 Test and Analyses of Modification

6.1 Analyses and Component Test

The evaluation of the failure modes utilizing hot functional test data, analyses and experimental measurements on components and on entire CEA shrouds identified two potential failure mechanisms for the original shroud design. Similar analyses and component testing on the modified shroud should give confidence that the modified shroud will not fail. A description of mechanical testing on a modified single shroud tube is given in Section 6.1.1. Analytical models described previously in Section 4.2 are applied in Section 6.1.2 to the modified design. As a final check on the response calculated for the CEA shroud during normal operation, testing will be done in the Palo Verde Unit 1 reactor after all modifications are completed. Section 6.2 describes this planned Demonstration Test. The final CEA shroud report will summarize the results from the test and compare them to analytical predictions.

6.1.1 Mechanical Excitation Test

The purpose of this test is to characterize the vibration of a single CEA shroud tube after the modifications described in Section 5.1 are completed. The test arrangement was described previously in Section 4.1.4. This test is underway and results will be presented in the final CEA shroud report.

6.1.2 Analyses of Modified CEA Shroud Assembly

Structural analyses of the modified upper guide structure were performed using models of a full length single tube and the CEA shroud assembly. The structural modifications are the removal of the four finger CEA guides and the top three inches of the tubes which contain these guides, the removal of the twelve finger CEA guides, and the addition of snubbers to prevent lateral motion of the peripheral shrouds. Preliminary results of base excitation analyses indicate that the snubbers help by limiting deflections. In addition, the removal of the guides eliminates regions with stress concentration factors. Stresses are being calculated at selected locations throughout the structure and will be used to determine the structural integrity of the various shroud tubes. Because of the size of the model and the amount of deflection data, the evaluations are still continuing in order to fully assess the response of the modified structure. The results of this prediction analysis will be compared to actual measurements from the planned Demonstration Test.

6.2 Demonstration Test

A demonstration test is planned for Palo Verde Unit 1 to confirm the adequacy of the repairs to the upper guide structure under operating conditions which are similar to those during the pre-core hot functional test. During the test, data will be taken for various reactor coolant pump combinations at selected coolant system temperatures and pressures. The maximum pressure for the test is 2250 psi and the maximum temperature is 550°F.

The CEA shroud will be instrumented during the demonstration test to determine the loadings and structural responses. Instruments will be located at the top and bottom of the shroud assembly as shown in Figures 6.2-1 and 6.2-2. Table 6.2-1 defines the purpose for each of the instruments. The vibratory motion of several shroud tubes will be determined with bi-directional accelerometers; strain gages will be used to determine the stress levels in selected tubes and webs. Dynamic strain will be correlated with dynamic pressures measured at the top and bottom of the same tubes. The basis for selecting these instruments is to determine the response and loading at key locations, especially where structural failures occurred, in order to learn which contributing mechanisms led to the failures. The measurement results will be compared to analytical forcing functions and responses.

TABLE 6.2-1

UGS Instrumentation List

Transducer	Purpose
A-1	Measure motion of previous failed tube and measure snubber impact if occurring.
A-2 A-3 A-4	Measure CEA shroud axial motion and measure snubber impact if occurring.
A-6	Measure response of outermost tube next to UGS barrel wall.
A-5	Measure response of center tube for comparison with outer tube motion.
A-7	Measure motion of Tube #6 where high cross flow occurs. (Designated A-7 in CVAP)
A-8	Measure motion of UGS plate.
A-9	Measure fuel alignment plate motion.
SG-1	Obtain strain distributions.
SG-2	Obtain strain distributions.
SG-3 SG-4	Measure strain in previously failed tube.
SG-5 SG-6	Record strains on previously unfailed tube toward the interior of the package for comparison.
SG-7 SG-8	Measure strain on previously failed tube and obtain strain distributions.
SG-9	Measure bending strain in outer web.
SG-10 SG-11	Obtain strain distributions. Obtain strain distributions.
SG-12 SG-13	Determine strains in location of failed tube in the inner row.

TABLE 6.2-1 (cont'd)

UGS Instrumentation List

Transducer	Purpose
SG-14	Measure strain in high cross flow
SG-15	region (previously designated S-9 & S-10 in CVAP)
SG-16	Measure strain on web interior to tie rods.
SG-17	Measure bending strain in web near tie rod.
SG-18	Measure strain on web interior to tie rods.
P-1	Measure forcing function in
P-2	previously failed tubes.
P-3	Measure forcing function in web area.
P-4	Measure forcing function in
P-5	previously failed tubes.
P-6	Measure pressure fluctuations on UGS plate to be compared with Unit 1 CVAP results. (Designated P-13 in CVAP).
P-7	Measure forcing function on highly instrumented tube.
P-8	Measure acoustic pulses
P-9	exiting RCP. (Not shown in Figures 6.2-1 & 6.2-2.)

INSTRUMENTATION LOCATIONS
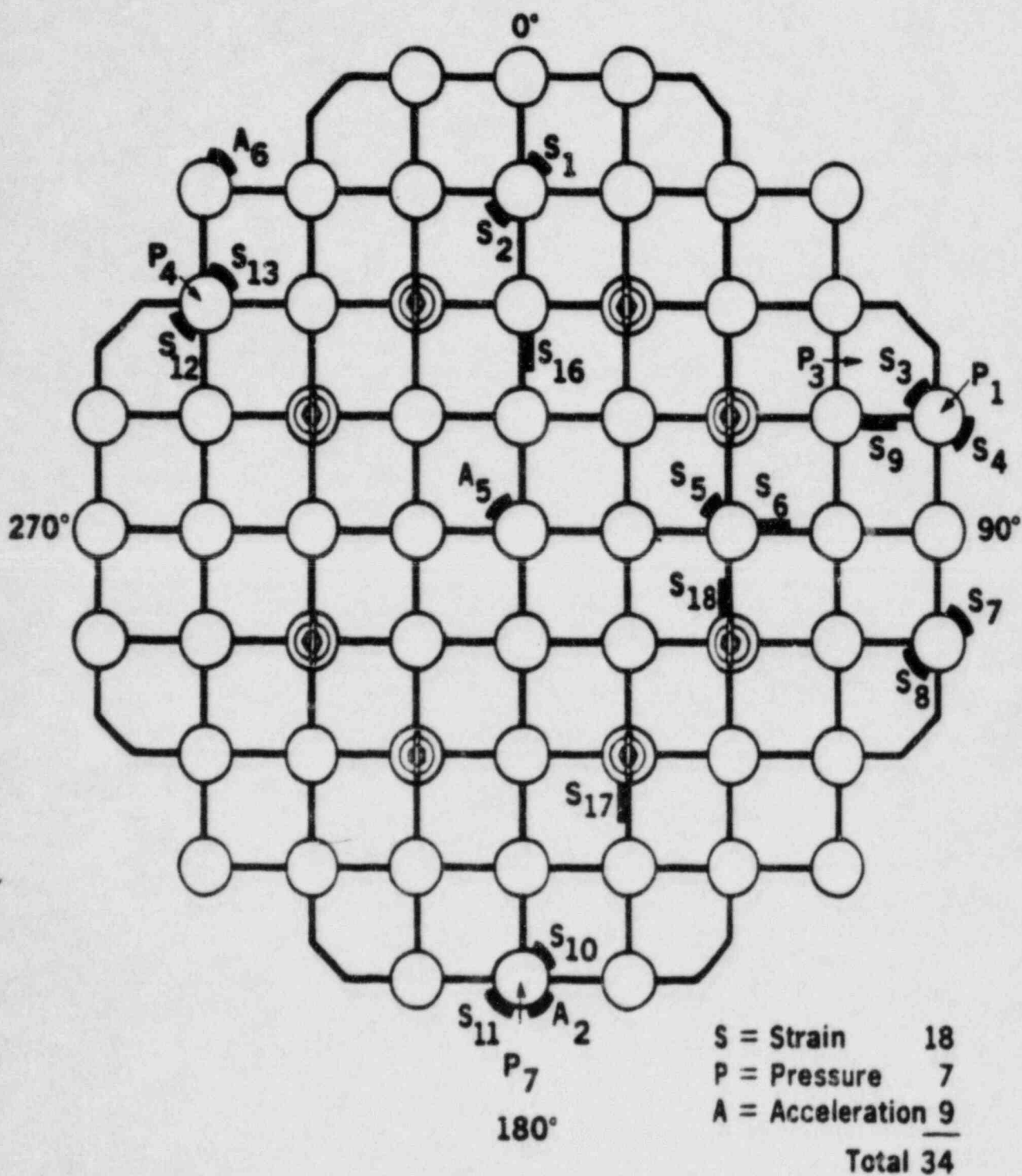## (Only Top Locations Shown)
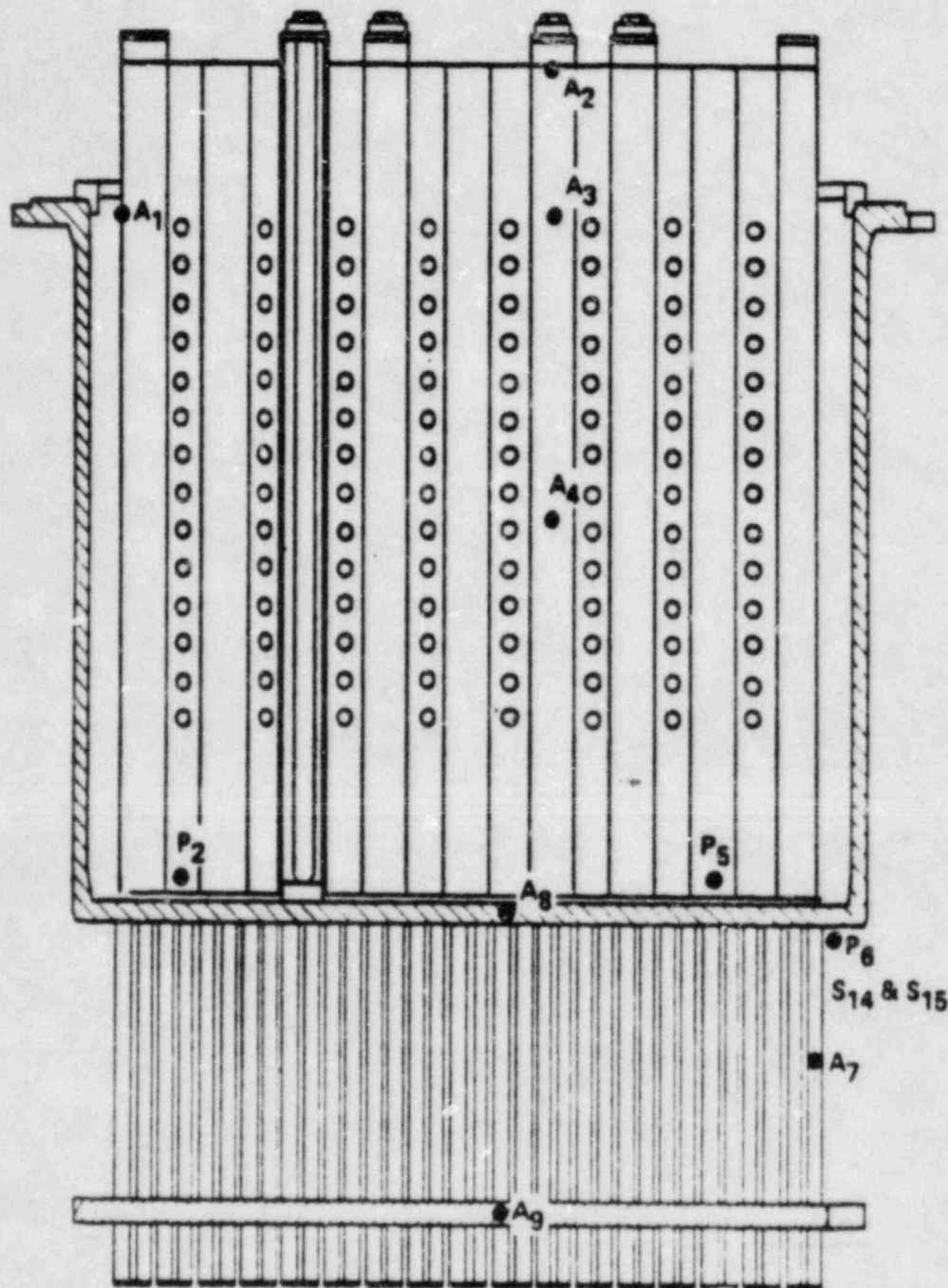

FIGURE 6.2-1

INSTRUMENT LOCATIONS
(ELEVATION VIEW)

FIGURE 6.2-2

COMBUSTION ENGINEERING, INC.